Model-order reduction for the parametric analysis of damage in reinforced concrete structures

Matthieu Vitse

université PARIS-SACLAY

école normale supérieure paris—saclay

NNT : 2016SACLN055

Thèse de doctorat
de l'Université Paris–Saclay
préparée à
l'École Normale Supérieure de Cachan
(École Normale Supérieure Paris–Saclay)

Ecole doctorale n°579
Sciences mécaniques et énergétiques, matériaux et géosciences - SMEMAG
Spécialité de doctorat : solides, structures, matériaux

par

M. Matthieu Vitse

Réduction de modèle pour l'analyse paramétrique de l'endommagement dans les structures en béton armé

Thèse présentée et soutenue à Cachan le 9 décembre 2016.

Composition du Jury :

M.	David Dureisseix	Professeur INSA Lyon	(Président)
M.	Pedro Díez	Professeur UPC–BarcelonaTech	(Rapporteur)
M.	Jean-Charles Passieux	Maître de conférences HDR INSA Toulouse	(Rapporteur)
M.	Udo Nackenhorst	Professeur HSU Hannover	(Examinateur)
M.	Benjamin Richard	Ingénieur–chercheur HDR CEA Saclay	(Examinateur)
M.	Pierre-Alain Boucard	Professeur ENS Paris–Saclay	(Co-directeur de thèse)
M.	David Néron	Professeur ENS Paris–Saclay	(Directeur de thèse)

Enfin ! L'écriture de ces lignes fait office d'ultime bilan de ces années de thèse, un bilan humain extrêmement riche, à l'image des nombreuses interactions que j'ai pu avoir dans mon travail ou ma vie privée.

Je souhaite tout d'abord remercier les membres du jury, en particulier les rapporteurs de ce manuscrit, pour m'avoir accordé un peu de leur temps en cette fin d'année je l'imagine très chargée. Je les remercie en particulier pour leurs commentaires et leurs remarques qui m'ont permis de préparer la soutenance avec plus de sérénité.

Je souhaite ensuite bien évidemment remercier Pierre-Alain et David, qui m'ont guidé et encouragé pendant ces trois (et quelques) années. Je n'oublierai pas ces sessions de débuggage code à distance, ou ces tapes amicales sur l'épaule qui redonnaient un peu de courage (une fois la douleur passée!) quand rien ne voulait fonctionner.

Je ne peux également pas penser à ces années sans remercier les personnes que j'ai côtoyé au quotidien au sein du laboratoire, depuis mon premier bureau en salle 211 jusqu'au centre de calcul où j'ai passé le plus clair de mon temps : Paul, Camille, Rana, Maxime, Basile, Elena, Hadrien, John-Éric, Stéphane N., Charles et bien d'autres. Je ne saurai non plus oublier Martin, Jan, Yoann, Peter, Stéphane R., Boubou, Frisou, Danielle et Lydia. Un immense merci à Marie pour son soutient et dont la présence était souvent réconfortante.

Je n'oublie pas mes amis d'ailleurs, qui ont joué un rôle important en me donnant cette bouffée d'air bien nécessaire parfois : Adrien, Mélanie, Victor, Lisou, Pierre, Kate, Tifenn, Hélène, Mathieu, Noémie.

À ma famille, pour son soutien sans failles, en particulier à mon père qui a toujours su, à sa manière, me conseiller dans les choix décisifs de ma vie : un simple "merci" n'est certainement pas suffisant.

Florent, Elisabeth, Maxence et Paul, (vaga)merci.

Contents

Nomenclature

Mathematical notations

x	continuous variable or function
x	discrete variable or function
$\boldsymbol{x}$	continuous vector
$\mathbf{x}$	discrete vector
$\boldsymbol{X}$	continuous tensor of order ≥ 2
$\mathbf{X}$	discrete tensor of order ≥ 2
$\mathcal{X}$	continuous space
$\boldsymbol{\chi}$	discrete space
$\mathbf{I}_1(\square)$	first invariant of the tensor $\square$ (trace operator)
$\square : \square$	contracted product, $\boldsymbol{A} : \boldsymbol{B} = \mathbf{I}_1(\boldsymbol{A} \cdot \boldsymbol{B})$
$\langle \square \rangle_+$	Macaulay brackets - positive part of tensor $(\cdot)$
$\bar{\times}_k$	mode-k tensor-vector product
$[\![\square]\!]_{(c,r)}$	jump of quantity $\square$ at the interface (c, r)
$\otimes$	outer product of vectors $\boldsymbol{u}$ and $\boldsymbol{v}$

Mechanical problem

$\boldsymbol{C}^c$	fourth-order Hooke tensor for the concrete medium
$\boldsymbol{C}^r$	fourth-order Hooke tensor for the reinforcement
$\boldsymbol{C}$	assembled Hooke tensor
$\mathcal{D}_i$	interval of definition of the parameter μ_i
$\mathcal{I}$	time interval of definition of the solution ($\equiv \mathcal{D}_1$)
$\mathcal{U}$	displacement space
$\boldsymbol{u}^c$	displacement field for the concrete medium
$\boldsymbol{u}^r$	displacement field for the reinforcement
$\boldsymbol{u}$	assembled displacement field
$\boldsymbol{u}_d$	prescribed displacement over $\partial_1 \boldsymbol{\Omega}$

Y^c part of the energy rate released due to damage
Z^c thermodynamic force associated with z
$\boldsymbol{\varepsilon}^c$ second-order strain tensor in the concrete medium
$\boldsymbol{\varepsilon}^{c,f}$ homogenized contribution of the crack opening to the total strain
$\boldsymbol{\varepsilon}^f_{\max}$ maximum of crack strain that affects the evolution of the proportion of closed cracks
$\boldsymbol{\varepsilon}^r$ second-order strain tensor in the reinforcement
$\boldsymbol{\varepsilon}$ assembled strain tensor
φ^m non-associated pseudo-potential of dissipation
$\boldsymbol{\Omega}$ spatial domain ($\boldsymbol{\Omega} \in \mathbb{R}^n$, $n = 1, 2, 3$)
$\partial_1\boldsymbol{\Omega}$ spatial domain restricted to prescribed displacements (Dirichlet condition)
$\Psi^{c,f}$ Helmholtz free energy associated with the closed cracks
$\Psi^{c,m}$ Helmholtz free energy associated with the cracked continuum medium
$\boldsymbol{\sigma}^c$ second-order Cauchy stress tensor in the concrete medium
$\boldsymbol{\sigma}^{c,m}$ second-order Cauchy stress tensor in the cracked continuum medium
$\boldsymbol{\sigma}^{c,f}$ second-order Cauchy stress tensor in the cracks when closed
$\boldsymbol{\sigma}^r$ second-order Cauchy stress tensor in the reinforcement
$\boldsymbol{\sigma}$ assembled stress tensor

Algorithmic

ς_{crit} stopping criterion

Model parameters

A_d brittleness coefficient in tension
d assembled damage variable
d^c damage variable of the concrete medium
d^r damage variable of the reinforcement
E^c Young modulus of the concrete medium
E^r Young modulus of the reinforcement
f_t^c maximum strength in tension for the concrete medium
H consolidation function
Y_0 initial threshold for damage activation
z^c isotropic hardening variable of the concrete medium
α_0 parameter controlling the variance of the event “a crack closes”

LATIN and reduced-order modeling

s solution ensemble set
$\boldsymbol{\Phi}_k$ k^{th} space function in the separated-variable decomposition
a_k k^{th} parameter function in the separated-variable decomposition
$\boldsymbol{\Gamma}$ space of the local –nonlinear– equations
$\boldsymbol{A_d}$ space of the global –linear– equations
η_{crit} update criterion

Introduction

The study of the variability in materials is an open subject in computational mechanics when dimensioning structures. This variability can be the result of the manufacturing of the material (choice of the constitutive elements, manufacturing process), but also can come from the description of its physical model. Hence, it is easy to understand that the stronger the uncertainties, the more difficult the computations can get, whichever the scale considered (from a micro-scale point of view to the scale of an engineering structure). This is especially true for reinforced concrete which has been (and still is) extensively used for civil engineering purposes, even if its long-term mechanical behavior and the degradation mechanisms that result from the aging of the structures are not perfectly known or even understood. Chemical reactions, mechanical degradations (see Fig. 1) can occur along the life of a given structure, which makes it even more difficult, even with the advanced numerical tools available nowadays, to predict the behavior of a building to a certain loading. Among the numerous areas of interest in this field, the simulation of reinforced concrete structures under cyclic loading has shown a growing interest, especially since the Fukushima incident from 2011. This was the trigger event of the *SINAPS@* project[1], funded by the French national research agency (ANR) and led by the CEA, which also involves many industrial and academic partners such as EDF, AREVA, École Centrale de Nantes or École Normale Supérieure Paris–Saclay. Its goal was set to explore the uncertainties related to the physical processes and the methods used to evaluate the seismic risk and the vulnerability of structures and nuclear components. It mostly aims at providing tools to describe the seismic hazard as well as its impact on a given structure, to identify the seismic margins and to propose recommendations on the evolution of regulations regarding the seismic hazard.

Our interest, as part of this project, lies in the fact that when studying the response of a reinforced concrete structure to seismic loading, one can consider several time scales, all having an important impact on the final behavior of the structure:

(i) early-age concrete's mechanical properties evolve quickly due to the hydration of the concrete paste, with highly exothermic reactions, which can impact the stress and strain state of the structure. The long-term effects of those mechanisms on the global mechan-

[1] www.institut-seism.fr/en/projet/sinaps/

ical response of a structure are not well known in particular for massive constructions, for which the high gradients of temperature can initiate cracks within the structure;

(iii) inner and desiccation creeps, which are independent from the hydration, have long-term effects which impact the strain state of the structure;

(iii) chemical and mechanical degradations may occur over the life of the structure, weakening it and changing its mechanical properties.

The seismic hazard itself is also not well understood and modeled. The problem faced here is the following: one has to compute the mechanical response, at time t, of a structure for which the loading conditions are defined over a short time scale, but has to take into account the whole history of the structure (sometimes several decades in the case of massive civil engineering structures). Some models do exist to do so, however their numerical implementation

Figure 1: Example of degradations in a reinforced concrete medium

can often be complex ([Hilaire et al., 2014] provides an extended overview of the state of the art). Yet, this works does *not* intend to provide advances in the modeling of those long-term mechanisms previously exposed, but rather focuses on the numerical strategy to solve such problems. To do so, we propose to consider a reinforced concrete structure *at a given instant* for which some of the mechanical properties face a variability on some of their coefficients such that whichever the degradation mechanisms that may have occurred over the life of the structure, we will only consider their potential effects on (loading or material) parameters solely defined by an interval of variation. The aim here is not to compute the response of the structure over several months, years or decades but to assess the mechanical response of such family of structures under cyclic loading conditions, with the behavior of the material highlighting both strong nonlinearities and variabilities.

Despite the rise of algorithms and technologies for high-performance computing, the resolution of such parametric problems is still an issue as the cost of the computation (both CPU and storage) increases exponentially with the number of parameters in the formulation of the problem (dozens, potentially hundreds of parameters). Among the classes of methods that arose over the last decades to circumvent such issue, we focus here on model-reduction techniques, based on a separated-variable representation of the unknown fields (let say the

displacement field) which show the double advantage of reducing the computation cost of parametric problems and providing a good framework for the storage of the solution (and its post-treatment). Those methods, unlike meta-modeling techniques, do not intend to simplify the model itself but rather to provide a framework for approximating the solution of the mechanical problem associated with a rather complex physical model. The choice of such techniques is especially motivated by the fact that the number of uncertain parameters, as well as their intervals of variation, can be very large, which might make probabilistic approaches too computationally expensive to carry out.

Model-order reduction methods usually rely on a two phase approach (summarized on Fig. 2): the first step consists in building the reduced-order model, seen in our case as a database of solutions (which will also be referred to as "virtual charts" of solutions, an analogy to the engineering charts used in the past), which can be expensive when dealing with nonlinear parametric problems but which encompasses all the different possible occurrences, whereas the second step consists in particularizing the solution for a given purpose, a strategy which makes conceivable the possibility of obtaining rapidly (in real time) the mechanical response of the system. Among those techniques, the proper orthogonal decomposition (POD) method [Kosambi, 1943, Chatterjee, 2000], the reduced-basis (RB) method [Maday and Ronquist, 2004, Patera and Rozza, 2007] and the proper generalized decomposition (PGD) method [Ladevèze, 1999, Chinesta et al., 2010, Nouy, 2010] have been quite extensively used over the last decade in numerous areas such as fluid dynamics, study of composite structures, real-time surgery, ..., with a recent emphasis on verification and validation aspects [Patera and Rozza, 2007, Ammar et al., 2010a, Bouclier et al., 2013]. The two first approaches rely on a learning phase, for which the solution of the problem is partially computed for given instants or values of parameters (snapshots) in order to extract the reduced-order basis which can be used online to find the approximation of another similar problem. The RB method goes a step further as it provides a way to choose the best snapshots to accurately cover the dynamics of the solution to approximate. On the other hand, proper generalized decomposition techniques do not rely on such learning stage as they directly build a separated-variable approximation of the solution fields using a greedy algorithm, without any prior information on this solution.

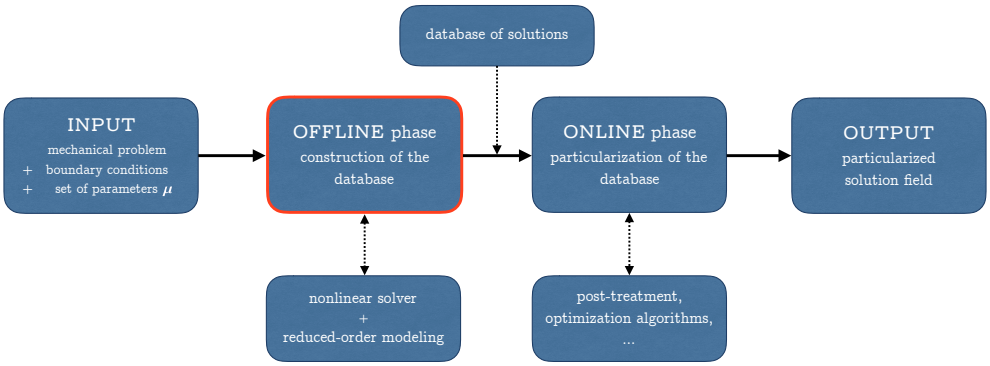

Figure 2: Offline/online approach in reduced-order modeling

However, such approaches used alone are not well-suited for solving nonlinear problems as the ones encountered in civil engineering calculations. Linearization strategies, such as Newton-Raphson techniques [Nocedal and Wright, 1999], the asymptotic numerical method [Cochelin et al., 1994] or the LATIN method [Ladevèze, 1999] can be used to solve this issue. Newton methods (Newton-Raphson, quasi-Newton, ...) are probably the most commonly used, especially with POD and RB methods during the learning phase of the process. They are usually quite efficient when the number of parameters stays low, as they requires to enrich the reduced-order model at each iteration (increment) of the process, which can become expensive. Their coupling with POD is illustrated in [Kerfriden et al., 2011] and with RB in [Jung et al., 2009]. For PGD, see [Ammar et al., 2010b]. Asymptotic numerical method, coupled with POD, was introduced to tackle hyper-elasticity problems [Niroomandi et al., 2010], or with PGD in [Chinesta et al., 2013] for heat transfer problems. It relies on an asymptotic expansion of the variables of interest, but its main drawback it that it requires a high-order interpolation of the nonlinear term to obtain accurate results. This approach can however be interesting as it enables to take into account the bifurcation phenomena [Beringhier et al., 2016]. Finally, the LATIN method relies on a simple but powerful concept: a separation of the linear/nonlinear problems and an alternative resolution of the two subproblems. This approach, coupled with PGD (let us recall that PGD –denominated "radial approximation" at the time– was at first a tool of the LATIN algorithm [Ladevèze, 1985]), is very attractive as it iteratively provides an approximation of the solution field under a separated representation, which can be enriched until reaching a given quality criterion. It has been extensively used in the last couple of decades in numerous research fields, such as the study of multi-scale [Ladevèze and Nouy, 2003] or multi-physics [Dureisseix et al., 2003] problems for example.

Considering the parametric aspect of the equations, two approaches must be mentioned in particular: (i) Newton-Raphson–RB methods have shown to be very efficient [Drohmann et al., 2012], especially thanks to the way the parametric domain is covered to select the most interesting parameter sets (most energetic solutions) in order to build the approximation; (ii) the LATIN–PGD association is fairly natural in this context and provides a great framework for parametric studies, based for example on successive enrichments of solutions (multi-parametric strategy [Boucard and Ladevèze, 1999, Allix and Vidal, 2002]).

This LATIN–PGD approach is at the core of the developments presented in this work, as it enables to tackle the two problems at stake in our study: on the one hand, damage mechanisms are often modeled by strongly nonlinear equations, whereas on the other hand some equations of the mechanical model depend on parameters which may have an important variability. This present work is, in a sense, in the continuity of the ones of [Heyberger et al., 2013] and [Relun et al., 2013] which intended, for example, to take into account the variability on material parameters to compute the failure probability of an mechanical component, using the multi-parametric strategy and a wise sampling of the parametric space. In both cases, those approaches may show some limits when too many parameters are considered, as the parametric space becomes very rich and the solutions associated with different sets of parameters may not be close enough one another, which is the main assumption of this method. It also follows some older work from [Allix et al., 1989] for which the LATIN–PGD

algorithm has been used for damage mechanics problems (for composite structures) with a time-space variable separation.

The strategy chosen here to take the parametric dependency into account in the LATIN–PGD framework is however different and two contributions are presented in this work. The first one is a new extension of the classical LATIN–PGD algorithm to parametric studies for which, unlike the multi-parametric strategy, the parameters are considered as extra-variables for the PGD decomposition. This enables to work on larger parametric spaces, as the basis is iteratively enriched to take into account all the different occurrences (sometimes even non-physical/irrelevant ones). The feasibility of this extension was shown in [Vitse et al., 2014] on a simple 1-D heat evolution problem, with a variability on the thermal conductivity. This present work provides a more general framework for the resolution of nonlinear parametric problems, and the numerical implementation of the 3-D model led to the development of a new tool for computational mechanics at LMT (ROMlab). The second novelty is the application of such strategy to reinforced concrete structures, with an isotropic damage model and unilateral effect. Particular importance is given to first introducing the different notions in a continuous manner to present the main concepts, and in a discrete framework in order to highlight the numerical aspects and problems that were encountered.

It must be pointed out that several works used different approaches for the simulation of damage mechanics in a reduced-order modeling framework: [Ryckelynck et al., 2011] with Newton-Raphson–POD, [Metoui et al., 2014] with PGD for the delamination in cohesive zones and [El Halabi et al., 2016] with a Newton-Raphson–PGD approach. [Kerfriden et al., 2012] also proposed a local/global approach for the simulation of quasi-brittle fracture using a POD local enrichment.

Regarding the objectives of the *SINAPS@* project, this work does *not* intend to provide criteria related regarding the mechanical strength of civil engineering structures under cyclic loading conditions. Our objective is to provide a tool to accurately and quickly compute databases of solutions (first step of the model reduction strategy) which take into account all the different sets of parameters, that can be afterwards used by engineers for design purposes for example.

This manuscript is divided into four chapters.

- In Chap. 1 the models of the concrete and reinforcement media are recalled, based on the work of [Richard and Ragueneau, 2012] and [Vassaux et al., 2015]. The damage behavior and the unilateral effect equations are presented, with an emphasis on the different material parameters studied and the influence of their variability on the mechanical response of a 0-D structure.

- Chap. 2 details the state of the art of nonlinear model-order reduction and the recent extensions to parametric studies. It first presents different ways to obtain a separated-variable decomposition for evolution problems, based on the use of POD, RB and PGD methods. The extension to parametric problems is then presented with methods either based on the enrichment of an already computed basis or considering the new parameters as extra-coordinates of the decomposition. Different variations of the algorithm

for generating PGD modes are proposed. Finally, different couplings with linearization methods for solving non-linear evolution problems are recalled and a focus on the LATIN–PGD algorithm is made.

- In CHAP. 3, a reinforced concrete medium is considered. The different ingredients of the LATIN–PGD algorithm are detailed, with a continuous then a discrete point of view. The extension to a full parametric decomposition of the LATIN linear stage is detailed and the main differences with the classical time-space decomposition are highlighted. This study lead to the development of a 3-D finite element-based tool, ROMlab, coupling LATIN and PGD algorithms for multi-materials structures, with variabilities on material and loading parameters. Some elements of the numerical implementation are given.

- CHAP. 4 gives numerical results, post-treated from databases generated with ROMlab: first a tensile test is simulated to ensure that the algorithms provides a good approximation of the model. A parametric dependency is set on the loading condition, and this test shows that the local and global behaviors are recovered with a few iterations. Then the algorithm is used to compute the response of a reinforced concrete beam during a 4-points bending test, with this time a variability on both the amplitude of the loading and the mean value of the Young modulus of the concrete medium. Simulations on the full beam shows that the damage patterns are globally recovered within a few iterations. Those results are obtained by particularizing the computed databases for different sets of parameters. Finally, the numerical study is validated with the simulation of the response of a T-shaped concrete beam subjected to complex loading conditions (see a picture of the experiment on FIG. 3) and our numerical results are compared to Cast3M simulations from [Iskef, 2016], which intended to study the behavior of beam-column assemblies (*SMART testing* project at LMT).

Figure 3: *SMART testing* project experiment

Chapter 1

Concrete: a widely used complex medium

Preamble We must point that no work has been done during this thesis on the modeling of the behavior of the concrete medium. The purpose of this chapter is only to recall the main aspects of the model implemented in the algorithm developed during the thesis, and highlight its main characteristics.

We study herein a reinforced concrete medium. In the following sections, $\square^c$ (respectively $\square^r$) will refer to mechanical quantities relative to the concrete medium (respectively the reinforcement). The concrete model considered in this thesis derives from [Richard and Ragueneau, 2012, Vassaux et al., 2015], with the difference that the plasticity in compression and the hysteresis effects are neglected in order to simplify the model (but could be relatively easily taken into account for industrial applications). Concrete is modeled under a continuum damage mechanics theory, where a unique damage variable associated with an isotropic hardening is assumed in tension. Under this assumption, the crack openings are not directly computed but may be obtained by a post-treatment of the damage field. A summary of the different mechanisms that are taken into account in this work is presented in Tab. 1.1. To improve the reader's comprehension, the main elements of the damage model are recalled in Sec. 1.1. The unilateral effect is also taken into account and is described in Sec. 1.2. A summary of the state and internal variables and thermodynamic forces for the concrete medium is given in Tab. 1.2. Reinforcements are elastic steel bars and the interface between the concrete and the bars is chosen to remain perfect (see Sec. 2). The variability aspects of the concrete medium are detailed in Sec. 5 and numerical examples highlighting their influence on the mechanical response of a 0-D structure (Gauss point) are given in Sec. 6.

1 The concrete medium

A decomposition of the stress tensor within the representative volume element (RVE) is assumed [Sellier et al., 2013]. The total stress $\boldsymbol{\sigma}^c$ is split into two independent parts:

$$\boldsymbol{\sigma}^c = \boldsymbol{\sigma}^{c,m} + \boldsymbol{\sigma}^{c,f} \tag{1.1}$$

Table 1.1: Summary of the mechanisms studied

Mechanisms	
Asymmetry between tension and compression	✓
Stiffness degradation in tension	✓
Quasi-brittle behavior in tension	✓
Hardening / softening behavior in compression	×
Permanent strain in tension	✓
and in compression	×
Unilateral effect	✓
Hysteretic phenomena	×

where $\boldsymbol{\sigma}^{c,m}$ is the stress in the cracked continuum medium (neglecting the interactions between the cracks) and $\boldsymbol{\sigma}^{c,f}$ is the stress in the cracks when closed. The total free energy of the specimen writes:

$$\Psi = \Psi^m + \Psi^f \tag{1.2}$$

where Ψ^m and Ψ^f are the Helmholtz free energies respectively associated with the two aforementioned stress tensors. The formulation of those two energies is detailed in the next sections.

1.1 Modeling of the cracked behavior

Fracture processes are modeled using the continuum damage theory. The experimental response for a uni-axial tension test [Terrien, 1980] is given on Fig. 1.1 and highlights the classical softening behavior of quasi-brittle materials. To model so, an isotropic damage model is formulated, implying a unique scalar damage variable d^c. The free Helmholtz energy associated with the cracked continuum medium then writes:

$$\Psi^m = \frac{1}{2}(1 - d^c)\,\boldsymbol{\varepsilon}^c : \boldsymbol{C}^c : \boldsymbol{\varepsilon}^c + \Psi^{m,d}(z^c) \tag{1.3}$$

where d^c is the isotropic damage variable; $\boldsymbol{\varepsilon}^c$ is the second-order total strain tensor; $\boldsymbol{C}^c$ is the fourth-order Hooke tensor; z^c is the isotropic hardening variable; $\Psi^{m,d}$ represents the energy locked through the damage process and can be seen as a consolidation function which drives the post-peak behavior in tension. This function is associated with the isotropic hardening related to damage.

From the Clausius-Duhem inequality, the state equations are obtained by differentiating the state potential with respect to the state variables. The Cauchy stress tensor writes:

$$\boldsymbol{\sigma}^{c,m} = \frac{\partial\, \Psi^m}{\partial\, \boldsymbol{\varepsilon}^c} = (1 - d^c)\,\boldsymbol{C}^c : \boldsymbol{\varepsilon}^c \tag{1.4}$$

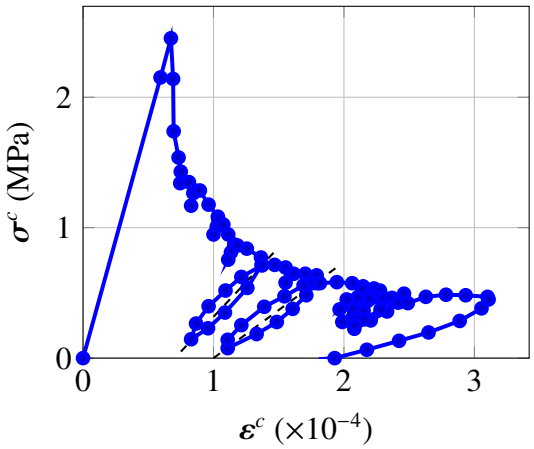

Figure 1.1: Uniaxial tension test – stress/strain relation [Terrien, 1980]

and the energy rate released by the damage mechanism Y^c is expressed by:

$$Y^c = -\frac{\partial \Psi^m}{\partial d^c} = \frac{1}{2}\,\boldsymbol{\varepsilon}^c : \boldsymbol{C}^c : \boldsymbol{\varepsilon}^c \tag{1.5}$$

Finally, the thermodynamic force Z^c associated with the isotropic hardening z^c writes:

$$Z^c = \frac{\partial \Psi^m}{\partial z^c} = \frac{\mathrm{d}\,\Psi^{m,d}(z^c)}{\mathrm{d}\,z^c} \tag{1.6}$$

The non-associated pseudo-potential of dissipation φ^m is based on a Mazars-like failure criterion [Mazars, 1984], expressed in terms of energy variables:

$$\varphi^m(\overline{Y}^c, Z^c\,;\, Y_0) = \overline{Y}^c - (Y_0 + Z^c) \tag{1.7}$$

where: (i) Z^c is the thermodynamic force associated with z^c; (ii) $\overline{Y}^c$ is the energy released rate, with:

$$\overline{Y}^c(\boldsymbol{\varepsilon}^c\,;\, E^c) = \frac{1}{2}\,\langle \boldsymbol{\varepsilon}^c \rangle_+ : \boldsymbol{C}^c : \langle \boldsymbol{\varepsilon}^c \rangle_+ \tag{1.8}$$

where the Macaulay brackets $\langle \square \rangle_+$ denote the positive part of $\square$ such that:

$$\langle \boldsymbol{X} \rangle_+ = \sum_{i=1}^{3} \langle X_i \rangle\; \boldsymbol{n}_i \otimes \boldsymbol{n}_i \tag{1.9}$$

with $\langle X_i \rangle_+$ the positive part of the i^{th} eigenvalue of matrix $\boldsymbol{X}$ ($\langle X_i \rangle_+ = \frac{1}{2}(X_i + \mathrm{abs}(X_i))$) associated with the eigenvector $\boldsymbol{n}_i$. One may notice that, the damage state being linked with positive extensions, $\overline{Y}^c$ will be used instead of Y^c as the latter is not an increasing function of the total strain. An associated flow is assumed and the flow rules can be written considering

the normality rules:

$$\dot{d}^c = \dot{\lambda}_d \frac{\partial \varphi^m}{\partial \overline{Y}^c} = \dot{\lambda}_d \tag{1.10}$$

$$\dot{z}^c = \dot{\lambda}_d \frac{\partial \varphi^m}{\partial Z^c} = -\dot{\lambda}_d \tag{1.11}$$

where $\dot{\lambda}_d$ is the Lagrange multiplier determined from the loading / unloading conditions and can be computed explicitly using the consistency condition $\varphi^m = \dot{\varphi}^m = 0$, provided that the consolidation function $H(z^c)$ is known (assuming the arbitrary choice $\Psi^{m,d}(z^c) = H(z^c)$, such that $Z^c = \frac{\mathrm{d}\, H(z^c)}{\mathrm{d}\, z^c}$). The following choice for the consolidation function is made:

$$H(z^c) = \frac{1}{A_d}\left[-z^c + \ln(1 + z^c)\right] \tag{1.12}$$

with A_d a material parameter which drives the brittleness of the softening part of the stress / strain relation [Richard et al., 2010]. The expression of damage (only satisfied during loading) can be obtained analytically and is written as follows:

$$d^c(\overline{Y}^c\,;\, A_d, Y_0) = 1 - \frac{1}{1 + A_d(\overline{Y}^c - Y_0)} \tag{1.13}$$

and the isotropic hardening variable z^c states:

$$z^c = -d^c \tag{1.14}$$

where A_d and Y_0 are parameters of the study. For the sake of simplicity and for the reasons exposed above $\overline{Y}^c$ will be written Y^c in the rest of this manuscript.

1.2 Modeling of the cracked closure phenomenon (unilateral effect)

Concrete, during cyclic loadings, undergoes tension and compression phases which activate alternatively cracks in the direction of the loading as well as in the transverse directions, as shown on Fig. 1.2. Even though the concrete medium is permanently damaged during tension, it appears to behave in compression independently from its history in tension. This mechanism is called the unilateral effect [Mazars et al., 1990]. This section deals with the modeling of the constitutive laws related to the cyclic effects.

Whereas classical theories separate the tension to the compression (where the damage is assumed to have a null value), [Vassaux et al., 2015] uses only one damage variable and shows two aspects at stakes here:

(i) a nonlinear elastic modeling reproduces the progressive crack closure and regain of stiffness induced by the initiated contacts within the cracks when unloading a damaged sample in tension;

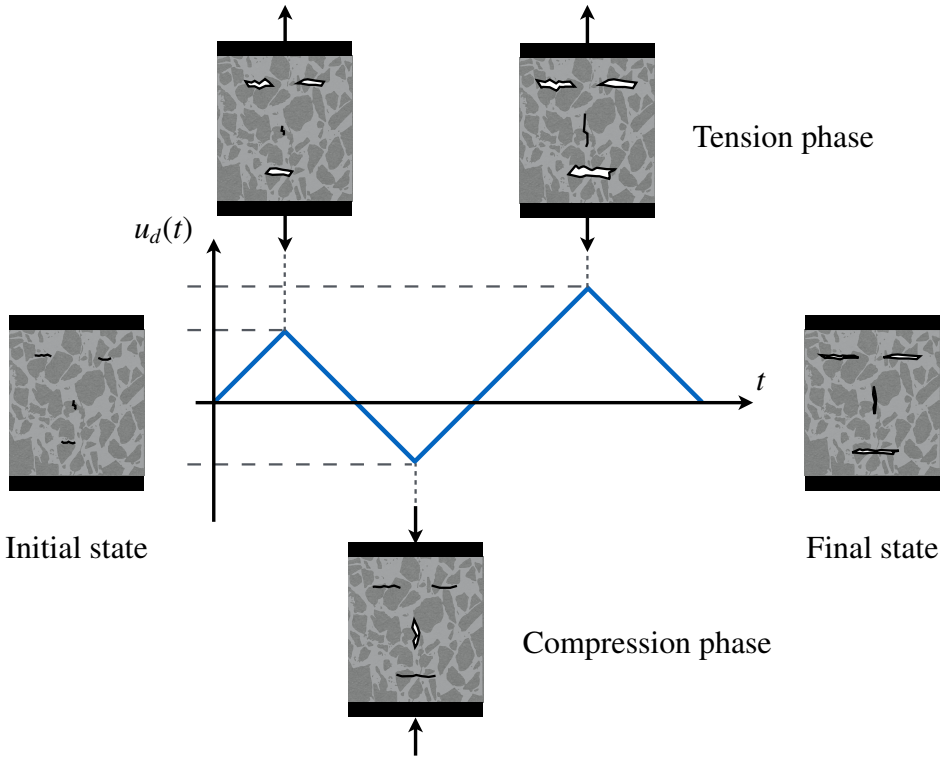

Figure 1.2: Schematic representation of the behavior of a concrete medium under a uni-axial cyclic prescribed displacement

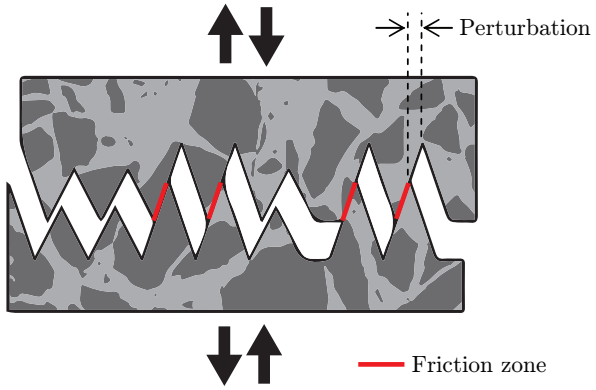

Figure 1.3: Crack under cyclic loading [Mihai and Jefferson, 2011] (courtesy of M. Vassaux)

(ii) a dissipation mechanism (plasticity) can be introduced to reproduce the friction initiated at the surface of the closing cracks and which is associated with hysteresis effects, as shown in Fig. 1.3. However, this phenomenon will not be taken into account in our study.

The mechanical behavior of the cracks is described by a stress tensor $\boldsymbol{\sigma}^{c,f}$, which is a non-linear function of the strain tensor $\boldsymbol{\varepsilon}^{c,f} = d^c\,\boldsymbol{\varepsilon}^c$ (note that this relation remains elastic). $\boldsymbol{\varepsilon}^{c,f}$

can be considered as the homogenized contribution of crack opening to the total strain of the representative elementary volume [Matallah et al., 2010]. The following assumption is made:

$$\dot{\boldsymbol{\sigma}}^{c,f}(\boldsymbol{\varepsilon}^{c,f}\,;\,E^c) = \nu(\boldsymbol{\varepsilon}^{c,f})\,\boldsymbol{C}^c : \dot{\boldsymbol{\varepsilon}}^{c,f} \tag{1.15}$$

where the function ν is chosen to be scalar, meaning that the tangent modulus is proportional to the undamaged Hooke elastic tensor. It represents the part of the stiffness lost during tension which is recovered during compression and $0 < \nu < 1$. As ν evolves with the loading state, it is considered dependent on $\boldsymbol{\varepsilon}^{c,f}$. The free energy Ψ^f then writes:

$$\Psi^f = \int_0^T \left[\int_0^T \nu(\boldsymbol{\varepsilon}^{c,f})\,\boldsymbol{C}^c : \frac{\mathrm{d}\boldsymbol{\varepsilon}^{c,f}}{\mathrm{d}t}\,\mathrm{d}t \right] \frac{\mathrm{d}\boldsymbol{\varepsilon}^{c,f}}{\mathrm{d}t}\,\mathrm{d}t \tag{1.16}$$

with $\mathbf{I}_1$ the trace operator and the function ν is defined in [Vassaux et al., 2015] as:

$$\nu = 1 - \frac{1}{1 + \exp\left[-\dfrac{\alpha_0}{\mathbf{I}_1(\boldsymbol{\varepsilon}^f_{\max})} \mathbf{I}_1(\boldsymbol{\varepsilon}^{c,f}) \right]} \tag{1.17}$$

where: (i) $\boldsymbol{\varepsilon}^f_{\max}$ is the maximum of crack strain that affects the evolution of the proportion of closed cracks; (ii) α_0 is a parameter controlling the variance of the event "a crack closes". ν is a sigmoid function, thus integrable and the continuity of the total free energy is ensured. $\boldsymbol{\sigma}^{c,f}$ can then be computed by integrating Eq. (1.15).

Table 1.2: Summary of the model variables for the concrete medium

Mechanism	State variable	Internal variable	Thermodynamic force
Total strain	$\boldsymbol{\varepsilon}^c$		$\boldsymbol{\sigma}^c$
Elasticity		$\boldsymbol{\varepsilon}^{c,e}$	$\boldsymbol{\sigma}^{c,m}$
Isotropic damage		d^c	$-Y^c$
Isotropic hardening related to damage		z^c	Z^c
Crack closure		$\boldsymbol{\varepsilon}^{c,f}$	$\boldsymbol{\sigma}^{c,f}$

2 The reinforcement

2.1 Modeling of the behavior of the reinforcement

The goal of our study is primarily to focus on the degradation of the concrete medium. As a consequence, an elastic behavior of the steel reinforcement is considered:

$$\boldsymbol{\sigma}^r = \boldsymbol{C}^r : \boldsymbol{\varepsilon}^r \tag{1.18}$$

$$d^r = 0 \tag{1.19}$$

2.2 Interface between the concrete and the reinforcement

Degradation mechanism (corrosion of the interface for example [Richard et al., 2010]) and sliding may appear at the interface between concrete and steel. We will however consider this interface to be perfect for the rest of the study and consider the following kinematic relation between the nodes of the (c, r) interface:

$$[\![\boldsymbol{u}]\!]_{(c,r)} = \boldsymbol{u}^c_{(c,r)} - \boldsymbol{u}^r_{(c,r)} = \boldsymbol{0} \tag{1.20}$$

3 Summary of the constitutive relations

State laws

$$\begin{aligned}
\boldsymbol{\sigma}^{c,m} &= (1 - d^c)\, \boldsymbol{C}^c : \boldsymbol{\varepsilon}^c \\
\dot{\boldsymbol{\sigma}}^{c,f} &= \nu\, \boldsymbol{C}^c : \dot{\boldsymbol{\varepsilon}}^{c,f} \\
Y^c &= \frac{1}{2} \langle \boldsymbol{\varepsilon}^c \rangle_+ : \boldsymbol{C}^c : \langle \boldsymbol{\varepsilon}^c \rangle_+ \\
Z^c &= \frac{\mathrm{d}\, H(z^c)}{\mathrm{d}\, z^c} \\
\boldsymbol{\sigma}^r &= \boldsymbol{C}^r : \boldsymbol{\varepsilon}^r
\end{aligned} \tag{1.21}$$

Evolution equations

$$\begin{aligned}
d^c &= 1 - \frac{1}{1 + A_d(Y^c - Y_0)} \\
z^c &= \frac{1}{1 + A_d(Y^c - Y_0)} - 1 \\
\boldsymbol{\varepsilon}^{c,f} &= d^c\, \boldsymbol{\varepsilon}^c \\
d^r &= 0
\end{aligned} \tag{1.22}$$

4 Regularization of the problem

The loss of ellipticity of problems involving softening behaviors is a recurrent problem when simulating reinforced concrete structures [Hill, 1958], leading to a localization of the deformations. To solve this problem, a regularization of the equations must be done. A short overview of the existing methods to do so is given in App. A. For our study, the damage variable d^c is regularized using a viscosity law [Ladevèze, 1991, Dubé et al., 1996, Allix and Deü, 1997, Allix, 2012, Allix et al., 2003]:

$$\dot{d}^c = \frac{1}{\tau_c} \left[1 - \exp(-a \langle d^c_s(Y^c) - d^c \rangle_+)\right] \tag{1.23}$$

where d^c_s is the non-regularized damage variable, d^c is the regularized one, τ_c is called the characteristic time and a is a parameter usually equal to 1.

5 Uncertainties and parametric dependency

The study of reinforced concrete leads engineers to face difficulties related to the variability on some constitutive parameters of the medium. This variability comes from different sources: the manufacturing itself, for example for massive structures made from several batches of concrete; its design, involving geometrical parameters; the loading conditions (either coming from the loading itself or from the boundary conditions); the aging of a structure, which may also induce a variability on some parameters of the constitutive laws as a result of delayed phenomena as presented in the introduction of this manuscript. Those uncertainties have a direct influence on the mechanical behavior of the structure. Usual techniques to assess this influence rely on probabilistic tools (Monte Carlo simulations for example) or statistical data (from extensive experimentation campaigns). For example, [Choi and Kwon, 2000] provide numerical values of the coefficient of variation (the ratio between the standard deviation of a given value and its mean value, also referred to as relative standard deviation) of the Young modulus around (0.10–0.15) and (0.20–0.30) for the tensile strength, for which a normal distribution is assumed, based on Monte Carlo simulations in order to assess the variability in deflections of reinforced concrete beams. However, the cost associated with this techniques is high, due to the numerous experiments or numerical simulations to be performed.

The approach chosen in our study to model those uncertainties is to set a variability on N^p parameters $\boldsymbol{\mu} = \{\mu_i\}_{i=1\cdots N^p}$ of the mechanical formulation, for which a uniform distribution is considered. The main difference with the usual techniques will rely on the numerical tools used to simulate the response of structures associated with those parameters, which will be the point of the next chapters. Two types of parameters are studied here: material (Young modulus for example) or boundary condition parameters (amplitude of the loading, frequency, ...) and for which the intervals of variation are known. For example, $\boldsymbol{\mu} = \{\mu_1, \mu_2\}$ where μ_1 affects the brittleness coefficient $A_d = A_d(\mu_1)$ and μ_2 affects the Young modulus such that $E^c = E^c(\mu_2)$.

Note that: (i) geometrical parameters are *not* taken into account; (ii) only material parameters of the concrete model are considered, even if the reinforcement may also face high material variabilities.

6 0-D results

This section provides some numerical examples computed with M. Vassaux's (slightly modified Matlab) code in order to show the influence of the variability on some parameters on the mechanical behavior at the scale of a Gauss point. The material can be considered as a homogenized concrete medium. First, the mechanical response (without variability) is computed in order to illustrate the different aspects of the model mentioned in the previous sections. Then, a variability is set on some material parameters (see Tab. 1.3) and the mechanical behavior is computed for several values of those parameters.

Table 1.3: Studied parameters, variability

Parameter	Name	Mean value	Variability	Bounds of variation
E^c	Young modulus	36×10^9 Pa	$+/-30\%$	$[25.2 - 46.8] \times 10^9$
A_d	Brittleness coefficient	8×10^{-3} J^{-1}.m^3	$+/-20\%$	$[6.4 - 9.6] \times 10^{-3}$
Y_0	Initial threshold for damage activation	180 J.m^{-3}	$+/-20\%$	$[144 - 216]$

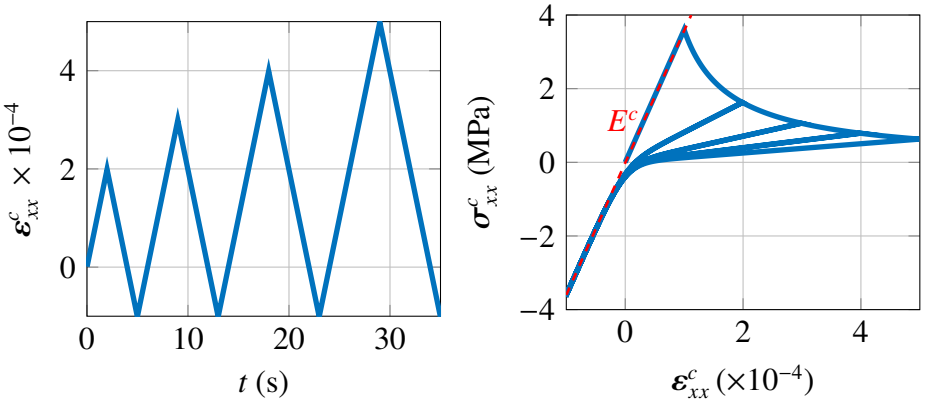

(a) (b)

Figure 1.4: Prescribed strain (Fig. 1.4a) and according mechanical response $\boldsymbol{\sigma}^c_{xx} = f(\boldsymbol{\varepsilon}^c_{xx})$ at a Gauss point (Fig. 1.4b)

6.1 Mechanical response to uni-axial cyclic loading

Fig. 1.4b shows the behavior $\boldsymbol{\sigma}^c_{xx} = f(\boldsymbol{\varepsilon}^c_{xx})$ for a cyclic uni-axial loading (4 cycles) for which the amplitude of the tension part of the loading increases with the time, as shown on Fig. 1.4a. This figure illustrates the evolution of both the damage mechanism and the unilateral effect over the different cycles. The quasi-brittle aspect of the response is observed and the damage state increases over the different cycles along with the amplitude of the loading. The undamaged elasticity modulus (linear part of the curve) is also progressively (and completely) recovered during the unloading (and compression) phase, inducing permanent strains in tension.

6.2 Influence of the variabilities on the mechanical response of the structure

A variability is set on the Young modulus E^c, the energy threshold Y_0 and the brittleness coefficient A_d. Their mean value, variability and according intervals of variation are summed up in Tab. 1.3. The goal of this section is to highlight the influence of those parameters on the mechanical response of a structure.

Variability on the Young modulus. FIG. 1.5a shows the influence of a $+/-30\%$ variability on the Young modulus E^c on the mechanical response of the medium, which directly intervenes in the behavior equation (1.4) and in the formulation of the unilateral effect (1.15). It is noticeable that after a few cycles the behavior reaches the same damaged state, showing that this parameter has a strong influence on the first few cycles.

Variability on the energy. FIG. 1.5b shows the influence of a $+/-20\%$ variability on the initial threshold for damage activation Y_0 (which is linked to the maximum strength in tension for the concrete medium $f_t^c = 3.6 \times 10^6$ Pa) on the mechanical behavior of the medium. Note that uncertainties on this parameter may accelerate or delay (in terms of stress reached) the activation of damage, and as a consequence have an important role on the integrity of a structure.

Variability on the post-peak coefficient. FIG. 1.5c shows the influence of a $+/-20\%$ variability on the brittleness coefficient A_d, which drives the post-peak behavior (see EQ. 1.13), on the mechanical response of the medium. As a consequence, this parameter has a strong influence on the fracture energy, which is proportional to the area under the $\boldsymbol{\sigma}_{xx} = f(\boldsymbol{\varepsilon}_{xx})$ curve. Numerically, this property is used in the energy regularization as the post-peak coefficient is locally adjusted in order to keep a consistent energy whichever the mesh discretization (see APP. A).

7 To put it in a nutshell ...

The material behavior of the reinforced concrete medium was presented, with a unique damage variable activated in tension and a unilateral effect representing the cracks closure in compression. The influence of the variability on some material parameters on the 0-D mechanical response of the medium has been studied. Such modeling highlights two difficulties that have to be taken into account for the simulation of engineering structures: (i) the strong nonlinearity of the behavior equations of the concrete medium; (ii) the material variability in such problems which has a strong influence on the global mechanical response of the structure. The simple 0-D examples highlight the importance of taking into account those uncertainties, as the local behavior is strongly influenced by those parameters (and we will see in a further chapter that the same observation applies to the macroscopic response of 3-D structures). Probabilistic or stochastic approaches are usually used to take into account this second issue. Monte-Carlo methods however require numerous numerical simulations, which can be costly depending on the complexity of the model. Perturbation methods, such as developments in Taylor series, are not suitable for large variations of the parameters. Spectral methods (for example combined with the finite element method [Ghanem and Spanos, 1991]) are interesting but require a high order of decomposition to be precise enough, with once again a high computational costs. We will present in the next chapter an alternative way to directly take into account material and loading variabilities in the formulation of the mechanical problem using a deterministic approach.

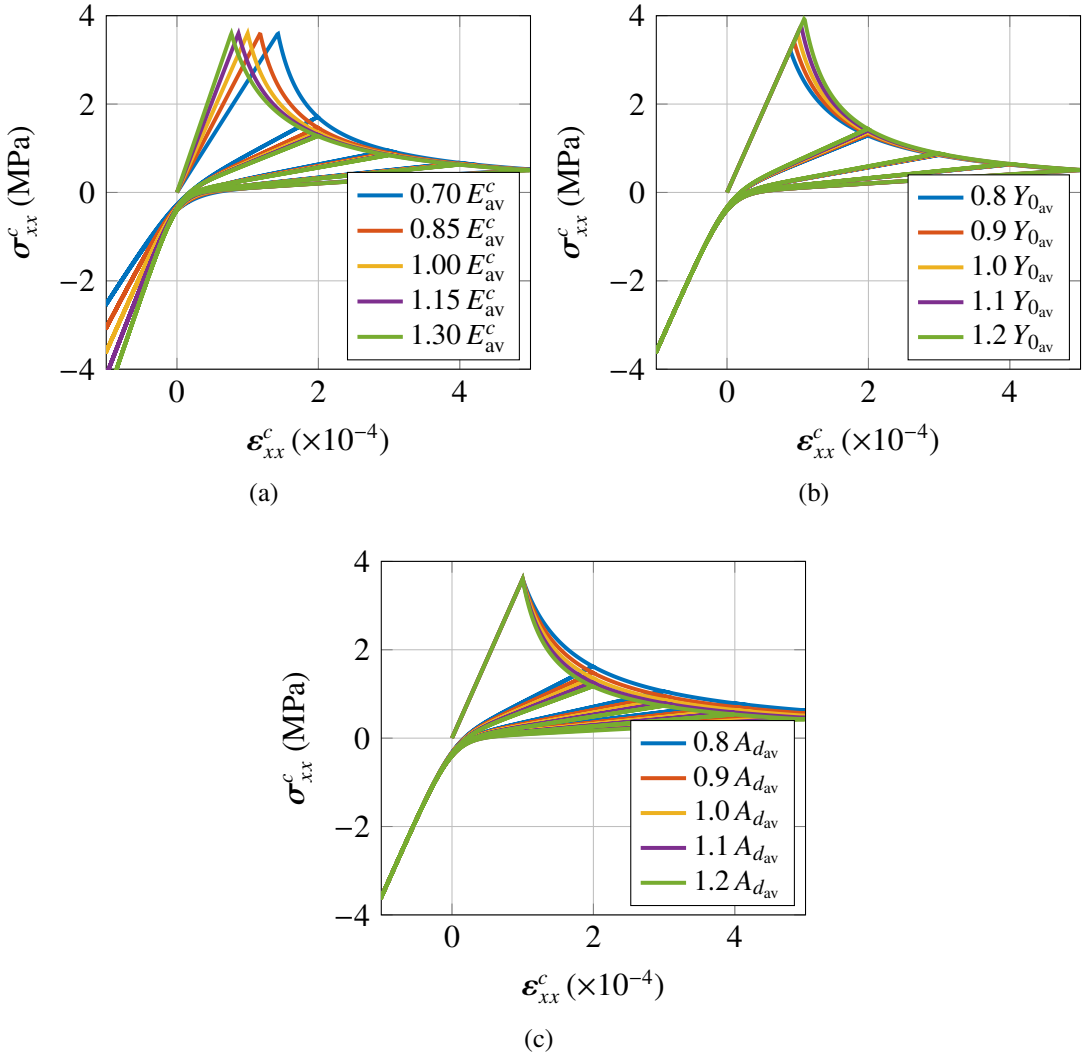

Figure 1.5: Influence of the variability on the Young modulus E^c (Fig. 1.5a), the energy threshold Y_0 (Fig. 1.5b) and the brittleness coefficient A_d (Fig. 1.5c) on the mechanical response at a Gauss point

Chapter 2

Nonlinear parametric model reduction – state of the art

It is obvious that the more parameters are added to the mechanical formulation of an evolution problem, the more complex the computation gets and dedicated numerical strategies need to be implemented to circumvent this issue, especially when facing strong nonlinearities as the ones encountered in damage mechanics. This difficult problem led over the last decades to the developments of different types of model reduction techniques used to reduce the complexity of a given time-dependent partial differential equations problem involving many variables, whether they are material or geometrical parameters. As a matter of fact, classical approaches consisting in using explicit or implicit incremental techniques may require a rather refined time discretization and as a result may be very costly to use when solving parametric problems. An alternative resolution consists in seeking the solution of this problem under a separated-variable representation, as a sum of products of time and space functions:

$$\boldsymbol{u}(\boldsymbol{x},t) \approx \boldsymbol{u}_m(\boldsymbol{x},t) = \sum_{k=1}^{m} a_k(t)\,\boldsymbol{\Phi}_k(\boldsymbol{x}) \tag{2.1}$$

where the set of the coefficients $\{a_k(t)\}_{k=1\cdots m}$ is associated with the rank-m reduced-order basis (ROB) $\{\boldsymbol{\Phi}_k(\boldsymbol{x})\}_{k=1\cdots m}$.

Different methods to construct such approximations are given in Sec. 1 for evolution problems, with an emphasis and on the proper orthogonal decomposition (POD) and the proper generalized decomposition (PGD). The extension to parametric problems is given in Sec. 2, for which the PGD method provides a very convenient framework. The treatment of nonlinear problems in the context of reduced-order modeling is addressed in Sec. 3, where different linearization techniques are recalled and a focus is done on the LATIN method.

For a better understanding of this chapter, the different notations are given:

- intervals of definition:

  - $\boldsymbol{x} \in \boldsymbol{\Omega}$, a non-zero bounded regular domain, with $\boldsymbol{\Omega} \subset \mathbb{R}^d$ $(d = 1, 2, 3)$;
  - $\mathcal{D} = \prod_{i=1}^{N^p} \mathcal{D}_i$ with $\mathcal{D}_i = [\mu_i^{\min}, \mu_i^{\max}]$ (where "$\prod$" is used in the sense of "$\times$") is the space associated with the variable μ_i, with the particular case: $\mathcal{D}_1 \equiv \mathcal{I} = [0, T]$ associated with the time variable $\mu_1 \equiv t$;
  - $\mathcal{P} = \boldsymbol{\Omega} \times \mathcal{D}$;

- vector spaces:

  - $\mathcal{W} \equiv \mathcal{H}^1(\boldsymbol{\Omega}) = \left\{\boldsymbol{u} \in \boldsymbol{L}^2(\boldsymbol{\Omega}), \nabla \boldsymbol{u} \in \boldsymbol{L}^2(\boldsymbol{\Omega})\right\}$, with $\|\square\|_{\mathcal{W}} = \left(\int_{\boldsymbol{\Omega}} \square^2 \, \mathrm{d}\boldsymbol{\Omega}\right)^{1/2}$, $\boldsymbol{L}^2$ norm on $\mathcal{W}$;
  - $\mathcal{U} \equiv \boldsymbol{L}^2(\mathcal{D}, \mathcal{W}) = \left\{\boldsymbol{u} \,:\, \mathcal{D} \to \mathcal{W}, \int_{\mathcal{D}} \|\boldsymbol{u}\|_{\mathcal{W}}^2 \, \mathrm{d}\mu < +\infty\right\}$;
  - $\mathcal{S}_m$, a subspace of $\mathcal{U}$ of the fields that write (2.1) with $\boldsymbol{\Phi} \in \mathcal{W}$ and $a_i \in \mathcal{F}_i$;
  - $\mathcal{F}_i \equiv \boldsymbol{L}^2(\mathcal{D}_i, \mathbb{R})$;
  - $\mathcal{F} = \prod_{i=1}^{N^p} \mathcal{F}_i$;
  - $\mathcal{T}_{\boldsymbol{u}_m}(\mathcal{S}_m)$, the tangent linear space to $\mathcal{S}_m$ at $\boldsymbol{u}_m$;

1 Reduced order modeling for evolution problems

1.1 Data analysis using the proper orthogonal decomposition technique

Let us consider a field $\boldsymbol{u}(\boldsymbol{x}, t) \in \mathcal{U}$ explicitly known. One seek to find the best rank-m approximation $\boldsymbol{u}_m \in \mathcal{S}_m$ of $\boldsymbol{u}(\boldsymbol{x}, t)$ under the form presented in (Eq. 2.1). This can be achieved by solving the following minimization problem:

$$\min_{(a_i, \boldsymbol{\Phi}_i) \in (\mathcal{F} \times \mathcal{W})} \|\boldsymbol{u} - \sum_{i=1}^{m} a_i \, \boldsymbol{\Phi}_i\|_{\mathcal{U}}^2 \tag{2.2}$$

with the constraint of orthogonality of the functions $\{\boldsymbol{\Phi}_i\}_{i=1\cdots m}$: $(\boldsymbol{\Phi}_k, \boldsymbol{\Phi}_l)_{\mathcal{W}} = \delta_{kl}$, which can be rewritten, considering $a_i = (\boldsymbol{u}, \boldsymbol{\Phi}_i)_{\mathcal{W}}$, where $(\cdot, \cdot)_{\mathcal{W}}$:

$$\min_{\substack{\boldsymbol{\Phi}_i \in \mathcal{W} \\ (\boldsymbol{\Phi}_k, \boldsymbol{\Phi}_l)_{\mathcal{W}} = \delta_{kl}}} \|\boldsymbol{u} - \sum_{i=1}^{m} (\boldsymbol{u}, \boldsymbol{\Phi}_i)_{\mathcal{W}} \, \boldsymbol{\Phi}_i\|_{\mathcal{U}}^2 \tag{2.3}$$

which leads to the resolution of an eigenvalue problem.

This decomposition is optimal in the sense that the modes are orthogonal and their norm monotonically decreases with m. Its accuracy depends on the number of modes (i.e. number of products of functions) m. As an example of those properties, Fig. 2.1a shows the incremental (direct) solution $\boldsymbol{u}_{\text{ref}}(\boldsymbol{x}, t)$ of a heat evolution problem on a beam and the truncation error for several number of modes in the decomposition:

$$\text{Err} = \frac{\|\boldsymbol{u}_{\text{ref}} - \boldsymbol{u}_m\|_{\mathcal{W}}}{\|\boldsymbol{u}_{\text{ref}}\|_{\mathcal{W}}} \tag{2.4}$$

with $\|\boldsymbol{u}\|^2_{\mathcal{W}} \equiv \int_{\mathcal{I}} \|\boldsymbol{u}\|^2_{\mathcal{U}} \, \mathrm{d}t$.

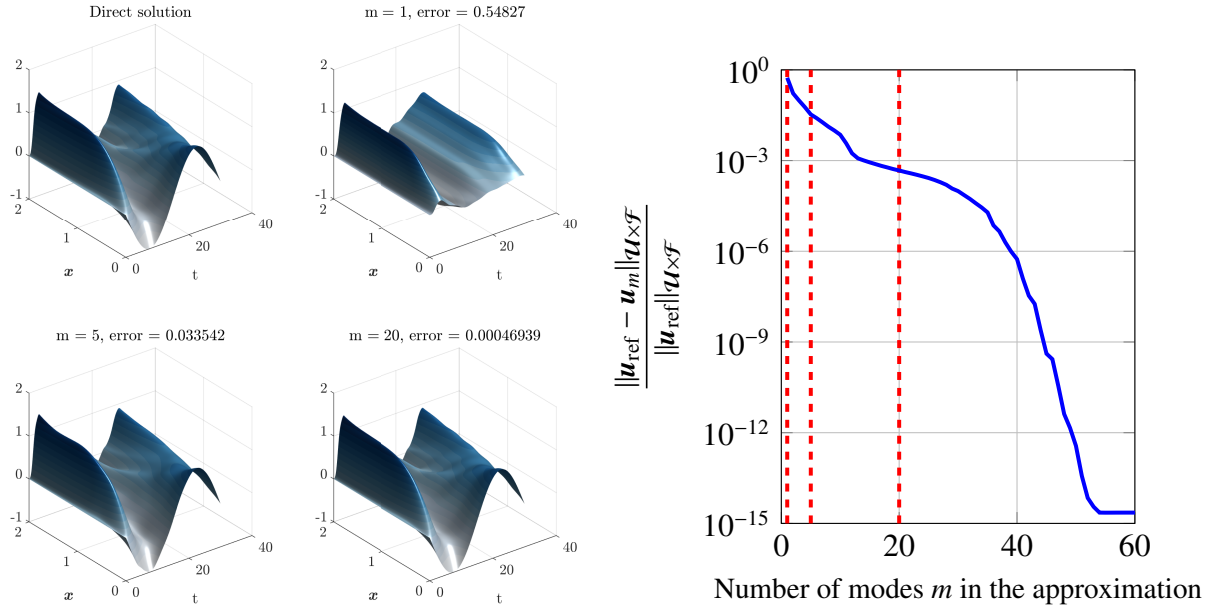

(a) POD of the function $\boldsymbol{u}(\boldsymbol{x}, t)$ for $m = 1$, $m = 5$ and $m = 20$ and the associated truncation error

(b) POD truncation error

Figure 2.1: SVD reconstruction $\boldsymbol{u}_m(\boldsymbol{x}, t)$ for different levels of truncation (Fig. 2.1a) and evolution of the associated truncation error with the number of terms m (Fig. 2.1b)

1.2 Construction of the reduced-order model when u is known implicitly (as the solution of a partial differential equation)

Let consider the following abstract evolution problem: find $\boldsymbol{u}(\boldsymbol{x}, \boldsymbol{\mu} \equiv t) \in \mathcal{U}$ solution of:

$$\mathcal{L}(\boldsymbol{u}; t) = \boldsymbol{f}(t) \tag{2.5}$$

where $\mathcal{L}$ is a linear differential operator. For example, $\mathcal{L} \equiv \mathbf{A}(t)$, symmetric positive definite time-dependent operator or $\mathcal{L} \equiv \frac{\mathrm{d}}{\mathrm{d}t}\mathbf{I} + \mathbf{A}(t)$. Different methods exist to build the rank-m approximation Eq. (2.1) on a subspace $\mathcal{S}_m \subset \mathcal{U}$. Those techniques are detailed in the following sections and their advantages and drawbacks are recalled.

1.2.1 Snapshot-based Galerkin POD

The proper orthogonal decomposition (POD) [Kosambi, 1943, Chatterjee, 2000], also known under similar forms as Karhunen–Loève (KL) decomposition [Karhunen, 1946] or principal component analysis (PCA) (all equivalent in the discrete case [Liang et al., 2002]), enables to approximate the solution of a problem on a given ROB $\{\boldsymbol{\Phi}_k\}_{k=1\cdots m}$ computed thanks to snapshots of solutions of similar problems. Those snapshots can be engendered by experimental data or numerical solutions computed over either a coarse mesh or time discretization,

and must be chosen so that they represent the dynamics of the system. The orthogonal basis $\{\boldsymbol{\Phi}_k\}_{k=1\cdots m}$ can be computed offline by performing a POD of the collection of snapshots and the problem lies in finding, online, the corresponding most adequate set of coefficients $\{a_k\}_{k=1\cdots m}$ to obtain the best approximation of the function $\boldsymbol{u}(\boldsymbol{x}, t)$:

$$a_k = (\boldsymbol{u}, \boldsymbol{\Phi}_k)_{\boldsymbol{\mathcal{W}}} \tag{2.6}$$

To be more precise, let us consider this problem in a discrete framework, for example using finite elements in space (n_x degrees of freedom –DOFs), and a sampling $\mathfrak{I}_p = [\mathrm{t}_1, \cdots, \mathrm{t}_p]$ of the time interval $\mathcal{I}$. The expressions are now given using the discretized fields and operators using non-italic letters. The matrix (database) $\boldsymbol{\Xi} \in \boldsymbol{\mathcal{M}}_{n_x,p}$ is assembled from the snapshots of solutions of the initial problem (2.5) computed from the full-order model for given instants $\{\mathrm{t}_k\}_{k=1\cdots p}$:

$$\boldsymbol{\Xi} = \left(\begin{bmatrix} \\ \mathbf{u}(\mathrm{t}_1) \\ \\ \end{bmatrix} \begin{bmatrix} \\ \mathbf{u}(\mathrm{t}_2) \\ \\ \end{bmatrix} \begin{bmatrix} \\ \mathbf{u}(\mathrm{t}_3) \\ \\ \end{bmatrix} \cdots \begin{bmatrix} \\ \mathbf{u}(\mathrm{t}_p) \\ \\ \end{bmatrix} \right) \tag{2.7}$$

where $\mathbf{u}(\mathrm{t}_j)$ is the computed field $\mathbf{u}$ at instant t_j. Two approaches to compute the ROB $\{\boldsymbol{\Phi}_k\}_{k=1\cdots m}$ can be highlighted:

1. a Karhunen-Loève decomposition [Karhunen, 1946] can be computed from determining the eigenvalues and eigenvectors of the covariance matrix $\mathbf{C} = \boldsymbol{\Xi}\,\boldsymbol{\Xi}^{\mathrm{T}}$:

$$\mathbf{C}\,\boldsymbol{\Phi} = \alpha\,\boldsymbol{\Phi} \tag{2.8}$$

   where $(\alpha, \boldsymbol{\Phi})$ are the eigenvalues and eigenvectors of the $\mathbf{C}$.

   Remark. An alternative approach could consist in sampling the spatial domain and assembling $\boldsymbol{\Xi}$ as a collection of the time functions associated with those sample points. However, the spatial problems is usually much bigger than the time discretization that is why the first approach is mostly used;

2. another approach to obtain the desired decomposition is to perform a singular value decomposition of the matrix $\boldsymbol{\Xi}$, which gives a factorization of the form:

$$\Xi = \mathbf{U}\,\boldsymbol{\Lambda}\,\mathbf{V}^{\mathrm{T}} \tag{2.9}$$

   where $\mathbf{U} \in \boldsymbol{\mathcal{M}}_m(\mathbb{R})$ and $\mathbf{V} \in \boldsymbol{\mathcal{M}}_p(\mathbb{R})$ are orthogonal matrices (see App. B), which can be rewritten:

$$\Xi = \sum_{i=1}^{m} \lambda_i\,\mathbf{U}_i \otimes \mathbf{V}_i^{\star} \tag{2.10}$$

where $\otimes$ represents the outer product of the vectors $\mathbf{U}_i$ and $\mathbf{V}_i^\star$ (first m vectors of $\mathbf{V}$). The analogy with the KL decompositions shows that the singular values λ_i are the square roots of the eigenvalues α_i of the covariance matrix $\mathbf{C}$ and the first m eigenvectors $\{\mathbf{\Phi}_i\}_{i=1\cdots m}$ of $\mathbf{C}$ are the first m columns of $\mathbf{U}$.

The Galerkin-POD method is summed up in Alg. 1. The main advantage of such technique is that if the expected results are similar enough from one computation for a given set of parameters to an other, the ROB $\{\mathbf{\Phi}_k\}_{k=1\cdots m}$ can be re-used and only a new set of coefficients $\{\mathrm{a}_k\}_{k=1\cdots m}$ has to be re-computed. However, the main drawback lies in the choice of the initial sampling of the snapshots and that, hopefully, $p \ll n_t$, which highly depends on the dynamics on the problem.

Algorithm 1: snapshot-based Galerkin POD

Offline stage:

Step 1: the time space $\mathfrak{I}$ is sampled: $\mathrm{t}_i \in [1, p]$;

Step 2: problem (2.5) is solved for each t^i in order to get the solutions $\mathbf{u}^i = \mathbf{u}(\mathbf{x}, \mathrm{t}^i)$;

Step 3: the database $\mathbf{\Xi} = \{\mathbf{u}^i\}_{i=1\cdots p}$ is assembled ;

Step 4: a PCA of $\mathbf{C}$ *or* a SVD of $\mathbf{\Xi}$ gives the reduced basis $\{\mathbf{\Phi}_i\}_{i=1\cdots m}$.

Online stage:

Step 5: Galerkin method on Span$(\{\mathbf{\Phi}_i\}_{i=1\cdots m})$.

1.2.2 Proper generalized decomposition

On the other hand, proper generalized decomposition (PGD) techniques aim at approximating the evolution problem (2.5) by building the ROB $\{\boldsymbol{\Phi}_k\}_{k=1\cdots m}$ and finding its coefficients $\{a_k\}_{k=1\cdots m}$ at the same time during an iterative process, by successively enriching the approximation until a given criterion is reached [Ladevèze, 1999, Nouy, 2010]:

$$\boldsymbol{u}_m(\boldsymbol{x}, t) = \sum_{k=1}^{m} a_k(t)\, \boldsymbol{\Phi}_k(\boldsymbol{x}) \tag{2.11}$$

with $\{(\boldsymbol{\Phi}_k, a_k)\}_{k=1\cdots m} \in [\boldsymbol{\mathcal{U}} \times \boldsymbol{\mathcal{F}}]^m$. We recall in this section two methods for building the approximation: the first one based on a Galerkin orthogonality criterion and the second one based on the minimization of a residual function. Note that this kind of approximation was first introduced in the late 80s as the "radial approximation" in the LATIN algorithm [Ladevèze, 1985].

Algorithm based on the Galerkin orthogonality criterion. We now consider that the problem is semi-discretized in space, with $\boldsymbol{\mathcal{L}} \equiv \mathbf{L}$, symmetric, constant and positive definite matrix and we assume the rank-m approximation of $\mathbf{u}$ is known, such that one seeks the rank-$(m+1)$ approximation as:

$$\mathbf{u}_{m+1} = \mathbf{u}_m + \mathrm{a}_{m+1}\, \mathbf{\Phi}_{m+1} \tag{2.12}$$

with $(\mathbf{\Phi}_{m+1}, \mathrm{a}_{m+1}) \in \mathcal{U} \times \mathcal{F}$. The classical definition of this new approximation consists in writing the orthogonality of the residue $\mathbf{L}(\mathbf{u}_{m+1}) - \mathbf{f}$ with respect to the function $\mathrm{a}^\star\, \mathbf{\Phi}_{m+1} + \mathrm{a}_{m+1}\, \mathbf{\Phi}^\star$ with $(\mathbf{\Phi}^\star, \mathrm{a}^\star) \in \mathcal{U} \times \mathcal{F}$:

$$(\mathbf{L}(\mathrm{a}_{m+1}\, \mathbf{\Phi}_{m+1}), \mathrm{a}^\star\, \mathbf{\Phi}_{m+1} + \mathrm{a}_{m+1}\, \mathbf{\Phi}^\star)_{\mathcal{I}} = (\mathbf{f} - \mathbf{u}_m, \mathrm{a}^\star\, \mathbf{\Phi}_{m+1} + \mathrm{a}_{m+1}\, \mathbf{\Phi}^\star)_{\mathcal{I}} \tag{2.13}$$

where $(\mathbf{u}, \mathbf{v})_{\mathcal{I}}$ is defined as:

$$(\mathbf{u}, \mathbf{v})_{\mathcal{I}} \equiv \int_{\mathcal{I}} \mathbf{v}^{\mathrm{T}}\, \mathbf{u}\, \mathrm{d}t \tag{2.14}$$

Such problem can be separated into two coupled equations:

$$(\mathbf{L}\, \mathrm{a}_{m+1}, \mathrm{a}_{m+1})_{\mathcal{I}}\, \mathbf{\Phi}_{m+1} = (\mathbf{f}_{m+1}, \mathrm{a}_{m+1})_{\mathcal{I}} \tag{2.15}$$

$$([\mathbf{\Phi}_{m+1}^{\mathrm{T}}\, \mathbf{L}\, \mathbf{\Phi}_{m+1}]\, \mathrm{a}_{m+1}, \mathrm{a}^\star)_{\mathcal{I}} = (\mathbf{\Phi}_{m+1}^{\mathrm{T}}\, \mathbf{f}_{m+1}, \mathrm{a}^\star)_{\mathcal{I}} \quad \forall \mathrm{a}^\star \in \mathcal{F} \tag{2.16}$$

with $\mathbf{f}_{m+1} = \mathbf{f} - \mathbf{u}_m$.

Algorithm based on the stationarity of the residual function. The second approach consists in finding the new couple of functions $(\boldsymbol{\Phi}_{m+1}, a_{m+1}) \in \boldsymbol{\mathcal{U}} \times \mathcal{F}$ minimizing the residual function:

$$\|\boldsymbol{f} - \boldsymbol{\mathcal{L}}(\boldsymbol{u}_{m+1})\|^2 = \left\|\boldsymbol{f}_{m+1} - \boldsymbol{\mathcal{L}}(a_{m+1}\, \boldsymbol{\Phi}_{m+1})\right\|^2 \tag{2.17}$$

where $\boldsymbol{f}_{m+1} = \boldsymbol{f} - \boldsymbol{u}_m$. Such kind of approximation then depends on the choice of the norm $\|\square\|$. On a discrete framework, if one again we consider $\boldsymbol{\mathcal{L}} \equiv \mathbf{L}$, symmetric, constant and positive definite matrix, the norm $\|\square\|$ is defined such that:

$$\|\boldsymbol{v}\|^2 \equiv \|\mathbf{v}\|^2_{\mathbf{L}^{-1}} = (\mathbf{L}^{-1}\, \mathbf{v}, \mathbf{v})_{\mathcal{I}} \equiv \int_{\mathcal{I}} \mathbf{v}^{\mathrm{T}}\, \mathbf{L}^{-1}\, \mathbf{v}\, \mathrm{d}t \tag{2.18}$$

The stationarity of this residue relative to a_{m+1} and $\mathbf{\Phi}_{m+1}$ writes: find $(\mathbf{\Phi}_{m+1}, \mathrm{a}_{m+1}) \in \mathcal{U} \times \mathcal{F}$ such that:

$$(\mathbf{L}(\mathrm{a}_{m+1}\, \mathbf{\Phi}_{m+1}), \mathrm{a}_{m+1}\, \mathbf{\Phi}^\star)_{\mathcal{I}} = (\mathbf{f}_{m+1}, \mathrm{a}_{m+1}\, \mathbf{\Phi}^\star)_{\mathcal{I}} \quad \forall \mathbf{\Phi}^\star \in \mathcal{U} \tag{2.19}$$

$$(\mathbf{L}(\mathrm{a}_{m+1}\, \mathbf{\Phi}_{m+1}), \mathrm{a}^\star\, \mathbf{\Phi}_{m+1})_{\mathcal{I}} = (\mathbf{f}_{m+1}, \mathrm{a}^\star\, \mathbf{\Phi}_{m+1})_{\mathcal{I}} \quad \forall \mathrm{a}^\star \in \mathcal{F} \tag{2.20}$$

Remark. One can notice that the two formulations are equivalent if $\boldsymbol{\mathcal{L}} \equiv \mathbf{L}$ symmetric, constant and positive definite and the orthogonality is done relative to the functions $\mathrm{a}^\star\, \mathbf{\Phi}_{m+1} + \mathrm{a}_{m+1}\, \mathbf{\Phi}^\star$ in the Galerkin formulation. This equivalence would not exist if $\dot{\mathbf{u}}$ terms appeared in the formulation (in the case of $\boldsymbol{\mathcal{L}} \equiv \frac{\mathrm{d}}{\mathrm{d}t}\mathbf{I} + \mathbf{L}(t)$ for example) [Nouy, 2010].

We know explain how to solve those problems.

Practical resolution. Problems (2.15 – 2.16) and (2.19 – 2.20) can be solve either by using a fixed-point algorithm or by substituting the space Eq. (2.15) (respectively (2.19)) into the time problem (2.16) (respectively (2.20)), which leads to the study of the stationarity of a Rayleigh ratio.

• **Fixed-point algorithm.** Following problem (2.15–2.16), this system of coupled equations can be solved using a fixed-point algorithm as shown on Alg. 2 [Néron and Dureisseix, 2008, Ammar et al., 2012]. A stationarity criterion is used to stop the process. Note that even though the maximum number of iterations to reach this stagnation is usually quite low (3–5), a maximum value of iterations $k_{\max}$ can be enforced to stop the fixed-point algorithm.

Algorithm 2: fixed-point procedure to generate the new functions $(\mathbf{\Phi}_{m+1}, \mathrm{a}_{m+1})$

Data: $\mathrm{a}_{m+1}^{(0)}$;
Result: $(\mathbf{\Phi}_{m+1}, \mathrm{a}_{m+1})$;
while $(\mathrm{a}_{m+1}^{k+1} - \mathrm{a}_{m+1}^{k})_{\mathcal{I}} > \epsilon$ **do**

1. compute $\mathbf{\Phi}_{m+1}^{(k+1)}$ solution of:

$$(\mathbf{L}\,\mathrm{a}_{m+1}^{(k)}, \mathrm{a}_{m+1}^{(k)})_{\mathcal{I}}\,\mathbf{\Phi}_{m+1}^{(k+1)} = (\mathbf{f}_{m+1}, \mathrm{a}_{m+1}^{(k)})_{\mathcal{I}} \tag{2.21}$$

2. compute $\mathrm{a}_{m+1}^{(k+1)}$ solution of:

$$[(\mathbf{\Phi}_{m+1}^{(k+1)})^{\mathrm{T}}\,\mathbf{L}\,\mathbf{\Phi}_{m+1}^{(k+1)}]\,\mathrm{a}_{m+1}^{(k+1)} = (\mathbf{\Phi}_{m+1}^{(k+1)})^{\mathrm{T}}\,\mathbf{f}_{m+1} \tag{2.22}$$

end

• **Substitution.** On the other hand, one can substitute the function $\mathbf{\Phi}_{m+1}$ from the first equation in problem (2.15) into Eq. (2.16) which leads to the study of the stationarity of a Rayleigh ratio to obtain a_{m+1}:

$$\mathbf{R}(\mathrm{a}_{m+1}) = (\mathbf{f}_{m+1}, \mathrm{a}_{m+1})_{\mathcal{I}}^{\mathrm{T}}\,[(\mathbf{L}\,\mathrm{a}_{m+1}, \mathrm{a}_{m+1})_{\mathcal{I}}]^{-1}\,(\mathbf{f}_{m+1}, \mathrm{a}_{m+1})_{\mathcal{I}} \tag{2.23}$$

and, knowing the a_{m+1} function, $\mathbf{\Phi}_{m+1}$ can then be computed accordingly from Eq. (2.15) or (2.19).

Remark. The PGD modes, unlike the POD ones, are not naturally orthogonal. A Gram-Schmidt algorithm can be used to form an orthonormal ROB (see App.. C).

1.3 Conclusion on the (x, t) reduced-order modeling

The classical separated-variable decompositions for evolution problems have been presented. Two distinct approaches can be used: on the one hand, the ROB can be computed from partial solutions (snapshots) determined during a learning phase; on the other hand, PGD provides a separated-variable representation without any prior information on the solution. The use of one method or the other is however case-sensitive, as the difference in computation cost mostly depends on the dynamics of the solution to approximate (which has an important role for the POD on the number of snapshots to compute in order to catch this dynamics). We know present the extensions of such methods to solve parametric evolution problems.

2 Dealing with parametric dependency

We now consider the following problem dependent on N^p parameters $\boldsymbol{\mu} = \{\mu_i\}_{i=1\cdots N^p}$ (for which the assumption $\mu_1 \equiv t$ is made to keep some consistency with the first section of this chapter). The problem lies now in finding $\boldsymbol{u}(\boldsymbol{x}, \boldsymbol{\mu})$ solution of:

$$\boldsymbol{\mathcal{L}}(\boldsymbol{u}; \boldsymbol{\mu}) = \boldsymbol{f}(\boldsymbol{\mu}) \tag{2.24}$$

Note that we will consider in this study only material and loading parameters. See [Ammar et al., 2014, Bognet et al., 2014, Courard et al., 2016, Zlotnik et al., 2015] for strategies taking into account geometrical parametric dependencies. Two methods are proposed to take into account the parametric dependency in a reduced-order modeling framework.

2.1 Enrichment strategies

The first approach consists in improving an already computed basis, calculated for an initial set of parameters, in order to solve the problems associated with the other sets of parameters (see Alg. 3).

Algorithm 3: time-space representation – enrichment procedure

Data: $\mathbf{u}^j(\mathbf{x}, \mathrm{t})$, solution associated with the j^{th} set of parameters $\boldsymbol{\mu}^j$;
Result: $\mathbf{u}^{j+1}(\mathbf{x}, \mathrm{t})$, solution associated with the $(j+1)^{th}$ set of parameters $\boldsymbol{\mu}^{j+1}$;
Step 1: computation of the coefficients $\{\mathrm{a}_k^{j+1}\}_{k=1\cdots m^j}$ associated with the $(j+1)^{\text{th}}$ problem, relative to the basis $\{\boldsymbol{\Phi}_k^j\}_{k=1\cdots m^j}$ (POD stage) ;
while $\varsigma > \varsigma_{crit}$ **do**
  Step 2: enrichment of the $(j+1)^{\text{th}}$ solution by adding new modes:

$$\mathbf{u}^{j+1}(\mathbf{x}, \mathrm{t}) = \sum_{k=1}^{m^j} \mathrm{a}_k^{j+1}\, \boldsymbol{\Phi}_k^j + \sum_{i=m^j+1}^{m^{j+1}} \mathrm{a}_i^{j+1}\, \boldsymbol{\Phi}_i^{j+1} \tag{2.25}$$

end

2.1.1 In the context of POD

Enrichment strategies. In the context of POD, enrichment step 2 of Alg. 3 is not easy to perform as the main advantage of this approach lies in the assumption that, once the initial basis is computed, the new problem to be solved will be similar enough such that this basis is accurate enough. If this is not the case, the original basis $\{\boldsymbol{\Phi}_k^0\}_{k=1\cdots m^0}$ needs to be enriched, which may not always be easy and may require the computation of new snapshots [Glüsmann and Kreuzer, 2009, Ryckelynck, 2005] (which increases the cost of the online phase of the process).

Reduced basis method. As a palliative to the case sensitivity of the POD, reduced basis (RB) methods [Maday and Ronquist, 2004, Patera and Rozza, 2007] provide a convenient framework for such kind of studies as they use a greedy algorithm to select the most relevant calculations to be performed (i.e. the most relevant snapshots) on the parametric space in order to enrich the ROB: a parametric manifold, analogue to an ensemble of snapshots, which intends to accurately represent the dynamics of the solution over the parametric space, is computed along a rigorous error estimator which quantifies the quality of the computed solution [Rozza and Veroy, 2007, Rozza et al., 2008].

Let assume a set of parameters $\boldsymbol{\mu}$, and a large number ψ of sets of parameters which can be obtained from a discretization of the variables $\{\mu_i\}_{i=1\cdots N^p}$ (in that case $\psi = \prod_{i=1}^{N^p} n_i$) or by using random processes (Monte Carlo method for example). The goal is to select only p of those sets and compute the according solutions $\{\boldsymbol{u}(\boldsymbol{x}, \boldsymbol{\mu}^i)\}_{i=1\cdots p}$ which will be used to build the reduced-order model. However, unlike PCA for which the approach consists in looking for the singular values and vectors of the covariance matrix formed with those solutions (see Sec. 1.2.1), those solutions will be directly kept and ortho-normalized one another (using a Gram-Schmidt algorithm for example) to build the ROM. The problem is here to choose the "best" sets of parameters $\boldsymbol{\mu}^i$. Let assume $m < M$ sets have already been chosen, associated with $\{\boldsymbol{\mu}^i\}_{i=1\cdots m}$ sets of parameters. $\boldsymbol{\mu}^{m+1}$ is chosen such that:

$$\boldsymbol{\mu}^{m+1} = \arg\max_{\boldsymbol{\mu}} \Delta_m^{\text{en}}(\boldsymbol{\mu}) \tag{2.26}$$

where Δ_m^{en} is an operator estimating the projection error (based on an energy norm). Different choices are possible for this operator [Patera and Rozza, 2007, Rozza et al., 2008], for example a function proportional to the residue of the equilibrium equation. This approach is especially interesting when the number of sets of parameters ψ is large.

2.1.2 In the context of PGD: the multi-parametric strategy

Similar to the enrichment method presented in Alg. 3, the multi-parametric strategy [Boucard and Ladevèze, 1999] uses the "on the fly generation" aspect of the PGD to enrich the reduced-order model over a parametric space. [Néron et al., 2015] gives an extended overview of the implementation of this technique. More recently, [Heyberger et al., 2013] presented improvements in order to browse in a more efficient way the parametric space. More informations will be provided in a later section once the LATIN method has been presented.

2.2 Higher-order decompositions

Another approach consists in taking the parameters $\boldsymbol{\mu}$ directly into the decomposition:

$$\boldsymbol{u}_m(\boldsymbol{x}, \boldsymbol{\mu}) = \sum_{k=1}^{m} \boldsymbol{\Phi}_k(\boldsymbol{x}) \prod_{i=1}^{N^p} a_k^i(\mu_i) \tag{2.27}$$

2.2.1 High-order decompositions

A canonical polyadic (CP) decomposition [Hitchcock, 1927] of the parametric ensemble of snapshots can be performed to compute such approximation. However such kind of decomposition requires numerous observations or computations and may be expensive to perform. Details about the construction of such kind of approximations are given in App. B.

2.2.2 "High-order" PGD

Another approach consists in using the PGD previously presented and introduce the new parameters as extra-coordinates of the decomposition [Ammar et al., 2012]. A greedy algorithm is then used to build iteratively the functions. Different approaches for the generation of such approximation are presented in this section, under a discrete form.

Method A: (classical) enrichment strategy. Back to Eq. (2.24) and using a similar approach than the one presented in Sec. 1.2.2, the correction $\Delta\mathbf{u}_m \in \mathcal{U}$ is sought under a separated-variable decomposition:

$$\Delta\mathbf{u}_m = \mathbf{\Phi}_{m+1} \prod_i \mathrm{a}^i_{m+1} \tag{2.28}$$

and by choosing the test function $\mathbf{u}^\star \in \mathcal{T}_{\boldsymbol{u}_{m+1}}(\mathcal{S}_{m+1})$ such as:

$$\mathbf{u}^\star = \mathbf{\Phi}^\star \prod_{j=1}^{N^p} \mathrm{a}^j_{m+1} + \sum_{i=1}^{N^p} (\mathrm{a}^i)^\star\, \mathbf{\Phi}_{m+1} \prod_{j\neq i} \mathrm{a}^j_{m+1} \tag{2.29}$$

problem (2.24) leads to the resolution of N^p+1 coupled equations, which can be solved using a fixed-point algorithm (similar to the one given in Alg. 2):

Enrichment method **A**:

(i) computation of the space function (assuming $\{(\mathrm{a}^j)^\star\}_{j=1\cdots N^p} = 0$):

$$\mathbf{\Phi}_{m+1} = \mathbf{L}^{-1}\left[\frac{\mathbf{f}_{m+1} \,\bar{\times}_{j+1}\, \left[\mathbf{I}_{\mathbf{D}_j}\, \mathrm{a}^j_{m+1}\right]}{\prod_{j=1}^{N^p} \left[(\mathrm{a}^j_{m+1})^{\mathrm{T}}\, \mathbf{I}_{\mathbf{D}_j}\, \mathrm{a}^j_{m+1}\right]}\right] \tag{2.30}$$

(ii) computation of the parametric functions (assuming $\mathbf{\Phi}^\star = \mathbf{0}$ and $\{(\mathrm{a}^j)^\star\}_{j=1\cdots N^p,\, j\neq i} = 0$):

$$\mathrm{a}^i_{m+1} = \frac{\mathbf{\Phi}^{\mathrm{T}}_{m+1}\left[\mathbf{f}_{m+1} \,\bar{\times}_{\substack{j+1\\ j\neq i}}\, \left[\mathbf{I}_{\mathbf{D}_j}\, \mathrm{a}^j_{n+1}\right]\right]}{[\mathbf{\Phi}^{\mathrm{T}}_{n+1}\, \mathbf{L}\, \mathbf{\Phi}_{n+1}] \prod_{j=1,\, j\neq i}^{N^p} [(\mathrm{a}^j_{m+1})^{\mathrm{T}}\, \mathbf{I}_{\mathbf{D}_j}\, \mathrm{a}^j_{m+1}]} \tag{2.31}$$

---

with $\mathbf{f}_{m+1} = \mathbf{f} - \mathbf{u}_m$, $\bar{\times}_k$ is the mode-k tensor-vector product [Bader and Kolda, 2007] and the integration operators $\mathbf{I}_{\mathbf{D}_i}$ are defined as:

$$\int_{\mathcal{D}_i} \boldsymbol{a}(\mu_i) \cdot \boldsymbol{b}(\mu_i)\, \mathrm{d}\mu_i \equiv \mathbf{a}^{\mathrm{T}}\, \mathbf{I}_{\mathbf{D}_i}\, \mathbf{b} \tag{2.32}$$

which gives the new product of functions $\Delta\mathbf{u}_m = \mathbf{\Phi}_{m+1} \prod_{i=1}^{N^p} \mathrm{a}^k_{m+1}$.

Method B: enrichment through tensor decomposition of the parametric functions. We still consider the problem (2.24) and the correction $\Delta\mathbf{u}_m$ is sought under the following separated-variable decomposition:

$$\Delta\mathbf{u}_m = \mathbf{\Phi}_{m+1}\,\mathbf{A}_{m+1} \tag{2.33}$$

where $\mathbf{A}_{m+1}(\mu) \in \mathcal{M}_{\mathbf{D}}(\mathbb{R})$ is initialized in the fixed point algorithm as:

$$\mathbf{A}_{m+1}(\boldsymbol{\mu}) = \prod_{i=k}^{N^p} \mathrm{a}_m^k(\mu_k) \tag{2.34}$$

and the test function is chosen as:

$$\mathbf{u}^\star = \mathbf{\Phi}^\star\,\mathbf{A}_{m+1} + \mathbf{\Phi}_{m+1}\,\mathbf{A}^\star \tag{2.35}$$

Once again, a fixed point algorithm enables to compute the different functions:

Enrichment method **B**:

(i) the space function is computed from Eq. (2.30) with $\mathbf{A}^\star = 0$;

(ii) assuming $\mathbf{\Phi}^\star = \mathbf{0}$ one computes $\mathbf{A}_{m+1}$ by solving the following problem:

$$\mathbf{A}_{m+1} = \frac{\mathbf{\Phi}_{m+1}^{\mathrm{T}}\,\mathbf{f}_{m+1}}{\mathbf{\Phi}_{m+1}^{\mathrm{T}}\,\mathbf{L}\,\mathbf{\Phi}_{m+1}} \tag{2.36}$$

(iii) a rank-1 CP-decomposition is performed on $\mathbf{A}_{m+1}$ to obtain the new set of functions $\{\mathrm{a}_{m+1}^k(\mu_k)\}_{k=1\cdots N^p}$.

This approach is especially interesting because: (i) $\mathcal{D}$ is alleged to be small compared to $\mathcal{P}$ (especially because of the size of $\boldsymbol{\Omega}$); (ii) we only assume a rank-1 decomposition; (iii) the orthonormalization of the basis is now much easier to perform (see App. C).

Method C: "Block" PGD. When the number of parameters increases too much (dozens, possibly hundreds) the assembly of the full operators $\{\mathbf{A}_i\}_{i=1\cdots m}$ can be too costly to perform (even for dedicated computers!). A way to balance this memory issue and the complexity of (and time spent) writing a full fixed-point algorithm (as shown on Eqs. (2.30–2.31)) is to mix both approaches, making blocks of parameters and building $\mathbf{A}^j$ operators associated with each of these groups, so that one does not exceed the memory available and that the CP decomposition converges quickly and with a good accuracy.

$$\mathbf{u}_m(\mathbf{x}, \{\mathrm{p}^h\}_{h=1}^{N^1}, \{\mathrm{q}^i\}_{i=1}^{N^2}, \{\mathrm{r}^j\}_{j=1}^{N^3}) = \sum_{k=1}^{m} \mathbf{P}_k\,\mathbf{Q}_k\,\mathbf{R}_k\,\mathbf{\Phi}_k \tag{2.37}$$

where:

$$\mathbf{P}_k = \prod_{h=1}^{N^1} \mathrm{a}_k^h(\mathrm{p}^h) \quad \mathbf{Q}_k = \prod_{i=1}^{N^2} \mathrm{b}_k^i(\mathrm{q}^i) \quad \mathbf{R}_k = \prod_{j=1}^{N^3} \mathrm{c}_k^j(\mathrm{r}^j) \tag{2.38}$$

A fixed-point algorithm can subsequently be used to obtain $(\mathbf{\Phi}_{m+1}, \mathbf{P}_{m+1}, \mathbf{Q}_{m+1}, \mathbf{R}_{m+1})$ and a rank-1 CP-decomposition is performed on those tensors to obtain the corresponding functions. This approach is similar to a tensor train decomposition [Oseledets, 2011].

2.3 Summary on parametric reduced-order modeling

Reduced-order modeling based on a separated variable representation has been introduced in the first section, first with a $(\boldsymbol{x}, t)$ decomposition for evolution problems with the introduction of the proper orthogonal decomposition and the proper generalized decomposition. The algorithms to generate the reduced basis have been presented in both cases.

The extension to parametric decompositions has now been presented. On the one hand, enrichment strategies aim at improving an already computed reduced order basis by adding new functions in the decomposition in order to obtain an approximation of the solution associated with a similar problem. Enrichment strategies within the POD framework do exist, but their numerical cost may be heavy as they sometimes rely on the computation of new snapshots. The reduced-basis method aims at palliating to this case-sensitivity by providing tools to efficiently browse the parametric space. The multi-parametric strategy uses the advantages of the PGD to provide an easy way to enrich the solution at a lower cost than the POD.

On the other, approaches consisting in taking the parametric dependency directly into the separated variable decomposition have been presented. They show the advantage of providing an approximation of the solution for all the possible outcome (sets of parameters). However, in the case of POD, they require the computation of numerous snapshots (in order to sweep the parametric space). PGD, once again, offers a more convenient framework for such studies.

However, those methods used alone are not suitable for the resolution of nonlinear problems, which is a strong aspect of our study. To do so, those methods need to be coupled with linearization strategies. We present in the next section the coupling between POD/PGD and different strategies.

3 Dealing with nonlinearities

As we have seen in the previous parts, classical problems in computational lead to the resolution of:

$$\boldsymbol{R}(\boldsymbol{u}; t) = \boldsymbol{\mathcal{L}}(\boldsymbol{u}; t) - \boldsymbol{f}(t) = \mathbf{0} \tag{2.39}$$

with $\boldsymbol{\mathcal{L}}$ a *nonlinear* differential operator. Different approaches have been investigated to solve such problems in a reduced-order modeling context, usually based on the linearization of the equations. Among those methods, one can cite:

(i) Newton-Raphson methods, mainly used with the POD [Kerfriden et al., 2011, Radermacher and Reese, 2014] and RB methods [Drohmann et al., 2012]. This however requires to build a reduced-order model at each iteration of the algorithm.

(ii) the asymptotic numerical method [Cochelin et al., 1994] has been employed with POD [Niroomandi et al., 2010, Niroomandi et al., 2012] and PGD [Leygue et al., 2013] and shows the advantage of requiring the computation of only one tangent operator, which stays constant over the iterations. However a higher interpolation order of the nonlinear term is thus required, leading to the generation of big (in number of terms) reduced-order bases.

(iii) the LATIN method [Ladevèze, 1999] lies in a separation of the difficulties of the problem, in our case the local problem (nonlinear) and the global problem (in space) which are solved iteratively and the solution of the problem is fully computed at each iteration of the algorithm.

Those methods are detailed in the following sections.

3.1 Newton algorithms for evolution problems

The semi-discretized version of (2.39) reads:

$$\mathbf{R}(\mathbf{u};t) = \mathbf{L}(\mathbf{u};t) - \mathbf{f}(t) = \mathbf{0} \tag{2.40}$$

which is a nonlinear vector equation. The usual approach to solve this problem consists in using a Newton algorithm, which leads to finding the correction $\Delta\mathbf{u}_j$ for each iteration step i and for each time increment t_j the equation:

$$\mathbf{R}(\mathbf{u}_j^i) + \mathbf{L}_T(\mathbf{u}_j^i)\,\Delta\,\mathbf{u}_j = \mathbf{0} \tag{2.41}$$

The solution $\mathbf{u}_j^{i+1}$ is then updated by $\mathbf{u}_j^{i+1} = \mathbf{u}_j^i + \Delta\,\mathbf{u}_j$. Different versions of the Newton algorithm exist, depending on the choice for the operator $\mathbf{L}_T$:

(i) Newton-Raphson, for which $\mathbf{L}_T$ is the tangent operator:

$$\mathbf{L}_T(\mathbf{u}_j^i) = \left.\frac{\partial\,\mathbf{L}(\mathbf{u}_j)}{\partial\,\mathbf{u}_j}\right|_{\mathbf{u}_j=\mathbf{u}_j^i} \tag{2.42}$$

(ii) quasi-Newton algorithms gather a large range of methods, which are used when the Jacobian or Hessian matrices are unavailable or too complicated to compute;

(iii) secant method, which is can be seen as a finite difference approximation of the Newton-Raphson method.

Example of coupling with POD. The coupling with the proper orthogonal decomposition is now presented, and summed up in Alg. 4. Let us consider the matrix $\mathbf{U} \in \boldsymbol{\mathcal{M}}_{n_x,m}(\mathbb{R})$, assembly of the m ROB vectors $\{\boldsymbol{\Phi}_i\}_{i=1\cdots m}$. The solution field $\mathbf{u}$ is searched under the form:

$$\mathbf{u} = \mathbf{u}(t_j) + \mathbf{U}\,\alpha_j \tag{2.43}$$

with the additional orthogonality constraint on the residue:

$$\mathbf{U}^{\mathrm{T}}\,\mathbf{R} = \mathbf{0} \tag{2.44}$$

The problem (2.40) can be rewritten, at each instant $\mathrm{t}_j \in [0, n_t]$ and at iteration i: find $\Delta\,\alpha_j^i \in \boldsymbol{\mathcal{M}}_{m,1}(\mathbb{R})$ solution of:

$$\mathbf{R}_R^i(\mathbf{u}_j) + \mathbf{L}_{T,R}(\mathbf{u}_j)\,\Delta\,\alpha_j^i = \mathbf{0} \tag{2.45}$$

where $\mathbf{R}_R^i$ is defined such that:

$$\mathbf{R}_R^i = \mathbf{U}^{\mathrm{T}}\,\mathbf{L}_T(\mathbf{u}_j + \mathbf{U}\,\alpha_j^i) + \mathbf{U}^{\mathrm{T}}\,\mathbf{f} \tag{2.46}$$

This enable to actualize the function $\alpha_j^{i+1} = \alpha_j^i + \Delta\,\alpha_j^i$ and to compute the new corrections (with classical Newton-Raphson tangent operator):

$$\mathbf{R}_R^{i+1} = \mathbf{U}^{\mathrm{T}}\,\mathbf{L}_T(\mathbf{u}_j + \mathbf{U}\,\alpha_j^{i+1}) \quad \text{and} \quad \mathbf{L}_{T,R}(\mathbf{u}_j^{i+1}) = \mathbf{U}^{\mathrm{T}}\;\left.\frac{\partial\,\mathbf{L}(\mathbf{u}_j + \mathbf{U}^{\mathrm{T}}\,\alpha_j)}{\partial\,\alpha_j}\right|_{\alpha_j=\alpha_j^{i+1}} \tag{2.47}$$

The algorithm stops when the norm of the residue $\mathbf{R}_R^{i+1}$ is lower than a threshold $\varsigma_{\mathrm{crit}}$.

Algorithm 4: Newton-Raphson–POD

Data: residue $\mathbf{R}$, $\|\,.\,\|$ a norm on $\mathbb{R}^{n_x}$, $\mathbf{U} \in \boldsymbol{\mathcal{M}}_{n_x,m}(\mathbb{R})$
;
Result: $\alpha_j = \{\mathrm{a}_k(t_j)\}_{k=1\cdots m}$
;
hypothesis: $\exists\,\mathbf{u}^* \in \mathbb{R}^{n_x,m}$ such that $\mathbf{R}(\mathbf{u}^*) = \mathbf{0}$, $\mathbf{R}'(\mathbf{u}^*)$ invertible ;
initialization: $\mathbf{u}_0 \in \mathbb{R}^{n_x,m}$, $\varsigma_0 = \|\mathbf{R}(\mathbf{u}_0)\|$, $i = 0$;
while $\varsigma_i > \varsigma_{crit}$ **do**

- solve: $\mathbf{R}_R^i(\mathbf{u}_j) + \mathbf{L}_{T,R}(\mathbf{u}_j)\,\Delta\,\alpha_j^i = \mathbf{0}$;
- actualize: $\alpha_j^{i+1} = \alpha_j^i + \Delta\,\alpha_j^i$;
- correction stage:

$$\mathbf{R}_R^{i+1} = \mathbf{U}^{\mathrm{T}}\,\mathbf{L}_T(\mathbf{u}_j + \mathbf{U}\,\alpha_j^{i+1}) \quad \text{and} \quad \mathbf{L}_{T,R}(\mathbf{u}_j^{i+1}) = \mathbf{U}^{\mathrm{T}}\;\left.\frac{\partial\,\mathbf{L}(\mathbf{u}_j + \mathbf{U}^{\mathrm{T}}\,\alpha_j)}{\partial\,\alpha_j}\right|_{\alpha_j=\alpha_j^{i+1}}$$

- computation of $\varsigma_{i+1} = \|\mathbf{R}_R^{i+1}\|$;

end

Remarks. (i) It is important to notice that due to the definition of the damage variable d^c in CHAP. 1, which depends on the positive part of the strain tensor $\boldsymbol{\varepsilon}^c$, classical Newton-Raphson can not be applied. Secant approaches are preferred for such problems, but this tends to slow down the convergence rate of the algorithm; (ii) the (natural) extension of such algorithm to a parametric case is very expensive. Some dedicated strategies must be employed to overcome the problem of recurrent computation of snapshots (once again, RB can be an interesting approach).

3.2 The asymptotic numerical method

The asymptotic numerical method (ANM), developed by [Azrar et al., 1993] is an extension to the method of asymptotic developments presented in [Potier-Ferry, 1979] and has been applied to numerous fields: nonlinear geometry, Navier-Stokes equations, contact, visco-plasticity, ... It consists in defining asymptotic expansions of the unknown fields, as well as a loading parameter λ affecting the nonlinear term, for example:

$$\begin{cases} \boldsymbol{u} = \boldsymbol{u}_0 + c\,\boldsymbol{u}_1 + c^2\,\boldsymbol{u}_2 + \cdots \\ \lambda = \lambda_0 + c\,\lambda_1 + c^2\,\lambda_2 + \cdots \end{cases} \tag{2.48}$$

Such expansion is introduced in the nonlinear equilibrium equation which leads to the resolution of a sequence of linear problems associated with the order of the expansion parameter c, for which the solution $\boldsymbol{u}_p$, associated with the order-p parameter c, depends on the $p-1$ terms $\{(\boldsymbol{u}_i, c^i)\}_{i=1\cdots(p-1)}$.

ANM–PGD algorithms have been investigated in [Leygue et al., 2013], for which a PGD approximation of the unknown terms $\boldsymbol{u}_p$ is built for the different successive linearized problems. Accordingly, the total number of enrichment phases of the reduced-order model is $n_{\text{total}} = \sum_{i=0}^{p} n_i$, which can be high depending on the order of expansion (e.g. the number of terms p), which is linked to the nonlinearity of the problem. The main advantage of this approach remains that the different problems share the same stiffness matrix, which then must be inverted only once.

3.3 The (classical) LATIN–PGD algorithm

More than being a nonlinear solver, the LATIN method [Ladevèze, 1989, Ladevèze, 1999] is a concept which relies on a simple but powerful idea: the separation of difficulties, which are solved alternatively during an iterative process, with search directions $\boldsymbol{E}^+$ and $\boldsymbol{E}^-$ coupling the two problems. At convergence, the solution $\boldsymbol{s}$ of the algorithm satisfies both groups of equations. The most classical example is the treatment of visco-plastic behavior, for which the global (linear) equilibrium and the local nonlinear behavior are solved alternatively. This idea is schematically represented on FIG. 2.3, where $\boldsymbol{\Gamma}$ denotes the space associated with the nonlinear equations and $\boldsymbol{A_d}$ the one for which the solution $\boldsymbol{s}$ satisfies the global equilibrium equations. $\boldsymbol{s}$ represent the exact solution, whereas $\boldsymbol{s}_M$ (red dot) represents the rank-M approximation of $\boldsymbol{s}$. Unlike Newton-like techniques, this approach provides a complete solution at

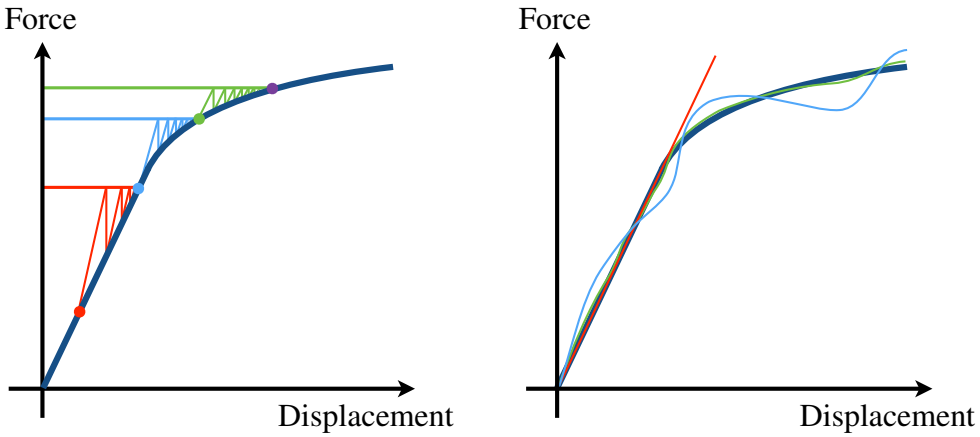

Figure 2.2: Schematic comparison of the Newton-Raphson (left) and LATIN (right) algorithms

each iteration of the algorithm (see FIG. 2.2 for a schematic description of both methods). Such strategy has also been applied for other types of problems: multi-scale, for which the micro and macro problems are solved alternatively; domain decomposition, for which the separation operates on the sub-domains on the one hand and the interfaces on the other hand; multi-physics, which separates the different models. In many cases, model-order reduction (PGD) is used to reduce the cost of resolution of the global problem. A thorough summary of the different works is provided in APP. D, with the according references.

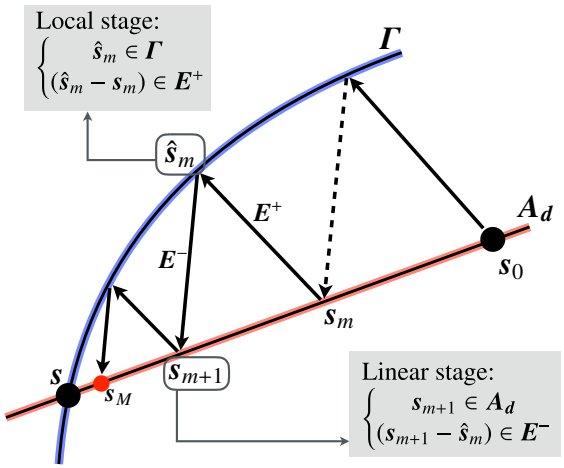

Figure 2.3: Schematic representation of the LATIN algorithm

We now briefly detail the different steps of the algorithm, which are summarized in ALG. 5.

3.3.1 The different steps of the algorithm

Let us first introduce the following spaces:

(i) space $\boldsymbol{A_d}$ of the admissible fields $\boldsymbol{s}$ such that the state equations are satisfied;

(ii) space $\boldsymbol{\Gamma}$ of admissible fields $\boldsymbol{s}$ such that the evolution equations are satisfied.

The solution of the problem satisfies the admissibility conditions and the evolution laws, such that it lies at the intersection of $\boldsymbol{A_d}$ and $\boldsymbol{\Gamma}$:

$$\boldsymbol{s} \in \boldsymbol{A_d} \cap \boldsymbol{\Gamma} \tag{2.49}$$

• **Initialization of the algorithm.** The algorithm is classically initialized by computing the elastic solution of the problem, such that $\boldsymbol{s}_0 \in \boldsymbol{A_d}$. However, more "clever" initialization can be done (partially converged solutions for example, which is the idea behind the multi-parametric strategy –see Sec. 3.3.2), provided that this initial solution belongs to $\boldsymbol{A_d}$. The iterative process then starts with a local stage.

• **The local stage.** The local stage (Fig. 2.4a) consists in finding $\hat{\boldsymbol{s}}_m \in \boldsymbol{\Gamma}$ knowing $\boldsymbol{s}_m \in \boldsymbol{A_d}$ and the search direction $\boldsymbol{E}^+$ defined such that $(\hat{\boldsymbol{s}}_m - \boldsymbol{s}_m) \in \boldsymbol{E}^+$. This local problem is solved incrementally (a Newton-Raphson technique -for example- can be used if required) at each Gauss point of the structure.

• **The linear stage.** The linear stage (Fig. 2.4b) consists in finding $\boldsymbol{s}_{m+1} \in \boldsymbol{A_d}$ knowing $\hat{\boldsymbol{s}}_m \in \boldsymbol{\Gamma}$ and the search direction $\boldsymbol{E}^-$ defined such that $(\boldsymbol{s}_{m+1} - \hat{\boldsymbol{s}}_m) \in \boldsymbol{E}^-$. To reduce the computational cost of this stage (which is global in space *and* time), the PGD technique is usually used to approximate the solution $\boldsymbol{s}_{m+1}$ under a separated-variable representation, which is enriched at each iteration of the algorithm, for which the quantity of interest $\boldsymbol{u}_{m+1}$ at iteration $m+1$ writes:

$$\boldsymbol{u}_{m+1} = \boldsymbol{u}_m + \Delta \boldsymbol{u}_m \tag{2.50}$$

with $\boldsymbol{u}_m = \sum_{i=1}^{m} a_i(t)\, \boldsymbol{\Phi}_i(\boldsymbol{x})$, known at this iteration, and one seeks the correction $\Delta \boldsymbol{u}_m = a_{m+1}\, \boldsymbol{\Phi}_{m+1}$ in the same way as the one presented in Sec. 1.2.2.

• **Stopping criterion.** Error estimation is still an open field when dealing with reduced-order models. In the LATIN framework, different criteria exist to quantify the error of approximation [Ladevèze, 1999], the most classical is based on an energy norm (as defined in 1.2.2):

$$\varsigma = \frac{\|\boldsymbol{\varepsilon}_{m+1} - \hat{\boldsymbol{\varepsilon}}_m\|_{\mathbf{C}}}{\left\|\frac{1}{2}(\boldsymbol{\varepsilon}_{m+1} + \hat{\boldsymbol{\varepsilon}}_m)\right\|_{\mathbf{C}}} \tag{2.51}$$

Other possibilities based on the norm of the residue or the norm of the modes can also be considered.

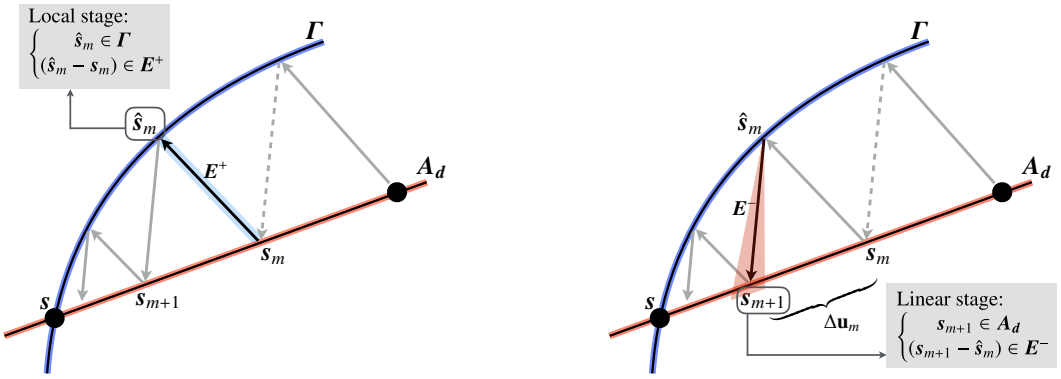

(a) Local stage at iteration $m + 1$

(b) Linear stage at iteration $m + 1$

Figure 2.4: Local (Fig. 2.4a) and linear stage (Fig. 2.4b) representations

Algorithm 5: LATIN algorithm - concept

Data: elastic solution satisfying the boundary conditions
;
Result: $\boldsymbol{u}_m$, approximation of $\boldsymbol{u}$
;
while $\varsigma > \varsigma_{crit}$ **do**
Iteration $m + 1$ starts:

- **Local stage:** knowing the solution $\boldsymbol{s}_m \in \boldsymbol{A_d}$ from previous iteration m, find the local solution $\hat{\boldsymbol{s}}_m \in \boldsymbol{\Gamma}$ using the search direction $\boldsymbol{E}^+$, parameter of the method:

$$\begin{cases} \hat{\boldsymbol{s}}_m \in \boldsymbol{\Gamma} \\ (\hat{\boldsymbol{s}}_m - \boldsymbol{s}_m) \in \boldsymbol{E}^+ \end{cases} \tag{2.52}$$

- **Linear stage:** knowing the solution $\hat{\boldsymbol{s}}_m \in \boldsymbol{\Gamma}$ just computed, find the linear solution $\boldsymbol{s}_{m+1} \in \boldsymbol{A_d}$ using the search direction $\boldsymbol{E}^-$, also parameter of the method:

$$\begin{cases} \boldsymbol{s}_{m+1} \in \boldsymbol{A_d} \\ (\boldsymbol{s}_{m+1} - \hat{\boldsymbol{s}}_m) \in \boldsymbol{E}^- \end{cases} \tag{2.53}$$

- **Computation of error indicator** ς ;

end

Remark: choice of the search directions. Tangent, secant or constant search directions have been investigated, depending on the applications. Tangent search directions are not well-suited for damage mechanics for example, but provide good results for elasto-plastic problems. [Ladevèze, 1999, Relun, 2011] provide some elements for optimized search directions when dealing with elastic-viscous-plastic materials.

3.3.2 The multi-parametric strategy

Let us come back to the multi-parametric strategy mentioned in Sec. 2.1.2. Its objective is to provide very quickly the solution of a nonlinear evolution problem for several values of parameters of the model, by re-using the solution of the same problem computed with different (but "close") values of parameters. This strategy relies on the non-incremental aspect of the LATIN method, which enables to initialize the algorithm with any solution already computed (as it belongs to $\boldsymbol{A_d}$). Fig. 2.5 illustrates this concept, for which the initial basis is successively enriched to provide the approximations $\boldsymbol{s}_{M^j}$ (red dots) of a unique problem associated with the parametric samplings $\{\mu^i\}_{i=1\cdots N^p}$ affecting only the nonlinear space $\boldsymbol{\Gamma}$. The number of iterations required to achieve the convergence of the algorithm is usually low due to this choice of the initialization.

The choice of the values of the parameters minimizing the number of iterations from one set to another is not trivial, and this question has been addressed in [Soulier and Boucard, 2009] (criteria on a distance in the space of parameters and in the space of the solutions) or [Heyberger et al., 2013] ("rational" multi-parametric strategy) using an approach similar to the RB method to select the most relevant sets of parameters to compute the enrichment.

It is worth mentioning that this approach has also been used without PGD at the linear stage in [Champaney, 1996, Boucard and Champaney, 2003], but the addition or reduced-order modeling in this framework tends to accelerate the process.

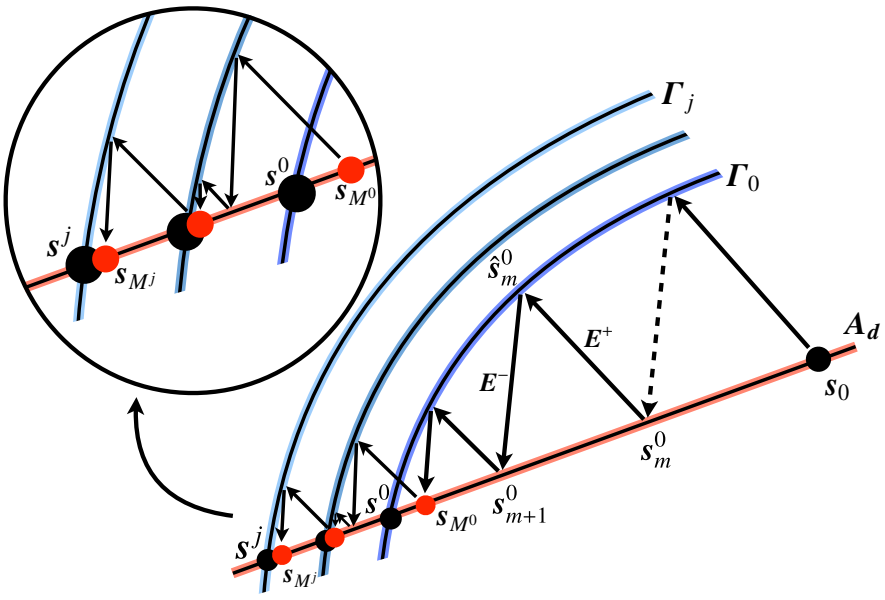

Figure 2.5: Schematic representation of the multi-parametric strategy

3.4 Limits of such approaches

The main drawback of these linearization methods, especially in a parametric context, is that they require the evaluation of the nonlinear term many times and [Chaturantabut and Sorensen, 2010] shows that the POD-Galerkin problem can be more costly to solve than the original full-order problem. The (expensive) computation of tangent operators is also often required.

Different techniques exist when working with reduced-order models to lessen the cost of such operations. Several methods are popular in the literature: one can cite the empirical interpolation method (EIM) which has been applied with POD [Barrault et al., 2004] or reduced basis [Grepl et al., 2007], and its discrete counterpart DEIM used with POD [Chaturantabut and Sorensen, 2010]; Gappy-POD techniques [Willcox, 2006] such as the a priori hyper-reduction method, used with POD [Ryckelynck, 2005, Ryckelynck et al., 2012], the Gauss-Newton with approximated tensors method also used with POD [Carlberg et al., 2013] or the energy-conserving sampling and weighting hyper reduction method used with POD [Farhat et al., 2014]; finally, the reference point method has been used with PGD withing the LATIN framework [Ladevèze, 1997, Capaldo, 2015].

4 To put it in a nutshell ...

The point of this chapter was to present at the same time the different existing techniques to solve nonlinear parametric problems, in a separated-variable-based reduced-order modeling framework, as well as the advantages and limits of those techniques. Classical time-space decompositions have been presented in the first section and the techniques to build the according approximations have been presented. Whereas POD techniques rely on partially known data (from experiments or numerical simulations), PGD techniques aim at building the reduced basis iteratively until a (user-defined) error criteria is reached. Used alone, those techniques are however very similar and the differences appear more clearly in a parametric context. Due to the need for partial data, POD shows the limit of being extremely case-sensitive, and enrichment techniques are not always easy to perform. Reduced basis methods however provide a convenient framework for parametric studies as they give tools to efficiently browse the parametric space in order to enrich the reduced-order model according to the dynamics of the problem. PGD techniques, on the other hand, provide a great framework for parametric studies, either through an enrichment of the solution similar to the POD one (multi-parametric strategy) or by fully decomposing the quantity of interest over its different variables.

The aspects linked to the nonlinearity of the problems encountered in mechanical engineering have also been investigated and different ways to tackle these issues in a ROM framework have been mentioned. The LATIN–PGD coupling offers great possibilities for the simulation of nonlinear parametric problems and this strategy will be at the basis of our work. This approach has already been used in a parametric context, the multi-parametric strategy, but for which only a time-space decomposition was assumed, and enriched progressively associated with the parametric path.

We propose in this work to consider another approach for which the parameters are taken as extra-variables of the PGD decomposition directly in the linear stage of the LATIN algorithm. This approach, compared to the RB and the MPS, is expected to be interesting in particular when the solution space is very large (either because it involves many parameters or because the variables ranges are wide). Preliminary results for a 1-D thermal problem have been published in [Vitse et al., 2014] but will not be recalled in this manuscript. The next chapter provides algorithmic elements of this coupling, and the direct application to a damage model with unilateral effect.

Remark: applications of LATIN–PGD algorithms to damage mechanics. The LATIN algorithm, in the context of damage mechanics, has mostly been used for the study of composite materials, without using PGD (except [Allix et al., 1989] which used a $(\boldsymbol{x}, t)$ decomposition). [Vandoren et al., 2013] proposed a version of the LATIN to simulate snap-back behaviors in reinforced concrete structures, once again without ROM.

More generally, concerning damage in the context of model reduction, one can cite [Ryckelynck et al., 2011] which showed the high potential of model reduction to deal with damage simulations, and some very recent works such as [Metoui et al., 2014] who introduced the coupling of PGD with a cohesive zone for delamination, or [El Halabi et al., 2016] who used a PGD-based multi-scale formulation for simulating problems with a rate-dependent damage model.

Chapter 3

LATIN nonlinear parametric model reduction applied to damage mechanics problems

We present in this part the improvements made to the classical LATIN–PGD algorithm given in the previous chapter in order to tackle the parametric dependency of the problem detailed in Chap. 1. The formulation of the damage problem in the framework of the LATIN method is presented. The enrichment strategy for the reduced model used here is the method **B** given in Chap. 2. Sec. 1 sets the hypothesis of the mechanical problem studied in this chapter. Sec. 2 provides the algorithmic developments of the method. The different stages of the LATIN method are shown in a continuous and discrete framework. Finally, as a significant part of this thesis has been dedicated to the computer implementation of the method (which led to the development of the ROMlab solver), Sec. 3 gives some details about technical elements on both the algorithm and some model aspects specifically linked to the numerical simulation of damage mechanics.

1 Mechanical problem formulation

We consider a reinforced concrete beam as illustrated on Fig. 3.1. The small perturbations assumption is made and the only load applied on the beam is a displacement $\boldsymbol{u}_d$ on its part $\partial_1\boldsymbol{\Omega}$ (body forces are neglected, which is a strong assumption for dynamical problems –which is not the case here– or the study of massive structures). The mechanical state of this structure is defined by the set of fields $\boldsymbol{s} = (\boldsymbol{\sigma}, Y, \boldsymbol{\varepsilon}, d)$, where $\boldsymbol{\varepsilon}$ (respectively Y, $\boldsymbol{\sigma}$, d) is the assembly of $\boldsymbol{\varepsilon}^c$ and $\boldsymbol{\varepsilon}^r$ (respectively Y^c, $\boldsymbol{\sigma}^c$, d^c and Y^r, $\boldsymbol{\sigma}^r$, d^r) relative to their corresponding degrees of freedom (DOFs).

Although the reinforcement is considered to remain in the elastic regime for our study, one can refer to [Relun et al., 2013] for the LATIN–PGD implementation of an Armstrong-Frederick elasto-visco-plastic behavior. A summary of the state laws and evolution equations

of the problem defined in Chap. 1 is given:

State laws.

$$\begin{aligned}
\boldsymbol{\sigma}^{c,m} &= (1-d)\,\boldsymbol{C}^c : \boldsymbol{\varepsilon}^c \\
\dot{\boldsymbol{\sigma}}^{c,f} &= \nu\,\boldsymbol{C}^c : \dot{\boldsymbol{\varepsilon}}^{c,f} \\
Y^c &= \frac{1}{2}\,\langle \boldsymbol{\varepsilon}^c \rangle_+ : \boldsymbol{C}^c : \langle \boldsymbol{\varepsilon}^c \rangle_+ \\
Z^c &= \frac{\mathrm{d}\,H(z^c)}{\mathrm{d}\,z^c} \\
\boldsymbol{\sigma}^r &= \boldsymbol{C}^r : \boldsymbol{\varepsilon}^r
\end{aligned} \tag{3.1}$$

Evolution equations.

$$\begin{aligned}
d^c &= 1 - \frac{1}{1 + A_d(Y^c - Y_0)} \\
z^c &= \frac{1}{1 + A_d(Y^c - Y_0)} - 1 \\
\boldsymbol{\varepsilon}^{c,f} &= d^c\,\boldsymbol{\varepsilon}^c \\
d^r &= 0
\end{aligned} \tag{3.2}$$

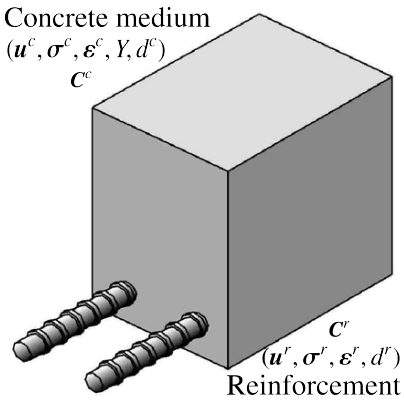

Figure 3.1: Representation of a reinforced concrete beam

The problem is defined over $\mathcal{P} = \boldsymbol{\Omega} \times \mathcal{D}$ associated with the set of variables $\boldsymbol{p} = \{\boldsymbol{x}, \boldsymbol{\mu}\}$, where $\boldsymbol{\Omega} = \{M(\boldsymbol{x})\} \in \mathbb{R}^3$ denotes the geometrical space of the specimen, and $\mathcal{D} = \mathcal{D}_1 \times \cdots \times \mathcal{D}_p$, in particular $\mathcal{D}_1 \equiv \mathcal{I} = [0, T]$ and the spaces $\mathcal{D}_i = [\mu_i^{\min}, \mu_i^{\max}]$ are respectively associated with the variables $\{\mu_i\}_{i=2\cdots N^p}$ (that will be, let us recall, affecting materials characteristics or the loading amplitude in this chapter). Those spaces are assumed to be sufficiently regular to allow the rewriting of the mechanical formulation below.

Let us also introduce the following spaces, as well as their corresponding homogeneous counterparts (denoted $\square_0$):

- space $\mathcal{W} \equiv \mathcal{H}^1(\Omega) = \left\{ \boldsymbol{u} \in \boldsymbol{L}^2(\Omega),\, \nabla \boldsymbol{u} \in \boldsymbol{L}^2(\Omega) \right\}$;
- $\|\square\|_{\mathcal{W}} = \left(\int_\Omega \square^2 \, \mathrm{d}\Omega \right)^{1/2}$, $\boldsymbol{L}^2$ norm on $\mathcal{W}$;
- $\mathcal{V} \equiv \boldsymbol{L}^2(\mathcal{D}, \mathcal{W}) = \left\{ \boldsymbol{u} \,:\, \mathcal{D} \to \mathcal{W},\, \int_{\mathcal{D}} \|\boldsymbol{u}\|^2_{\mathcal{W}} \, \mathrm{d}\mu < +\infty \right\}$;
- space $\mathcal{F}_i \equiv \boldsymbol{L}^2(\mathcal{D}_i, \mathbb{R})$;
- space $\mathcal{F} = \prod_{i=1}^{N^p} \mathcal{F}_i$;
- space $\mathcal{U}$ of the admissible fields $\boldsymbol{u}$ such that:

$$\boldsymbol{u} \in \mathcal{V} \text{ and } \boldsymbol{u}|_{t=0} = \boldsymbol{0} \text{ and } \boldsymbol{u} = \boldsymbol{u}_d \text{ on } \partial_1 \Omega \tag{3.3}$$

  and $\boldsymbol{u}_d$ may depend on $\boldsymbol{\mu}$;

- space $\mathcal{U}_0$ of the admissible fields $\boldsymbol{u}$ such that:

$$\boldsymbol{u} \in \mathcal{V},\, \boldsymbol{u}|_{t=0} = \boldsymbol{0} \text{ and } \boldsymbol{u} = \boldsymbol{0} \text{ on } \partial_1 \Omega \tag{3.4}$$

- space $\boldsymbol{S}_{\text{adm}}$ of the static admissible fields $\boldsymbol{\sigma}$ such that:

$$\forall \boldsymbol{u}^\star \in \mathcal{U}_0,\; -\int_{\mathcal{P}} \boldsymbol{\varepsilon}(\boldsymbol{u}^\star) : \boldsymbol{\sigma} \, \mathrm{d}\boldsymbol{p} = 0 \tag{3.5}$$

- space $\boldsymbol{A_d}$ of the admissible fields $\boldsymbol{s}$ such that $\boldsymbol{\sigma} \in \boldsymbol{S}_{\text{adm}}$ and the state equations (3.1) are satisfied;
- space $\boldsymbol{\Gamma}$ of the admissible fields $\boldsymbol{s}$ such that the evolution equations (3.2) are satisfied;
- space $\mathcal{T}_{\boldsymbol{u}_m}(\mathcal{U}_0)$, the tangent linear space to $\mathcal{U}_0$ at $\boldsymbol{u}_m$.

We now present the modified LATIN–PGD algorithm.

2 Extended LATIN–PGD algorithm

The most important changes to the classical LATIN–PGD algorithm are presented in this section. At the local stage, the behavior equations are solved at each Gauss point, for every set of values of parameters. This step can seem very costly, however this process is highly parallelizable with very important speedups (a numerical example is given in Chap. 4). At the linear stage, the enrichment to the approximation is sought under a time–space–parameter decomposition, using the method **B** presented in Chap. 1.

2.1 Initialization

Let us recall that the kinematic admissibility is usually contained in the initial elastic solution $\boldsymbol{u}_0 \in \boldsymbol{\mathcal{U}}$ such that the following corrections $\Delta\boldsymbol{u}_m$ are searched in $\boldsymbol{\mathcal{U}}_0$. This means that in the event a parameter is chosen to affect the loading conditions (in our case, its amplitude), the initial (kinematically admissible) solution must also comply with the parametric dependency. On the numerical point of view, in many cases, this computation can easily be parallelized over several CPUs, which does not increase the cost of the operation compared to the classical algorithm.

Although usual for plasticity or contact problems for example, this initialization may not be the most interesting choice for damage mechanics. The elastic solution provides an overall over-estimation of the strain field and as a consequence a damage state that may be widely spread over the structure at the first iterations instead of being very localized, whereas the converged solution tends to give confined damage areas concentrating the strain. This may impact the number of iterations of the algorithm to reach convergence. However, in our case, the damage tends to localize to only a few areas of the structure, which does not impact too much the number of iterations. For composites structures, for which the damage is localized to many areas over the structures (local delamination, ...) such initialization may lead to the generation, during the first iterations of the algorithm, to non-relevant modes that do not represent the damage state of the structure. Procedures enabling to "kill" those modes, depending on criteria to be defined, will need to be implemented but are not the core of this work.

2.2 Local Stage

The problem at the local stage consists in finding $\hat{\boldsymbol{s}}_m = (\hat{\boldsymbol{\sigma}}_m, \hat{Y}_m, \hat{\boldsymbol{\varepsilon}}_m, \hat{d}_m)$ knowing $\boldsymbol{s}_m = (\boldsymbol{\sigma}_m, Y_m, \boldsymbol{\varepsilon}_m, d_m)$, where the search directions are defined as:

$$\boldsymbol{E}^+ \left\{ \begin{array}{rcl} \hat{Y}_m & = & Y_m \\ (\hat{\boldsymbol{\sigma}}^c_m - \boldsymbol{\sigma}^c_m) + \boldsymbol{H}_m\,(\hat{\boldsymbol{\varepsilon}}^c_m - \boldsymbol{\varepsilon}^c_m) & = & \boldsymbol{0} \\ \hat{\boldsymbol{\varepsilon}}^r_m & = & \boldsymbol{\varepsilon}^r_m \end{array} \right. \tag{3.6}$$

The choice has been made to store the state of the energy rate variable Y between the previous linear stage and the local stage. Moreover, the search direction $\boldsymbol{H}_m$ is chosen to be equal to $\boldsymbol{H}^{\diamondsuit}_m$ (that is defined in Sec. 2.3).

At each Gauss point, for each time step t_j and value of parameters $\{\mu_i^j \in [\mu_i^{\min}, \mu_i^{\max}]\}_{i=2\cdots N^p}$, one has to solve Alg. 6. The more the number of parameters increases and the more the numerical cost (both CPU and storage) of this stage can be important. Note that however complex this stage can be, it is possible to parallelize the process at different scales: models (reinforcement and concrete media in our case), Gauss points, possibly parameter spaces. This issue is discussed in Sec. 3.

Algorithm 6: local stage

Data: $s_m = (\boldsymbol{\sigma}_m, Y_m, \boldsymbol{\varepsilon}_m, d_m)$, search direction (3.6) and behavior equations:

$$\hat{\boldsymbol{\sigma}}_m^{c,m} = (1 - \hat{d}_m^c)\, \boldsymbol{C}^c : \hat{\boldsymbol{\varepsilon}}_m^c \tag{3.7}$$

$$\hat{\boldsymbol{\sigma}}_m^r = \boldsymbol{C}^r : \hat{\boldsymbol{\varepsilon}}_m^r \tag{3.8}$$

Result: $\hat{s}_m = (\hat{\boldsymbol{\sigma}}_m, \hat{Y}_m, \hat{\boldsymbol{\varepsilon}}_m, \hat{d}_m)$;
For the concrete medium ;
Step 1: computation of the energy released $\hat{Y}_m$:

$$\hat{Y}_m^c = Y_m^c = \frac{1}{2} \langle \boldsymbol{\varepsilon}_m^c \rangle_+ : \boldsymbol{C}^c : \langle \boldsymbol{\varepsilon}_m^c \rangle_+ \tag{3.9}$$

Step 2: computation of the threshold $\varphi^m = \hat{Y}_m^c - (Y_0 + Z^c)$;

2.3 Linear Stage

The approach chosen to tackle the parametric dependency at the linear stage is to consider the parameters as extra-variables to the decomposition. This section provides the elements for the implementation of the different steps of the linear stage in a LATIN context, and the problems to be solved.

The search directions are defined as follows [Ladevèze, 1999]:

$$\boldsymbol{E}^- \begin{cases} d_{m+1} & = & \hat{d}_m \\ (\boldsymbol{\sigma}_{m+1} - \hat{\boldsymbol{\sigma}}_m) - \boldsymbol{H}_{m+1}^{\diamond} (\boldsymbol{\varepsilon}_{m+1} - \hat{\boldsymbol{\varepsilon}}_m) & = & \boldsymbol{0} \end{cases} \tag{3.20}$$

where one can notice the choice for d_{m+1} is made in order to linearize the problem, as d_{m+1} is then assumed to be fixed and is not an unknown at this stage anymore. A classical choice for search direction is to compute the tangent operator. However, this is not possible anymore in this study due to the use of positive parts ($\langle \square \rangle_+$) in the computation of the damage variable. As the assembly (and integration) of the secant matrix ([Vandoren et al., 2013]) is also complicated, the search direction operator $\boldsymbol{H}_{m+1}^{\diamond}$ at iteration $m+1$ is chosen to be constant over the iterations and equal to the undamaged stiffness matrix, such that $\boldsymbol{H}_{m+1}^{\diamond} = \boldsymbol{H}_0^{\diamond} = \boldsymbol{C}$ where $\boldsymbol{C}$ is the assembly of $\boldsymbol{C}^c$ and $\boldsymbol{C}^r$ relative to their corresponding DOFs. This also implies that $\boldsymbol{H}_m = \boldsymbol{H}_m^{\diamond} = \boldsymbol{C}$ (search direction operator at local stage). Other choices may be investigated, for example based on the use of a weighted stiffness matrix. By injecting the search direction (3.20) into Eq. (3.5), the problem becomes:

$\forall \boldsymbol{u}^\star \in \boldsymbol{\mathcal{T}}_{\boldsymbol{u}_{m+1}}(\boldsymbol{\mathcal{U}}_0)$,

$$\int_{\mathcal{P}} \boldsymbol{\varepsilon}(\boldsymbol{u}^\star) : \left[\boldsymbol{H}_{m+1}^{\diamond} : \boldsymbol{\varepsilon}(\boldsymbol{u}_{m+1}) \right] \mathrm{d}\boldsymbol{p} = - \int_{\mathcal{P}} \boldsymbol{\varepsilon}(\boldsymbol{u}^\star) : \left[\hat{\boldsymbol{\sigma}}_m - \boldsymbol{H}_{m+1}^{\diamond} : \hat{\boldsymbol{\varepsilon}}_m \right] \mathrm{d}\boldsymbol{p} \tag{3.21}$$

Algorithm 1 (continuation)

if $\varphi^m > 0$ **then**

Step 3.1: computation of $\hat{d}^c_m$:

$$\hat{d}^c_m = 1 - \frac{1}{1 + A_d(\hat{Y}^c - Y_0)} \tag{3.10}$$

Step 3.2: regularization of $\hat{d}^c_m$ using a damage-delay technique:

$$\hat{\dot{d}}^c_m = \frac{1}{\tau_c}\left[1 - \exp(-a\,\langle \hat{d}_s(\hat{Y}^c_m) - \hat{d}^c_m \rangle_+)\right] \tag{3.11}$$

Step 3.3: after injecting (3.7) into (3.6), one obtains $\hat{\boldsymbol{\varepsilon}}^c_m$ by solving the following system:

$$\left[(1 - \hat{d}^c_m)\,\boldsymbol{C}^c + \boldsymbol{H}_m\right] : \hat{\boldsymbol{\varepsilon}}^c_m = \boldsymbol{\sigma}^c_m + \boldsymbol{H}_m : \boldsymbol{\varepsilon}^c_m \tag{3.12}$$

Step 3.4: $\hat{\boldsymbol{\sigma}}^{c,m}_m$ is computed according to (3.7) ;
Step 3.5: computation of stress $\hat{\boldsymbol{\sigma}}^{c,f}_m$: integration of:

$$\dot{\hat{\boldsymbol{\sigma}}}^{c,f}_m = \nu\,\boldsymbol{C}^c : \dot{\hat{\boldsymbol{\varepsilon}}}^{c,f}_m \tag{3.13}$$

Step 3.6: computation of total stress $\hat{\boldsymbol{\sigma}}^c_m$:

$$\hat{\boldsymbol{\sigma}}^c_m = \hat{\boldsymbol{\sigma}}^{c,m}_m + \hat{\boldsymbol{\sigma}}^{c,f}_m \tag{3.14}$$

else

Step 3.1: element follows and elastic law:

$$\hat{\boldsymbol{\varepsilon}}^c_m = \boldsymbol{\varepsilon}^c_m \tag{3.15}$$

Step 3.2: compute the according stress field:

$$\hat{\boldsymbol{\sigma}}^c_m = \boldsymbol{C}^c : \hat{\boldsymbol{\varepsilon}}^c_m \tag{3.16}$$

This problem is semi-discretized in space using classical finite elements with basis functions that are continuous and polynomial by parts over each elements. The expressions are now given using the discretized fields and operators using non-italic letters. Assuming a rank-m approximation has been computed at the previous iterations of the algorithm:

$$\mathbf{u}_m = \mathbf{u}_0 + \sum_{j=1}^{m} \mathbf{\Phi}_j \prod_{i=1}^{N^p} \mathrm{a}^i_j(\mu_i) \tag{3.22}$$

with $\mathbf{u}_0 \in \mathcal{U} \times \mathcal{F}$ the initial solution satisfying the boundary conditions, the problem here lies

Algorithm 1 (continuation)
For the reinforcement ;
Step 4: computation of $\hat{\boldsymbol{\varepsilon}}^r_m$ and $\hat{\boldsymbol{\sigma}}^r_m$ from (1.19) and (3.6):

$$\hat{\boldsymbol{\varepsilon}}^r_m = \boldsymbol{\varepsilon}^r_m \tag{3.17}$$
$$\hat{\boldsymbol{\sigma}}^r_m = \boldsymbol{C}^r : \hat{\boldsymbol{\varepsilon}}^r_m = \boldsymbol{C}^r : \boldsymbol{\varepsilon}^r_m \tag{3.18}$$
$$\hat{d}^r_m = 0 \tag{3.19}$$

in finding a correction $\Delta\mathbf{u}_m \in \mathcal{U}_0$ such that:

$$\mathbf{u}_{m+1} = \mathbf{u}_m + \Delta\mathbf{u}_m \tag{3.23}$$

which leads to the resolution of the following problem: $\forall \mathbf{u}^\star \in \mathcal{T}_{\mathbf{u}_{m+1}}(\mathcal{U}_0)$ find $\Delta\mathbf{u}_m \in \mathcal{U}_0$ solution of:

$$\int_{\mathcal{D}} (\mathbf{u}^\star)^{\mathrm{T}} \underbrace{\left[\mathbf{B}^{\mathrm{T}}\, \mathbf{H}^{\Diamond}_{m+1}\, \mathbf{I}_{\boldsymbol{\Omega}}\, \mathbf{B}\right]}_{\mathbf{G}} \Delta\mathbf{u}_m \,\mathrm{d}\boldsymbol{\mu} = -\int_{\mathcal{D}} (\mathbf{u}^\star)^{\mathrm{T}} \underbrace{\left[\mathbf{B}^{\mathrm{T}}\, \mathbf{I}_{\boldsymbol{\Omega}} \left([\hat{\boldsymbol{\sigma}}_m + \mathbf{H}^{\Diamond}_{m+1}\, \hat{\boldsymbol{\varepsilon}}_m] + \mathbf{H}^{\Diamond}_{m+1}\, \mathbf{B}\, \mathbf{u}_m\right)\right]}_{\mathbf{Q}_m} \mathrm{d}\boldsymbol{\mu} \tag{3.24}$$

where $\mathbf{Q}_m \in \boldsymbol{\mathcal{M}}_{\mathcal{P}}(\mathbb{R})$ and $\mathbf{G} \in \boldsymbol{\mathcal{M}}_{\boldsymbol{\Omega}}(\mathbb{R})$. We also define the operators $\mathbf{B}$ such that $\boldsymbol{\varepsilon}(\mathbf{u}) = \mathbf{B}\,\mathbf{u}$ and $\mathbf{I}_{\boldsymbol{\Omega}}$:

$$\int_{\boldsymbol{\Omega}} \nabla\boldsymbol{\Phi} \cdot \nabla\boldsymbol{\Phi} \,\mathrm{d}\boldsymbol{\Omega} \equiv (\mathbf{B}\,\boldsymbol{\Phi})^{\mathrm{T}}\, \mathbf{I}_{\boldsymbol{\Omega}}\, \mathbf{B}\,\boldsymbol{\Phi} \tag{3.25}$$

The linear stage of the LATIN algorithm at this point consists of two steps: an update of the already computed time functions and (if necessary) the enrichment of the reduced-order model, as presented in the following sections and summed up in Alg. 7. Note that some recent advances obtained by [Giacoma et al., 2015, Giacoma et al., 2016] to generate a quasi-optimal decomposition can also be integrated into the algorithm.

2.3.1 Update of the basis

Once at least one iteration has been performed, an update stage is set in order to enrich the time functions of the already computed decomposition, directly after the local stage, in order to improve the approximation and possibly skip the rest of the linear stage [Boisse et al., 1990, Ladevèze and Nouy, 2003, Ladevèze et al., 2010]. Coming back to problem (3.24), one seeks to update the previously computed basis $\{\mathrm{a}^1_i(t)\}_{i=1\cdots m}$ and the correction $\Delta\mathbf{u}_m$ writes:

$$\Delta\mathbf{u}_m(\mathbf{x}, \boldsymbol{\mu}) = \sum_{i=1}^{m} \boldsymbol{\Phi}_i\, \overline{\mathrm{a}}^1_i \prod_{k=2}^{N^p} \mathrm{a}^k_i \tag{3.26}$$

with the test function $\mathbf{u}^\star$ chosen as:

$$\mathbf{u}^\star = \sum_{j=1}^{m} (\mathrm{a}^1)^\star \, \mathbf{\Phi}_j \prod_{k=2}^{N^p} \mathrm{a}_j^k \tag{3.27}$$

such that only the time functions are updated in the process, the other parameter functions being fixed. Other choices can be investigated but this method allows to recover the classical time-space approach if no other parameters than t are taken into account. The parametric spaces are now uniformly discretized using n_t and n_{e_i} values respectively for the spaces $\mathcal{I}$ and $\mathcal{D}_{i\,,\,i>1}$. Their discrete counterparts are respectively written $\mathfrak{I}$ and $\mathbf{D}_{i\,,\,i>1}$. Eq. (3.24) then writes: $\forall j \in [1, m]$, $\forall (\mathrm{a}^1)^\star$,

$$\sum_i \int_{\mathfrak{I}} ((\mathrm{a}^1)^\star)^{\mathrm{T}} \underbrace{\left[(\mathbf{\Phi}_i^{\mathrm{T}} \, \mathbf{G} \, \mathbf{\Phi}_j) \prod_{k=2}^{N^p} [(\mathrm{a}_i^k)^{\mathrm{T}} \, \mathbf{I}_{\mathbf{D}_k} \, \mathrm{a}_j^k] \right]}_{\mathrm{A}_{ji}} \overline{\mathrm{a}}_i^1 \, \mathrm{dt} = - \int_{\mathfrak{I}} ((\mathrm{a}^1)^\star)^{\mathrm{T}} \underbrace{\mathbf{\Phi}_j^{\mathrm{T}} \left(\mathbf{Q}_m \, \bar{\times}_{\substack{k+1 \\ k>1}} \left[\mathbf{I}_{\mathbf{D}_k} \, \mathrm{a}_j^k \right] \right)}_{\tilde{\mathrm{Q}}_{m,j}} \mathrm{dt} \tag{3.28}$$

with $\bar{\times}_k$ the mode-k tensor-vector product [Bader and Kolda, 2007] and where the integration operators $\mathbf{I}_{\mathbf{D}_i}$ are once again defined as:

$$\int_{\mathcal{D}_i} \boldsymbol{a}(\mu_i) \cdot \boldsymbol{b}(\mu_i) \, \mathrm{d}\mu_i \equiv \mathbf{a}^{\mathrm{T}} \, \mathbf{I}_{\mathbf{D}_i} \, \mathbf{b} \tag{3.29}$$

which leads to the resolution of the problem: find $\{\overline{\mathrm{a}}_i^1\}_{i=1\cdots m} \in \boldsymbol{\mathcal{M}}_{m,n_t}(\mathbb{R})$ (collection of the m time functions to be updated discretized over n_t time steps) solution of:

$$\mathbf{A} \cdot [\{\overline{\mathrm{a}}_i^1\}_{i=1\cdots m}] = \tilde{\mathbf{Q}}_m \tag{3.30}$$

where $\mathbf{A} \in \boldsymbol{\mathcal{M}}_m(\mathbb{R})$ and $\tilde{\mathbf{Q}}_m \in \boldsymbol{\mathcal{M}}_{m,n_t}(\mathbb{R})$, so that one gets the new approximation:

$$\overline{\mathbf{u}}_{m+1} = \mathbf{u}_0 + \sum_{i=1}^{m} \mathbf{\Phi}_i \, (\mathrm{a}_i^1 + \overline{\mathrm{a}}_i^1) \prod_{k=2}^{N^p} \mathrm{a}_i^k \tag{3.31}$$

Criterion for skipping the enrichment The following indicator is computed to decide whether a new PGD mode should be generated or not at iteration $m + 1$ [Heyberger et al., 2012] :

$$\eta = \frac{e_1 - e_2}{e_1} \tag{3.32}$$

$$e_1 = \frac{\|\boldsymbol{\varepsilon}_m - \hat{\boldsymbol{\varepsilon}}_{m-1}\|_{\mathbf{C}}}{\|\frac{1}{2} \, (\boldsymbol{\varepsilon}_m + \hat{\boldsymbol{\varepsilon}}_{m-1})\|_{\mathbf{C}}} \quad e_2 = \frac{\left\| \overline{\boldsymbol{\varepsilon}}_{m+1} - \hat{\boldsymbol{\varepsilon}}_m \right\|_{\mathbf{C}}}{\left\| \frac{1}{2} (\overline{\boldsymbol{\varepsilon}}_{m+1} + \hat{\boldsymbol{\varepsilon}}_m) \right\|_{\mathbf{C}}} \tag{3.33}$$

with $\|\mathbf{X}\|_{\mathbf{C}}^2 = \int_{\mathcal{D}} \mathbf{X}^{\mathrm{T}} \, \mathbf{I}_{\mathbf{\Omega}} \, \mathbf{C} \, \mathbf{X} \, \mathrm{d}\boldsymbol{\mu}$. If the value of this indicator is greater than a certain threshold η_{crit}, the computation of the new PGD mode is skipped and a new local stage is performed. Else, a new PGD mode is computed by solving Eq. (3.24) with $\mathbf{u}_m = \overline{\mathbf{u}}_{m+1}$ as explained in the next section.

2.3.2 Generation of a new mode

The new PGD mode is computed using a Galerkin orthogonality criterion, following the method **B** exposed in the previous chapter. Back to Eq. (3.24), the correction $\Delta\mathbf{u}_m$ is sought under a separated-variable decomposition:

$$\Delta\mathbf{u}_m = \mathbf{\Phi}_{m+1}\,\mathbf{A}_{m+1} \tag{3.34}$$

where $\mathbf{A}_{m+1}(\boldsymbol{\mu}) \in \mathcal{M}_{\mathbf{D}}(\mathbb{R})$ is initialized in the fixed point algorithm as:

$$\mathbf{A}_{m+1}(\boldsymbol{\mu}) = \prod_{i=k}^{N^p} \mathrm{a}_m^k(\mu_k) \tag{3.35}$$

and the test function is chosen as:

$$\mathbf{u}^\star = \mathbf{\Phi}^\star\,\mathbf{A}_{m+1} + \mathbf{\Phi}_{m+1}\,\mathbf{A}^\star \tag{3.36}$$

This leads to the resolution of a fixed-point algorithm:

(i) computation of the space function (assuming $\mathbf{A}^\star = \mathbf{0}$):

$$\mathbf{\Phi}_{m+1} = \mathbf{G}^{-1}\left[\frac{\mathbf{Q}_m\,\bar{\times}_{j+1}\left[\mathbf{I}_{\mathbf{D}_j}\,\mathrm{a}_{m+1}^j\right]}{\prod_{j=1}^{N^p}\left[(\mathrm{a}_{m+1}^j)^{\mathrm{T}}\,\mathbf{I}_{\mathbf{D}_j}\,\mathrm{a}_{m+1}^j\right]}\right] \tag{3.37}$$

(ii) computation of the parametric functions (assuming $\mathbf{\Phi}^\star = \mathbf{0}$):

$$\mathbf{A}_{m+1} = \frac{[\mathbf{Q}_m\,\mathbf{\Phi}_{m+1}]}{[\mathbf{\Phi}_{m+1}^{\mathrm{T}}\,\mathbf{G}\,\mathbf{\Phi}_{m+1}]} \tag{3.38}$$

(iii) a rank-1 CP-decomposition is performed of $\mathbf{A}_{m+1}$ to obtain the new set of functions $\{\mathrm{a}_{m+1}^k(\mu_k)\}_{k=1\cdots N^p}$ using an alternating least square algorithm (see App. B). This operation is done numerically using the *Tensor toolbox* [Bader and Kolda, 2007].

2.3.3 Orthonormalization of the basis

The new function $\mathbf{\Phi}_{m+1}(\mathbf{x})$ is orthonormalized with respect to the already computed orthonormal basis $\{\mathbf{\Phi}_i(\boldsymbol{x})\}_{i=1\cdots m}$, with the norm of the new mode being put on the time function a_{m+1}^1:

$$\mathrm{a}_{m+1}^1 \leftarrow \mathrm{a}_{m+1}^1[\mathbf{\Phi}_{m+1}^{\mathrm{T}}\,\mathbf{I}_{\mathbf{\Omega}}\,\mathbf{\Phi}_{m+1}]\prod_{k=2}^{N^p}[(\mathrm{a}_{m+1}^k)^{\mathrm{T}}\,\mathbf{I}_{\mathbf{D}_k}\,\mathrm{a}_{m+1}^k] \tag{3.39}$$

$$\mathbf{\Phi}_{m+1} \leftarrow \frac{\mathbf{\Phi}_{m+1}}{[\mathbf{\Phi}_{m+1}^{\mathrm{T}}\,\mathbf{I}_{\mathbf{\Omega}}\,\mathbf{\Phi}_{m+1}]} \tag{3.40}$$

$$\mathrm{a}_{m+1}^k \leftarrow \frac{\mathrm{a}_{m+1}^k}{[(\mathrm{a}_{m+1}^k)^{\mathrm{T}}\,\mathbf{I}_{\mathbf{D}_k}\,\mathrm{a}_{m+1}^k]} \qquad \forall k \in [2, N^p] \tag{3.41}$$

Note that this orthonormalization step is not natural with the method **A** presented in Chap. 2.2.2 and is now possible due to the use of the CP-decomposition (see App. C).

2.3.4 Update of the stress and strain fields

The computation of the search direction for the local stage requires the update of the strain et stress fields:

$$\boldsymbol{\varepsilon}_{m+1} = \mathbf{B}\,\mathbf{u}_{m+1} = \boldsymbol{\varepsilon}_0 + \sum_{i=1}^{m+1} \mathbf{B}\,\boldsymbol{\Phi}_i \prod_{j=1}^{N^p} \mathrm{a}_i^j \tag{3.42}$$

and the updated stress field is given according to (3.20):

$$\boldsymbol{\sigma}_{m+1} = \hat{\boldsymbol{\sigma}}_m + \mathbf{H}^{\Diamond}_{m+1}\,(\boldsymbol{\varepsilon}_{m+1} - \hat{\boldsymbol{\varepsilon}}_m) \tag{3.43}$$

Algorithm 7: linear stage

Data: $\hat{\mathbf{s}}_m = (\hat{\boldsymbol{\sigma}}_m, \hat{\mathrm{Y}}_m, \hat{\boldsymbol{\varepsilon}}_m, \hat{\mathrm{d}}_m)$, search direction (3.20)
;
Result: $\mathbf{s}_{m+1} = (\boldsymbol{\sigma}_{m+1}, \mathrm{Y}_{m+1}, \boldsymbol{\varepsilon}_{m+1}, \mathrm{d}_{m+1})$
;
Step 1: update of the existing basis (Eqs. (3.26 – 3.31)) ;
Step 2: computation of $\boldsymbol{\varepsilon}_{m+1}$ and $\boldsymbol{\sigma}_{m+1}$ from search direction (3.20) ;
Step 3: computation of the update indicator η;
if $\eta < \eta_{crit}$ **then**
  Step 4: computation and orthonormalization of a new PGD mode (Eqs. (3.34 – 3.43)) ;
end

2.4 Stopping criterion

The algorithm stops when the $\boldsymbol{L}^2$ norm of the new mode (i.e., the norm of the new time function) $\varsigma = \left\|\mathrm{a}^1_{m+1}\right\|_{\boldsymbol{L}^2}$ falls below a given criterion $\varsigma_{\mathrm{crit}}$. Such choice is interesting because it is inexpensive to compute.

It can however be questioned as it gives an overall indication of the influence of the correction (that is to say of the new mode) to the approximation. For very local phenomena, as it is our case, such estimator does not provide a relevant information on the local improvements to the solution, in the areas where the damage occur.

Error estimators, within this framework, are given in the literature for time-space PGD decompositions in [Ladevèze, 1999, Ladevèze et al., 2010]:

$$\varsigma = \frac{\|\boldsymbol{\varepsilon}_{m+1} - \hat{\boldsymbol{\varepsilon}}_m\|_{\mathbf{C}}}{\left\|\frac{1}{2}(\boldsymbol{\varepsilon}_{m+1} + \hat{\boldsymbol{\varepsilon}}_m)\right\|_{\mathbf{C}}} \tag{3.44}$$

where the norm $\|\boldsymbol{X}\|_{\mathbf{C}}^2$ is defined Sec. 2.3.1. However the extension to the parametric case is not an easy task as it is computationally extremely expensive, especially because, as explained in Sec. 3.6, the operator $\hat{\boldsymbol{\varepsilon}}_m$, of size $\mathcal{P}$, is full (in the sense of non-separated) and non-sparse.

Error estimators have been developed for high-dimensional PGD reduced-order models [Ammar et al., 2010a, Alfaro et al., 2015]. Once again, those indicators alone can not be used as they only provide an approximation of the error of the reduced-order modeling part, in our case associated with the global linear problem, but do not take into account the error linked to the approximation of the local nonlinear behavior.

2.5 Algorithm

The overall algorithm is summarized in Alg.. 8 which gives an overview of the main stages of the LATIN strategy.

Algorithm 8: LATIN–PGD algorithm

Data: $\mathbf{s}_0$, elastic solution satisfying the boundary conditions
;
Result: $\mathbf{u}_{m+1}$, rank-$m+1$ approximation of $\mathbf{u}$
;
while $\varsigma > \varsigma_{crit}$ **do**
  Local stage: (Alg.. 6)
  $\forall \mu_i \in \mathbf{D}_i$: incremental resolution of the local problem: $\mathbf{s}_m \rightarrow \hat{\mathbf{s}}_m$;
  Linear stage (Alg.. 7)
  • Update stage*: computation of the correction $\{\overline{\mathrm{a}}_i^1\}_{i=1}^m$ made to the time functions $\{\mathrm{a}_i^1\}_{i=1}^m$, assuming the basis $\{\boldsymbol{\Phi}_m, \{\mathrm{a}_m^j\}_{j>1}\}$ remains fixed;
  if $\eta > \eta_{crit}$ **then**
    A new iteration starts → local stage ;
    Break;
  else
    • Enrichment of the basis: alternated fixed point algorithm:
    → $\Delta\mathbf{u}_m = \boldsymbol{\Phi}_{m+1} \prod_i \mathrm{a}_{m+1}^i$;
    → $\mathbf{u}_{m+1} = \mathbf{u}_m + \Delta\mathbf{u}_m$
  end
  Computation of the indicator ς;
end
* At least one global stage has to have been undertaken to perform the update stage.

3 Computer implementation

The work done during this thesis led to the development of a finite-element based Matlab code, ROMlab (based on the *esbroufe*[1] program developed by J.C. Passieux), which not only provides the tools for nonlinear (PGD-)model reduction for multi-material models, but also intends to prepare a basis for more advanced methods and to help developing prototypes of algorithms with applications on 2-D or 3-D examples at LMT. The work done on this tool is the first step towards the development of more advanced solvers. This section aims at providing several pieces of information regarding computational aspects related to the modeling of reinforced concrete, the simulation of damage mechanisms in the LATIN–PGD framework, as well as more general remarks concerning the LATIN algorithm itself (and especially the cost associated with the local stage, which is detailed in Sec. 3.6).

3.1 Regularization of the problem

Different methods have been investigated for the regularization of the problem (see App. A). Even though nonlocal approaches are very classical for such kind of problem, their computational implementation is very heavy, especially for a 3-D demonstrator such as ours. The energy regularization is also difficult to implement due to the choice of the damage evolution law, which integration is not easy. Our choice finally focused on a damage-delay technique, which is usually used for dynamic problems for composite structures but showed interesting regularization results. However, its use with cyclic loading conditions tend to highlight some issues, especially when the loading reaches an extrema (for uni-axial loading, when switching from tension to unloading and compression) as the delay effect tends to increase the damage state even after the unloading phase started. The choice of the time constant τ_c is also difficult to justify as it does not have a physical sense, but has a strong influence on the post-peak behavior. Both aspects have to be taken into account when using this technique.

3.2 Concrete-reinforcement interface modeling

Different techniques exist to numerically represent a reinforced concrete medium, depending especially on the nature of the interface between the concrete and the steel media one wants to model. The classical approach consists in incorporating 2-nodes steel bar elements into the 3-D concrete mesh, where the nodes of the bars match some nodes of the volume elements (conformal meshes). The adherence is managed through kinematic relation between the different nodes. This however does not enable one to represent the degradation mechanisms at the concrete/steel interface. To do so, a first approach consists in using enrichment strategies [Casanova et al., 2012] in order to represent the progressive sliding of the nodes of the reinforcement relative to the nodes of the concrete mesh, but the numerical implementation can be delicate. Another approach consists in using 3-D cylinders with joint elements to model the interface. Those elements can either have a null value thickness but volume interfaces can also be used to take into account its progressive degradation and sliding mechanisms. The

[1] `http://jchpass.free.fr/index.php?id=fem`

drawbacks of such techniques are their numerical cost, as the meshes become heavier, and numerical instabilities that may appear at the interfaces.

We chose the most simple approach (i.e. 1-D steel bar elements into the 3-D concrete mesh, which is the most used technique in engineering applications and softwares) in the numerical examples presented in the next chapter, as shown on FIG. 3.2. A perfect interface is also assumed, meaning that no sliding will be taken into account.

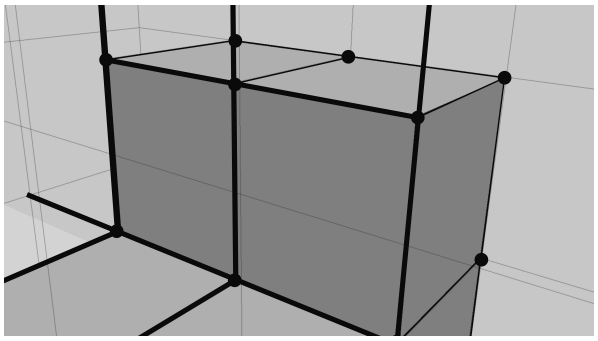

Figure 3.2: Numerical assembly of the 3-D hexahedron elements (concrete) and 1-D bar elements (thick black lines, reinforcement)

3.3 Damage initiation

Numerically, it is classical when studying concrete to represent the intrinsic heterogeneity of the material. This is done here by weighting the mean value of the Young modulus E^c with a uniform distribution ($+/-$ 5%, see FIG. 3.3a) in order to enable the localization of the initiation of the damage. Other methods such like the turning band method could also be implemented [Mantoglou and Wilson, 1982] (see FIG. 3.3b).

3.4 Damage limiters at the boundary conditions

Stress concentrations may occur in the areas where the boundary conditions are applied. An elastic behavior is assumed in those areas (in blue on FIG. 3.4) to avoid the initiation of damage in those zones where complex nonlinear phenomena may occur (although there is a high stress concentration, damage in this area may not lead to the crushing of the structure).

3.5 Visualization

The post-treatment and visualization of the PGD quantities is done using the PXDMF plug-in[2] developed by F. Bordeu within the ParaView[3] software. The PXDMF file format is used for storing solutions under a separated-variables representation. It enables to easily

[2] `https://rom.ec-nantes.fr/resources/separated-variables-representation-visualisation/`
[3] `http://www.paraview.org/`

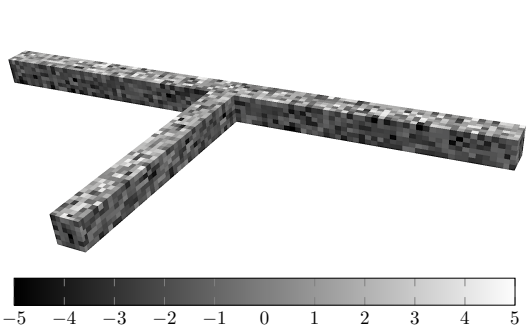

(a) Weighting distribution of the concrete medium's Young modulus E^c (in %)

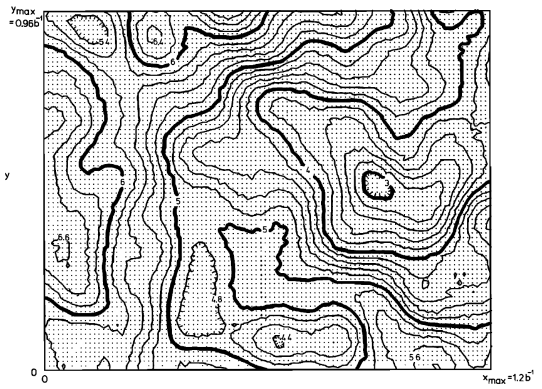

(b) Typical simulated realization of a 2-D stationary process, generated by the turning bands method [Mantoglou and Wilson, 1982]

Figure 3.3: Modeling of the heterogeneity of the medium

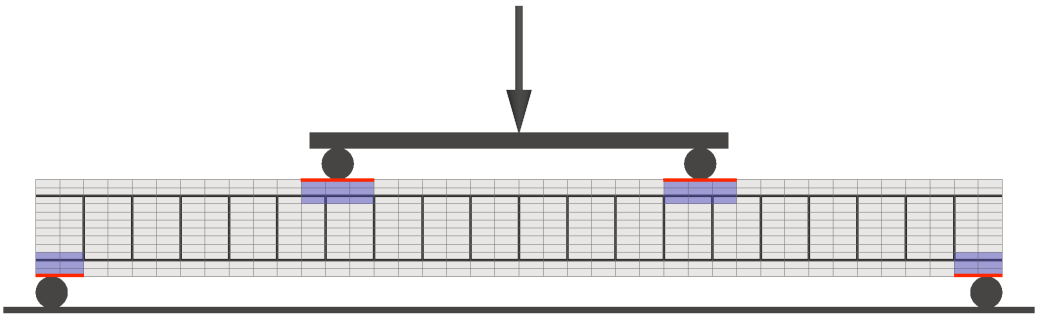

Figure 3.4: Boundary conditions areas (red) and damage limiter zones (blue areas) on a reinforced concrete beam under 4-points bending loading conditions

and quickly particularize the computed database for given sets of parameters (as the reconstruction only involves sums and products of vectors and scalars, depending on the choice of the values of the parameters), or post-process the different parametric functions to extract for example some local quantities of interest (using the internal filters of ParaView).

Remark. The damage variable d is also decomposed using a CP-decomposition (at convergence) to have some consistency in the format of the variables for the visualization. This is a relatively low-cost operation as d is sparse.

3.6 Discussion – numerical cost of the local stage

The algorithm of the local stage for 3 parameters is detailed in Alg. 9. Two problems can be highlighted here:

1. without any optimized strategy, the CPU cost of this stage increases exponentially with the number of parameters due to the nested *for* loops;

2. this stage requires the computation of the strain and stress tensors, which are (following the classical approach) full (non-separated) and non-sparse. To detail this issue, let assume a medium with an isotropic behavior (6 unknowns in the strain field), meshed with 10k 8-nodes hexahedron elements (that is to say 80k Gauss points, which is a fair number for a demonstrator but relatively small for an industrial case), for which the time interval is cut into 100 time steps (which is not a lot but rather classical for the kind of study we face) and for which the parametric spaces $\mathcal{D}_2$ and $\mathcal{D}_3$ are discretized with 10 values. The total size of the operator $\hat{\boldsymbol{\varepsilon}}_m$ is $\zeta = 80\times10^3\cdot6\cdot100\cdot10\cdot10 = 4.8\times10^9$ values, each of them being represented over 64 bits (e.g. 8 bytes) for a total size of 35.8 Gb. Such costly assembly not only is time-consuming, but sometimes too expensive to be performed.

   It is to be mentioned that the choice of the search direction is also important in this matter, as we chose a constant one. A secant search direction would require the computation of an operator of the size $\boldsymbol{\Omega} \times \mathcal{P}$ (n_x times bigger than the example given above), which is impossible to achieve with our tools.

Both the CPU and the storage costs of those operators are challenging without any optimization. Several approaches have been investigated to reduce those costs.

It is to be noticed that the process presented in Alg. 9 is time-dependent but the other parameters do not interfere one another. Hence, the local stage can easily (up to Matlab's capabilities) be parallelized over several cores. The machines available at LMT possess up to 32 cores and a numerical comparison between the serial and parallel runs for the same test case given in the next chapter presented very good speedup values. It is certain that programmed in a language incorporating message passing interface (MPI[4]) communications, this stage can be parallelized at the most elementary level (Gauss point), provided no nonlocal phenomena occur (but it still could be parallelized over the parametric spaces, with expected great speedups). Note that the parallelization can be implemented for other operations in the LATIN algorithm, such as the initialization stage, or several numerical procedures to be performed during the computation of the PGD functions.

Concerning the assembling of the stress and strain operators, different compression methods can be coupled to the LATIN algorithm to reduce the memory usage during this stage. The first approach could be to perform a PARAFAC decomposition of these operators in order to reduce their storage cost. This however still requires the computation of the full-order operators, which may not be feasible. Another approach could be to use the reference points method (RPM) [Ladevèze, 1997, Capaldo, 2015], which was developed in the LATIN framework and which provides tools for compressing massive operators in order to perform elementary algebraic operations on their compressed versions and finally reconstruct the approximations of those operators in a separated-variables representation. Finally, the quantities

[4] `https://en.wikipedia.org/wiki/Message_Passing_Interface`

at the local stage could be sought directly under a separated variable representation (which is however really problem-dependent), but once again the number of parameters may still cause memory issues. The resolution of problems with many (dozens) of parameters was the topic of the Master's thesis (and PhD to follow) of C. Paillet which I co-supervised during his Master's degree.

4 To put it in a nutshell ...

The extension of the LATIN–PGD algorithm to parametric problems using the parameters as extra-variables into the PGD decomposition has been introduced in this chapter. The enrichment of the reduced order model is done using a Galerkin orthogonality technique. Its formulation in a damage-mechanics problem was also presented. Such formulation, used alone, poses obvious computational problems in terms of CPU usage and memory allocation. However, several leads have been proposed to lower these costs for problems involving many of parameters. The choice of the indicator for the estimation of the quality of the approximation remains an open question, as one has to take into account both the global aspect of the approximated solution and the very local degradations that occur in confined zones. The next chapter provides numerical examples illustrating this technique.

Algorithm 9: local stage – computational aspects

Data: $\mathbf{s}_m = (\boldsymbol{\sigma}_m, \mathrm{Y}_m, \boldsymbol{\varepsilon}_m, \mathrm{d}_m)$, search direction
; **Result:** $\hat{\mathbf{s}}_m = (\hat{\boldsymbol{\sigma}}_m, \hat{\mathrm{Y}}_m, \hat{\boldsymbol{\varepsilon}}_m, \hat{\mathrm{d}}_m)$
; **for** $\mu_1 = 1 \cdots n_t$ **do**
  for $\mu_2 = 1 \cdots n_{e_2}$ **do**
    for $\mu_3 = 1 \cdots n_{e_3}$ **do**
      Concrete medium:
      for *each Gauss point k* **do**
        (all the (k, μ_1, μ_2, μ_3) *indexes are omitted –but must be kept in mind)*
        computation of $\langle \boldsymbol{\varepsilon}^c_m \rangle_+$:
          computation of the eigenvalues α_i and eigenvectors $\boldsymbol{\Lambda}_i$ of $\boldsymbol{\varepsilon}^c_m$
            $\langle \boldsymbol{\varepsilon}^c_m \rangle_+ = \sum_{i=1}^{3} \boldsymbol{\Lambda}_i^{\mathrm{T}} \langle \alpha_i \rangle_+ \boldsymbol{\Lambda}_i$
        computation of the energy released $\hat{\mathrm{Y}}^c_m$:
          $\hat{\mathrm{Y}}^c_m = \mathrm{Y}^c_m = \frac{1}{2} (\langle \boldsymbol{\varepsilon}^c_m \rangle_+)^{\mathrm{T}} \mathbf{C}^c \langle \boldsymbol{\varepsilon}^c_m \rangle_+$
        computation of the threshold $\varphi^m = \hat{\mathrm{Y}}^c_m - (\mathrm{Y}_0 + \mathrm{Z}^c_{m-1})$;
        if $\varphi^m > 0$ **then**
          computation of $\hat{\mathrm{d}}^c_m$:
            $\hat{\mathrm{d}}^c_m = 1 - \frac{1}{1 + A_d (\hat{\mathrm{Y}}^c_m - \mathrm{Y}_0)}$
          damage-delay regularization of $\hat{\mathrm{d}}^c_m$:
            $\hat{\dot{\mathrm{d}}}^c_m = \frac{1}{\tau_c} \left[1 - \exp(-a \langle \hat{\mathrm{d}}_s - \hat{\mathrm{d}}^c_m \rangle_+) \right]$
          computation of $\hat{\boldsymbol{\varepsilon}}^c_m$:
            $\hat{\boldsymbol{\varepsilon}}^c_m = \left[(1 - \hat{\mathrm{d}}^c_m) \mathbf{C}^c + \mathbf{H}_m \right] \backslash \left(\boldsymbol{\sigma}^c_m + \mathbf{H}_m^{\mathrm{T}} \boldsymbol{\varepsilon}^c_m \right)$
          computation of $\hat{\boldsymbol{\sigma}}^{c,m}_m$:
            $\hat{\boldsymbol{\sigma}}^{c,m}_m = (1 - \hat{\mathrm{d}}^c_m) \mathbf{C}^c \hat{\boldsymbol{\varepsilon}}^c_m$
          computation of stress $\hat{\boldsymbol{\sigma}}^{c,f}_m$ using an explicit Euler scheme ;
          computation of total stress $\hat{\boldsymbol{\sigma}}^c_m$:
            $\hat{\boldsymbol{\sigma}}^c_m = \hat{\boldsymbol{\sigma}}^{c,m}_m + \hat{\boldsymbol{\sigma}}^{c,f}_m$
          actualization of the hardening:
            $\hat{\mathrm{Z}}^c_m = \hat{\mathrm{Y}}^c_m - \mathrm{Y}_0$
        else
          element follows and elastic law:
            $\hat{\boldsymbol{\varepsilon}}^c_m = \boldsymbol{\varepsilon}^c_m$
          computation of stress field:
            $\hat{\boldsymbol{\sigma}}^c_m = \mathbf{C}^c \hat{\boldsymbol{\varepsilon}}^c_m$
        end
      end
      Reinforcement:
      for *each Gauss point k* **do**
          $\hat{\boldsymbol{\varepsilon}}^r_m = \boldsymbol{\varepsilon}^r_m$
          $\hat{\boldsymbol{\sigma}}^r_m = \mathbf{C}^r \hat{\boldsymbol{\varepsilon}}^r_m = \mathbf{C}^r \boldsymbol{\varepsilon}^r_m$
          $\hat{\mathrm{d}}^r_m = 0$
      end
    end
  end
end

Chapter 4

Numerical examples

This part illustrates the method presented in the previous chapter. Three numerical examples are provided for meshes of different sizes, and parameter variabilities on the loading and on material variables. The simulated concrete is a Portland blend cement *CEM I 52,5 N CE PM-CP2 NF* and the bars are *FE E 500*. Finite elements are 8-nodes hexahedron (brick) elements for the concrete and 2-nodes bar elements (only working in tension–compression) for the reinforcement. The meshes are set to be compatible, meaning that each node of the reinforcement elements matches at least one node of the concrete medium. The values of the material coefficients, identified in [Iskef, 2016], are summed up in Tab. 4.1 and algorithmic parameters are given in Tab. 4.2.

Table 4.1: Material coefficients

Symbol	Parameter	Value
E^c	Young modulus (concrete)	25.42×10^9 Pa
ν^c	Poisson ratio (concrete)	0.2
f_t	Tensile strength	3.6×10^6 Pa
Y_0	Threshold for damage activation	254.92 J.m^{-3}
A_d	Brittleness coefficient	1×10^{-3} J^{-1}.m^3
E^r	Young modulus (steel)	185.35×10^9 Pa
ν^r	Poisson ratio (steel)	0.3
D	Diameter of the section of the steel bars	8×10^{-3} m

The first example is a reinforced beam in tension and results illustrating the behavior implemented, so as a variability on the loading conditions, are given in Sec. 1. The second example is a 4-points bending test on a reinforced concrete beam, for which a variability is set on the amplitude of the loading and on the Young modulus of the concrete medium. Results are given in Sec. 2. The third example is a beam-column assembly arising from the *SMART testing* project at LMT. A cyclic displacement is prescribed at one extremity of the column, in the plane of the specimen, and a variability is set on the brittleness coefficient of the

Table 4.2: Algorithmic variables

Symbol	Parameter	Value
α_0	Unilateral effect parameter	6.5
a	Damage-delay parameter	1
τ_c	Characteristic time	$10 \cdot \Delta t$
η_{crit}	Update criterion	0.8
ς_{crit}	Stopping criterion	1×10^{-6}

concrete model (A_d), which affects the softening part of the damage evolution law. Numerical simulations and a comparison with Cast3M results are given in Sec. 3. Finally, Sec. 4 provides first hints concerning the performances of the algorithm, and deals with aspects linked to the parallel processing at the local stage.

1 Case 1 – tensile test

The first example is a tensile test on a reinforced concrete beam for which the geometrical description of both the concrete medium and its reinforcement are given on Fig. 4.1a and the discretization informations are given in Tab. 4.3. Homogeneous Dirichlet boundary condi-

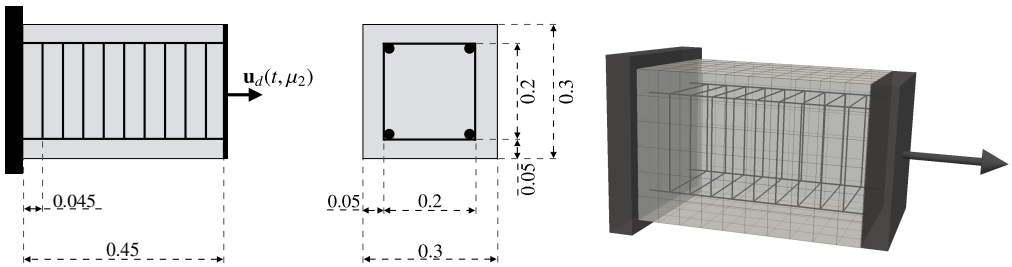

(a) Geometry of the beam (b) 3-D representation

Figure 4.1: Tensile test – geometry (left) and 3-D representation (right) of the beam

Table 4.3: Discretization of the first example

Variable space		Interval of variation – discretization
$\mathbf{\Omega}$	Concrete	3, 157 nodes, 2, 400 elements (9, 471 DOFs, 19, 200 GPs)
	Reinforcement	80 nodes, 112 elements (240 DOFs, 112 GPs)
$\mathbf{D}_1 \equiv \mathcal{I}$	Time	$t \in [0, 199]$ (200 time steps)
$\mathbf{D}_2$	Loading variability	$\mu_2 \in [1, 24]$ (24 values)

tions are enforced on one side of the beam (to the concrete surface as well as the corresponding reinforcement matching nodes) and a time-dependent prescribed displacement condition

$\mathbf{u}_d(t, \mu_2)$ is applied to the other extremity of the beam. Its amplitude is parameterized with a variable μ_2 and is represented on Fig. 4.3a for three values of μ_2, with a variability of around 25%:

$$\boldsymbol{u}_d(t, \mu_2^i) = (0.75 + 0.25\,\frac{\mu_2^i}{\mu_2^{\max}})\,\mathbf{saw}(t) \tag{4.1}$$

where the function $\mathbf{saw}(t)$ is shown Fig. 4.2a. This example is set to illustrate the strong influence of a variability on the loading conditions on the global mechanical response of the structure when the material parameters a kept invariant. This variability can either be due to a lack of knowledge on the loading conditions, or due to inaccuracies in the application of the load (improper fit of mechanical parts, ...). The following chart was computed:

$$\boldsymbol{u}_m(\boldsymbol{x}, t, \boldsymbol{u}_d(\mu_2)) = \sum_{i=1}^{m} \boldsymbol{\Phi}_i(\boldsymbol{x})\, a_i^1(t)\, a_i^2(\mu_2) \tag{4.2}$$

Fig. 4.2 shows the evolution of the $\sigma_{xx} = f(\varepsilon_{xx})$ relation at a given Gauss point for a given value of the parameter μ_2. One can see that the evolution of damage follows a similar pattern as in [Richard and Ragueneau, 2012] with the deterioration initiating at a threshold $f_t \approx 3.6$ MPa. The unilateral effect is also recovered, with the secant modulus after the first cycle going asymptotically towards the undamaged Young modulus.

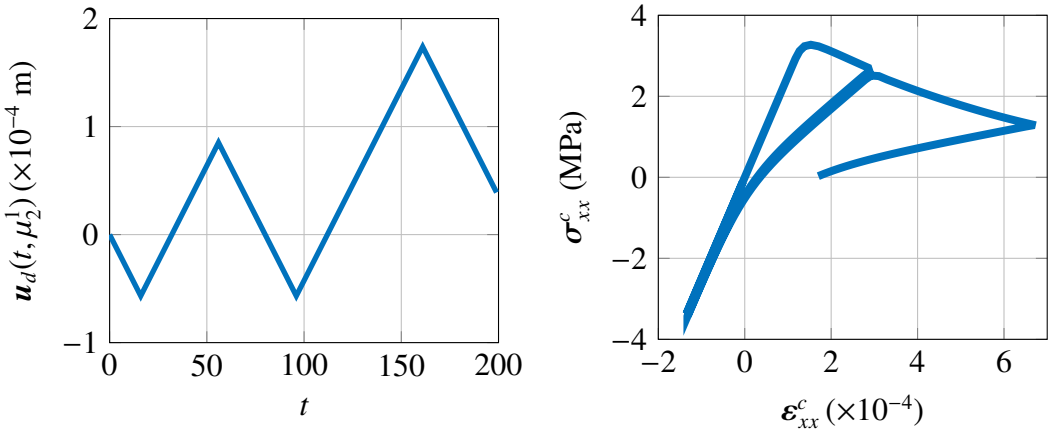

(a) Prescribed displacement

(b) Behavior at a Gauss point

Figure 4.2: Tensile test – behavior $\boldsymbol{\sigma}_{xx}^c = f(\boldsymbol{\varepsilon}_{xx}^c)$ at the Gauss point level for $\mu_2 = 12$

Fig. 4.3b shows the global reaction $\boldsymbol{F}|_{\partial_1\boldsymbol{\Omega}} = f(\boldsymbol{u}_d)$ and is particularized for the three previous values of μ_2. It illustrates the important influence of this parameter on the global response of the structure

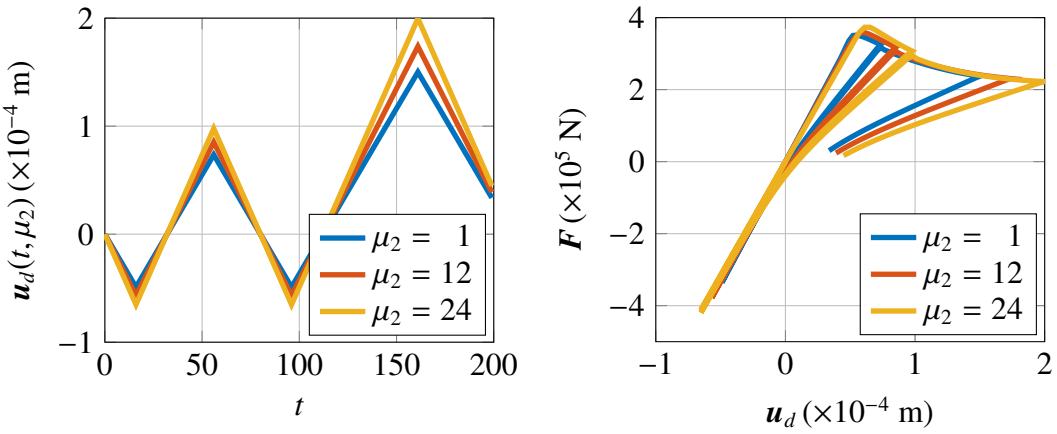

(a) Prescribed displacement particularized for three values of μ_2

(b) Mechanical response for three values of μ_2

Figure 4.3: Tensile test – $\boldsymbol{F}(\boldsymbol{u}_d)$ for several values of parameter μ_2

The first four spatial modes of the decomposition (4.2) are given on Fig. 4.4. One can notice that the more iterations, the more the modes localize and add specific information to certain areas. The parameter functions are given on Fig. 4.5a and 4.5b. The same remark can be done for the time functions, for which the information is added at instants during which the magnitude of the prescribed displacement is the most important. On the other hand, no specific indication can be deduced from the functions $a^2(\mu_2)$ as they are mostly linear. This can be explained by the fact that the parameter only affects the amplitude of the loading, and as a consequence the amplitude of the damage areas, which stays localized to the same zones. The damage patterns are then relatively similar from one value of μ_2 to another, which would not be the case if μ_2 affected the localization of the zone of enforcement of the prescribed displacements.

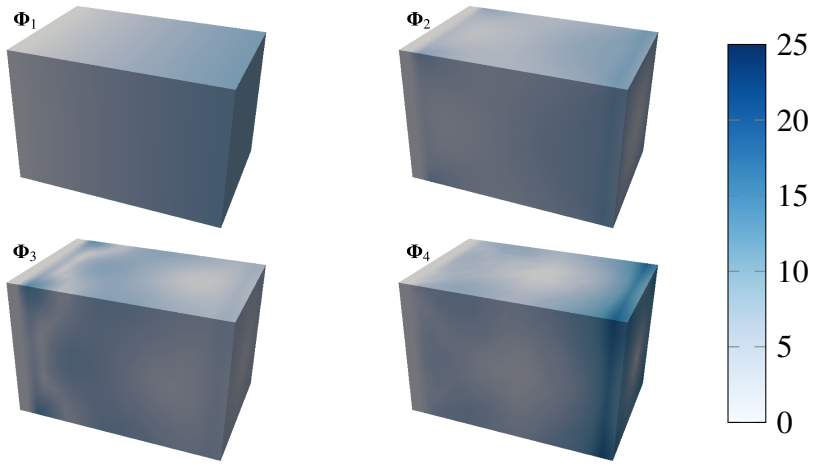

Figure 4.4: Tensile test – magnitude of the first four spatial modes $\{\boldsymbol{\Phi}_i\}_{i=1\cdots4}$

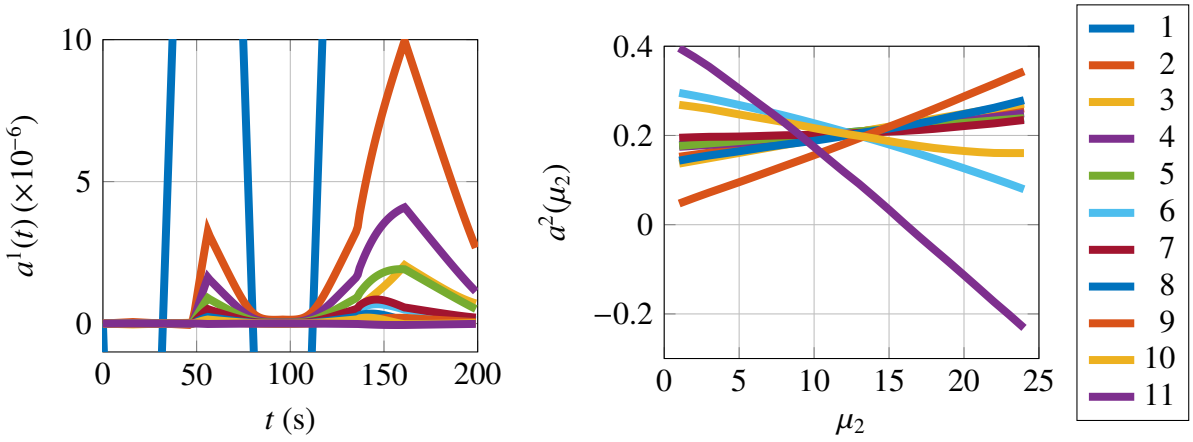

(a) Time functions $\{a_i^1(t)\}_{i=1\cdots11}$ (b) Functions associated with parameter μ_2 $\{a_i^2(\mu_2)\}_{i=1\cdots11}$

Figure 4.5: Tensile test – parametric functions $\{a_i^1(t)\}_{i=1\cdots11}$ (left) and $\{a_i^2(\mu_2)\}_{i=1\cdots11}$ (right)

Finally, Fig. 4.6 shows the evolution of the $\mathcal{L}^2$ norm of the time functions (and as a consequence the norm of the PGD modes as the other functions are normalized during the Gram-Schmidt orthonormalization phase). One can observe that the norm of the modes decreases rapidly with the iterations until reaching ς_{crit} after only 11 iterations.

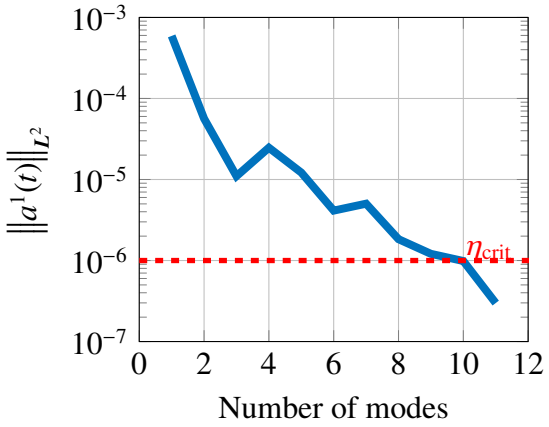

Figure 4.6: Tensile test – evolution of the $\mathcal{L}^2$ norm of the time functions with the number of modes in the decomposition

The results shown in this section highlight the fact that only a few modes were necessary to recover the local and global behavior of the structure, with both a complex model and a strong variability on the loading conditions. Whereas the first modes tend to represent the global elastic response of the medium, the more iterations and the more the modes tend to locally improve the solution in order to represent the very localized nonlinear phenomena.

The following section shows results on a rather more complex test case for which a variability is enforced on both material and loading parameters.

2 Case 2 – 4-points bending test

The goal of this second example is to simulate the response of a reinforced concrete beam, which geometry is given on Fig. 4.7, to a 4-points bending test (see Fig. 4.8 for a picture of an experiment at LMT, courtesy of A. Michou).

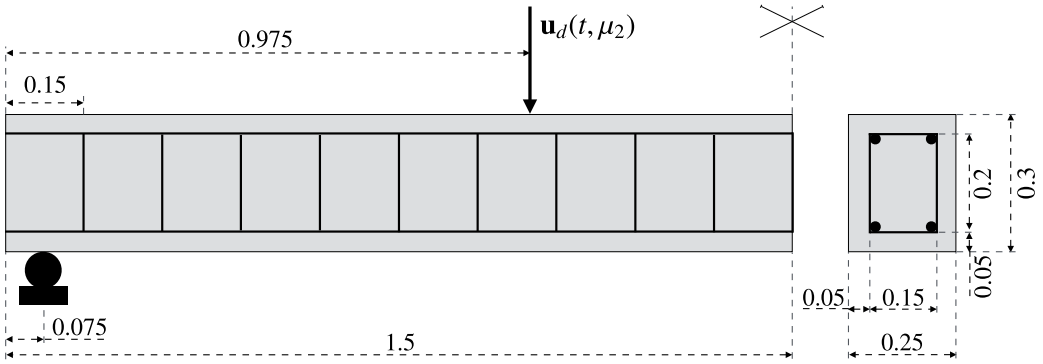

Figure 4.7: Bending test – longitudinal (half representation, left) and transversal (right) geometry of the reinforced beam (in m)

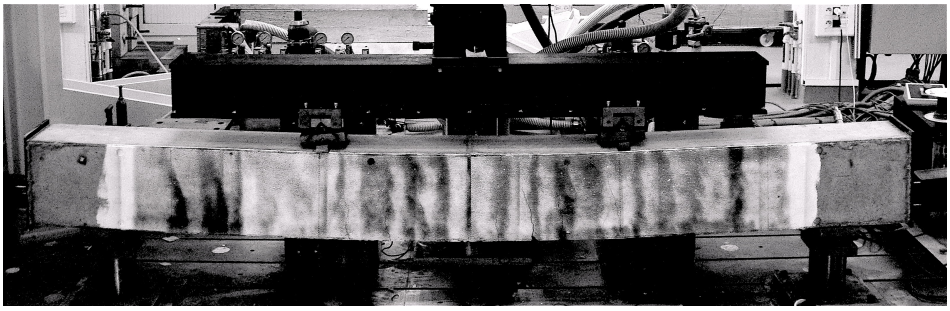

Figure 4.8: 4-points bending test at LMT (courtesy of A. Michou)

The discretization of the specimen as well as the parametric spaces is given in Tab. 4.4 and the boundary conditions are enforced over a band of elements along the width of the specimen (in red on Fig. 4.9).

The prescribed displacement $\mathbf{u}_d(t, \mu_2)$ is parameterized by a variable μ_2, with a variability of $+/-$ 30% which affects once again its amplitude using a law similar to the one presented in the first section (4.1) (but for which the maximum value of the prescribed displacement is set to 0 – see Fig. 4.10 for its particularization for three values of μ_2). The Young modulus of the concrete medium is also parameterized with a variable μ_3 affecting its mean value, with a variability of $+/-$ 15% around its mean value ($E^c \in [21.61, 29.23]$ GPa). The following

Table 4.4: Discretization of the second example

Variable space		Interval of variation – discretization
$\boldsymbol{\Omega}$	Space – concrete	3, 157 nodes, 2, 400 elements (9, 471 DOFs, 19, 200 GPs)
	Space – reinforcement	160 nodes, 232 elements (480 DOFs, 232 GPs)
$\mathbf{D}_1 \equiv \mathfrak{I}$	Time	$\mu_1 \equiv t \in [0, 99]$ (100 time steps)
$\mathbf{D}_2$	Loading variability	$\mu_2 \in [1, 12]$ (12 values)
$\mathbf{D}_3$	Young modulus variability	$\mu_3 \in [0.85, 1.15]$ (9 values)

chart was then computed:

$$\boldsymbol{u}_m(\boldsymbol{x}, t, \boldsymbol{u}_d(\mu_2), E^c(\mu_3)) = \sum_{i=1}^{m} \boldsymbol{\Phi}_i(\boldsymbol{x})\, a_i^1(t)\, a_i^2(\mu_2)\, a_i^3(\mu_3) \tag{4.3}$$

This example is more complex due to the strong variability on both material and loading parameters (especially for bending tests), which leads to more complex distributions of damage and stresses over the structure.

It enables to show the possibilities of the algorithm and especially the advantage of using a space-parameters PGD decomposition: on the one hand, it reduces the cost (both CPU and memory usage) of the linear problem, and it makes the post-treatment of the solution (visualization of global responses, but also computation of other local quantities of interest) quicker and interactive, thanks to the PXDMF plug-in.

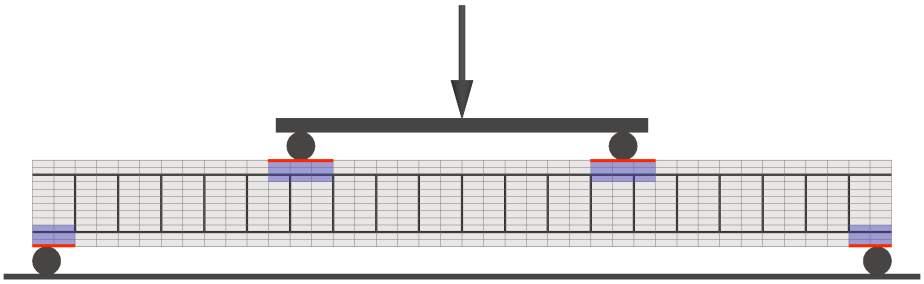

Figure 4.9: Bending test – boundary conditions (red) and elastic boxes (blue)

Some space modes, time and parameter functions of the decomposition (4.3) are respectively given on Figs. 4.11 and 4.12. Concerning the space modes, one can once again notice that the modes are more and more local showing that the approximation is progressively locally enriched with the number or iterations. Note that the focus has been made on Fig. 4.12a on the higher-order functions to show that once again those functions add corrections at time steps when damage occurs: when the load exceeds the value of the initial threshold during the first cycle (for example around $t = 10$s), or when the load exceeds the peak from the previous cycle (around $t = 40$s or $t = 90$s). The other parameter functions remain relatively smooth,

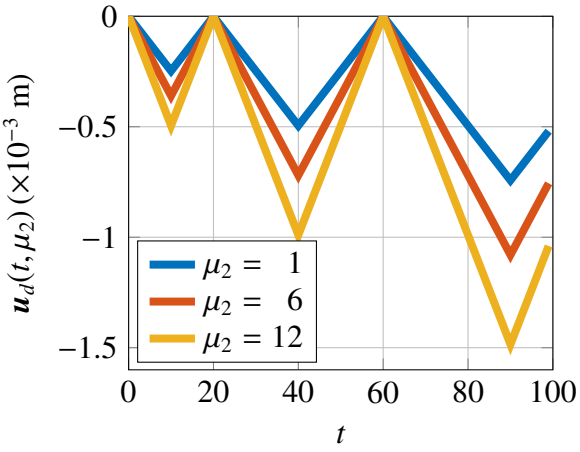

Figure 4.10: Bending test – variability on the prescribed loading $\boldsymbol{u}_d(t,\mu_2)$ for several values of parameter μ_2

as the variability on the loading seems to have a more important influence on the response.

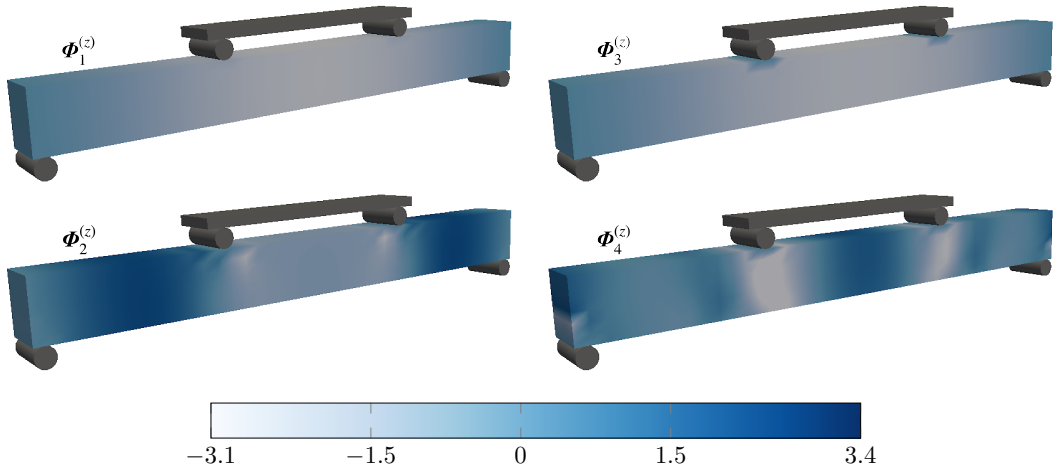

Figure 4.11: Bending test – z component of the spatial modes $\{\boldsymbol{\Phi}_i\}_{i=\{1,3,5,7\}}$ ($\boldsymbol{\Phi}_i^{(z)} = \boldsymbol{\Phi}_i \cdot z$)

Fig. 4.13 shows the particularization of the damage map for three given sets of parameters $\boldsymbol{\mu}_i = \{t^j, \mu_2^k, \mu_3^l\}_{i=1\cdots 3}$. One can notice the strong influence of the parameters μ_2 and μ_3 on the mechanical response of the beam, with more or less wide damaged zones depending on the sets of parameter. Once again, this reconstruction can be achieved really easily and quickly once the virtual chart is built thanks to the ParaView [Ayachit, 2015] PXDMF reader developed at École Centrale de Nantes[1], which recombines on the fly the different modes

[1] `https://rom.ec-nantes.fr/`

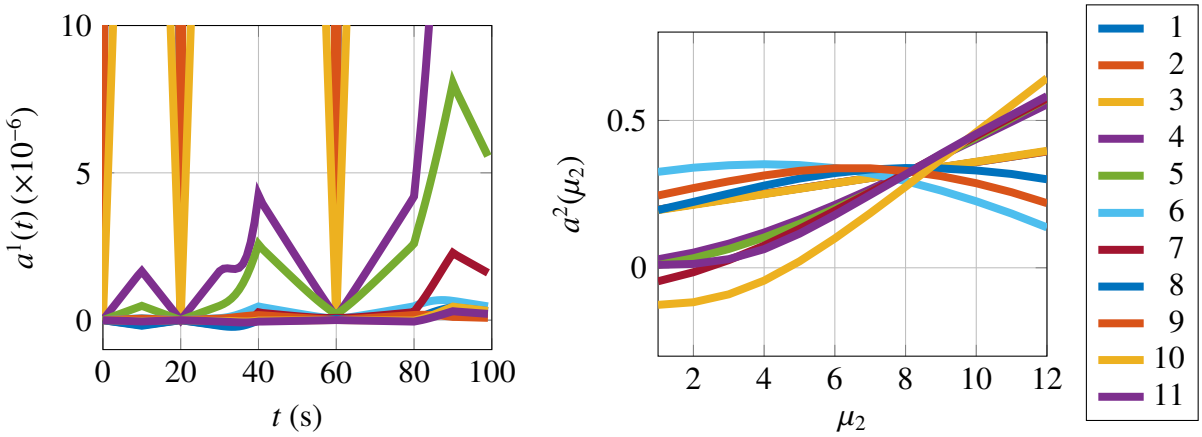

(a) Time functions $\{a_i^1(t)\}_{i=1\cdots11}$

(b) Functions associated with parameter μ_2 $\{a_i^2(\mu_2)\}_{i=1\cdots11}$

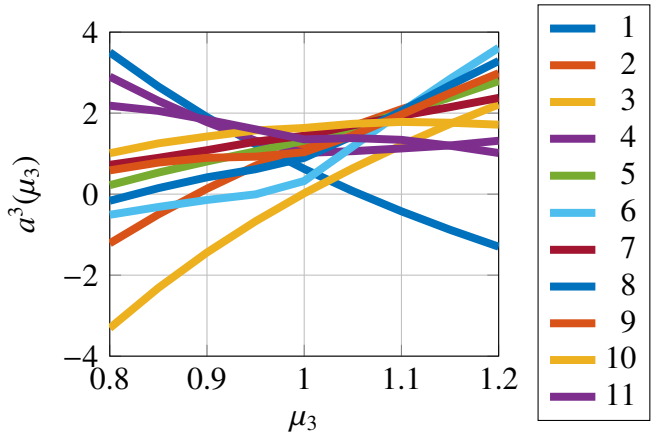

(c) Functions associated with parameter μ_3 $\{a_i^3(\mu_3)\}_{i=1\cdots11}$

Figure 4.12: Bending test – parametric functions $\{a_i^1(t)\}_{i=1\cdots11}$ (Fig. 4.12a), $\{a_i^2(\mu_2)\}_{i=1\cdots11}$ (Fig. 4.12b) and $\{a_i^3(\mu_3)\}_{i=1\cdots11}$ (Fig. 4.12c)

(depending on the user-chosen values of parameters) in order to assemble the particularized solution.

This finding is verified on a more local scale: Fig. 4.14 shows the evolution of the Mises stress σ_{VM} within an element of the damaged area for the different sets of parameters (μ_2, μ_3). Finally, one can notice on Fig. 4.15 the overall decrease of the norm of the modes along with the number of iterations.

Once again, only a few (11) iterations were necessary to compute the solution of a 4-points bending test on a reinforced concrete beam, with a variability on the amplitude of the prescribed displacement and on the Young modulus of the concrete medium. The use of PGD in this context is especially interesting as it lowers the cost of the linear stage of the problem, as well as it enables to easily compute local quantities of interest (here the Mises stress), which can be very quickly updated when changing the values of the parameters $\boldsymbol{\mu}$.

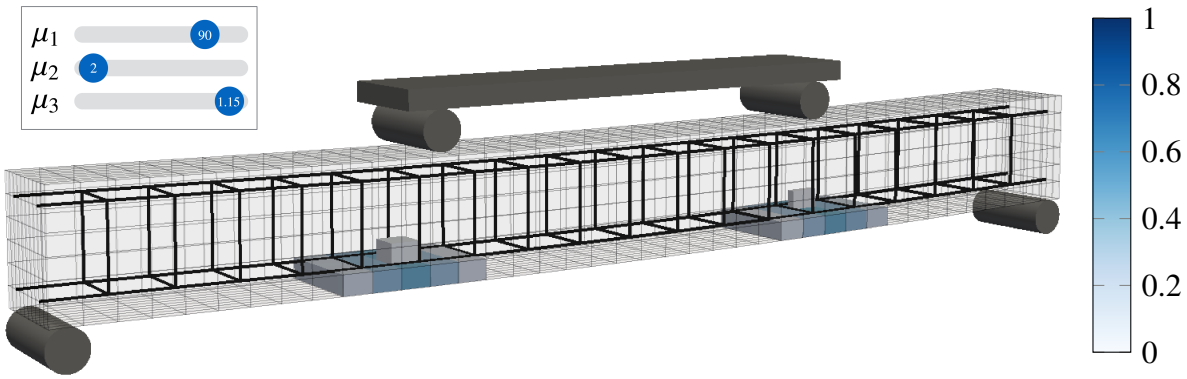

(a) Damage map for $\mu_1 = 90$, $\mu_2 = 2$ and $\mu_3 = 1.15$

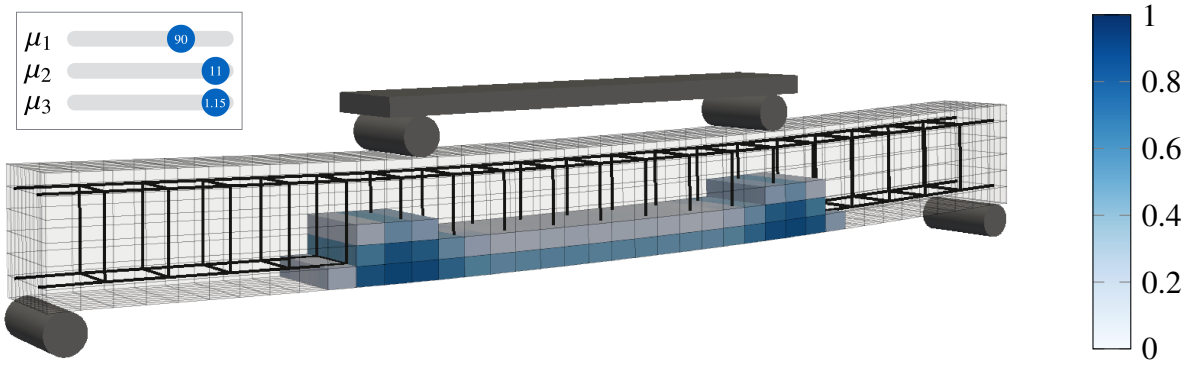

(b) Damage map for $\mu_1 = 90$, $\mu_2 = 11$ and $\mu_3 = 1.15$

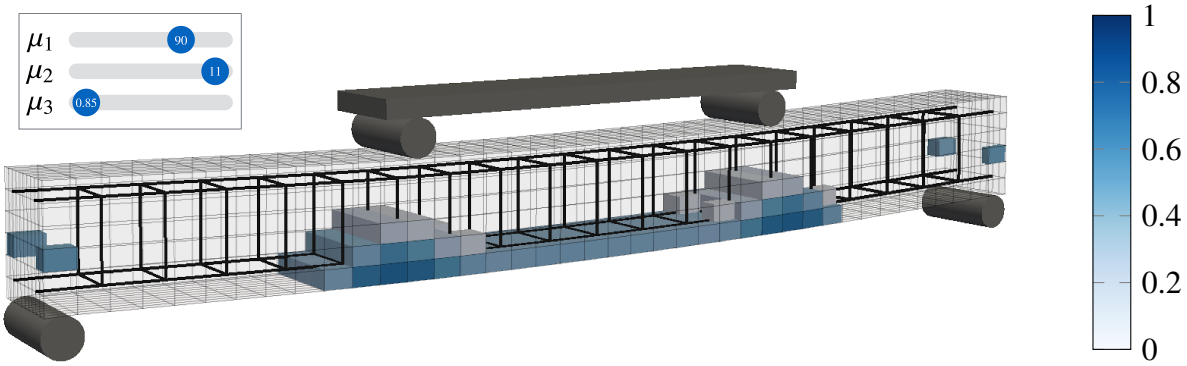

(c) Damage map for $\mu_1 = 90$, $\mu_2 = 11$ and $\mu_3 = 0.85$

Figure 4.13: Bending test – damage map for three particularized cases: (a) $(90, 2, 1.15)$; (b) $(90, 11, 1.15)$; (c) $(90, 11, 0.85)$

3 Case 3 – *SMART testing* project at LMT

The *SMART testing* project aims at studying the behavior of reinforced concrete beam–column assemblies (see Fig. 4.16) under complex simulations. Those assemblies are considered as one of the most critical zones in the dissipation of seismic energy, and can face

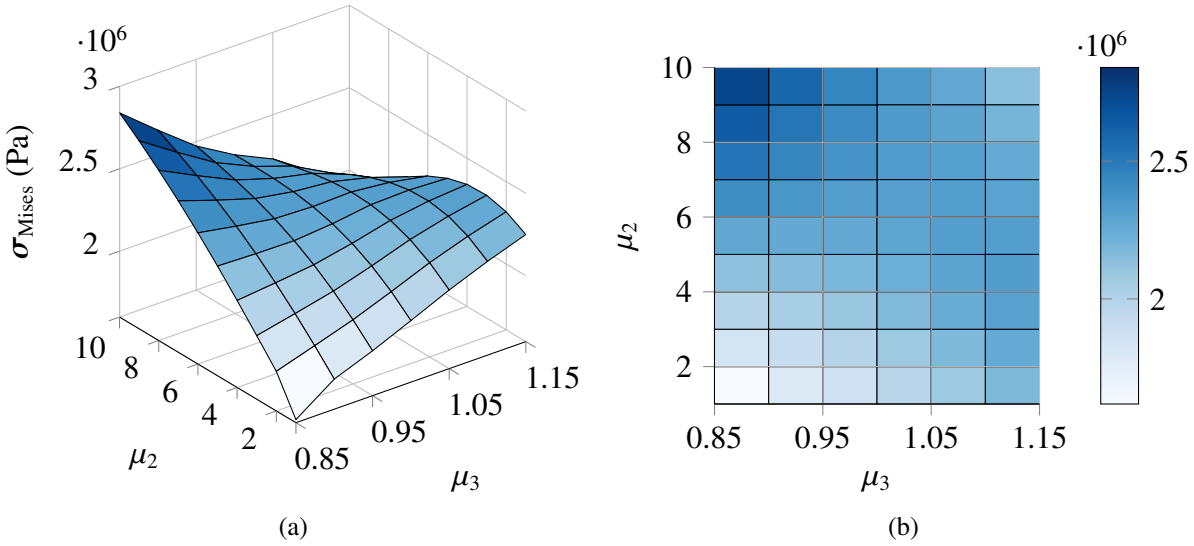

Figure 4.14: Mises stress on an element – response surface (4.14a) and projection (4.14b)

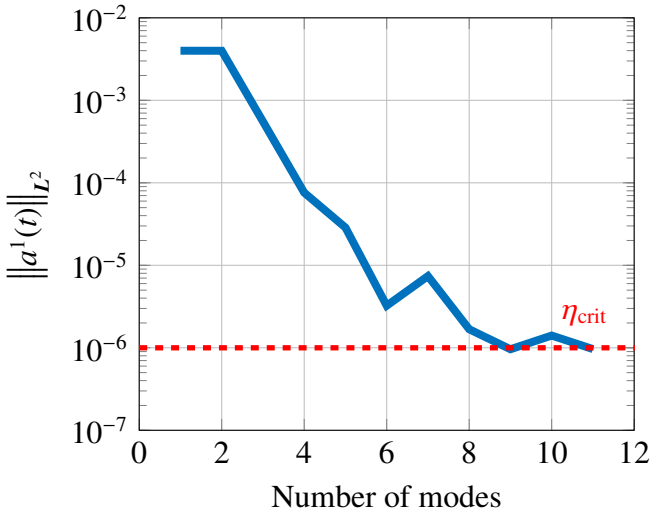

Figure 4.15: Bending test – evolution of the $\mathcal{L}^2$ norm of the time functions with the number of modes in the decomposition

different crushing mechanisms, due to the bending or shearing of the beam, to the bending or shearing of the column, to the shearing at the node, or a combination those different modes. The experiment was carried out at LMT during A. E. Iskef's PhD in 2015–16. The extremity of the column not attached to the beam is put inside a hexapod device, which is able to prescribe 6-DOFs displacements at the extremity of the column (see Fig. 4.17a). A load cell measures the reaction force at the hexapod–column interface and the displacement field is measured using digital image correlation [Sutton, 2013]. The geometry of the specimen is given on Fig. 4.16 and the meshes for the concrete and its reinforcement are given on Fig. 4.18. The discretization of the problem is given in Tab. 4.5.

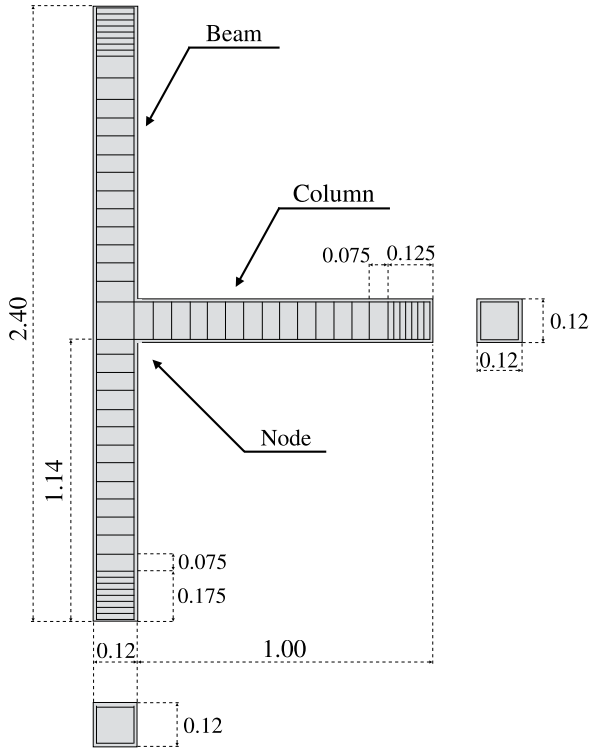

Figure 4.16: Beam–column assembly – geometry (in meters)

(a) *SMART testing* project experiment

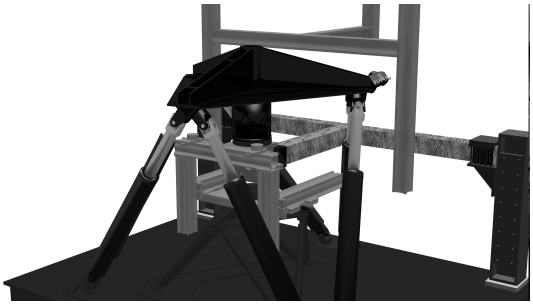

(b) Virtual representation

Figure 4.17: *SMART testing* project – experiment (top) and virtual representation (bottom)

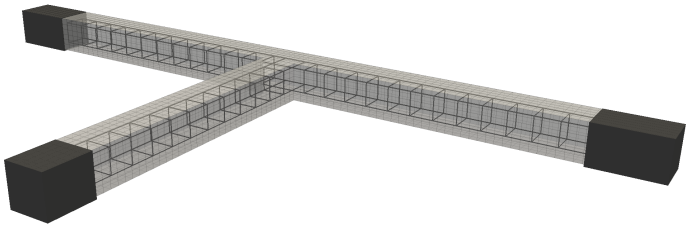

Figure 4.18: Beam–column assembly (in black the casks for the application of the prescribed displacements)

Remark. It has to be mentioned that I am also involved in this project for the virtual preparation of the testing, as shown on Fig. 4.17b. The goal of this aspect of the project is to use rendering softwares (in our case Blender[2]) to simulate the cameras (both specifications and positions) that will be used for the digital image correlation procedure, especially for such complex testing procedures involving up to 12 cameras and for which the set up can be very time-consuming.

[2] `https://www.blender.org`

Table 4.5: Discretization of the third example: *SMART testing* beam–column specimen

Variable space		Interval of variation – discretization
$\boldsymbol{\Omega}$	Space – concrete	6,860 nodes, 5,004 elements (20,580 DOFs, 40,032 GPs)
	Space – reinforcement	1,248 nodes, 1,476 elements (3,744 DOFs, 1,476 GPs)
$\mathbf{D}_1 \equiv \mathfrak{I}$	Time	$\mu_1 \equiv t \in [0, 260]$ (261 time steps)
$\mathbf{D}_2$	Post-peak variability	$\mu_2 \in [0.1, 1]$ (19 values)

[Iskef, 2016] presents experimental results for 3 phases of loading conditions. The first phase consists on a prescribed in-plane bending displacement of the extremity of the column, while the extremities of the beam are fixed, and for which the amplitude of the loading increases with the time, as shown on figure 4.19. The second and third loading phases are more complex as the prescribed displacement of the column's extremity follows a 2-D off-plan path.

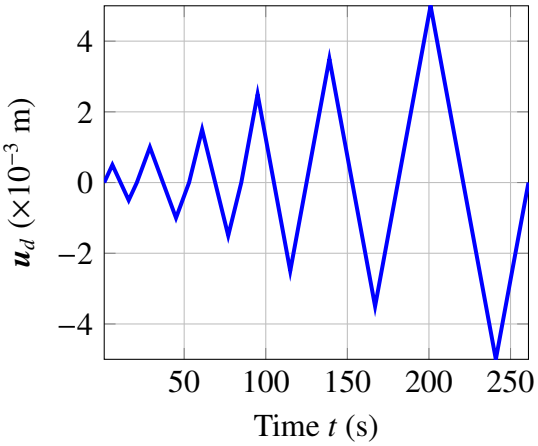

Figure 4.19: SMART testing – loading phase 1

In this section, only the first phase of the loading will be considered. A variability of the brittleness coefficient A_d, parameter which drives the post-peak behavior (highly nonlinear) during the softening part of the behavior, is assumed such that $A_d = A_d(\mu_2)$. This example is complex in a sense than the parameter μ_2 directly affects the nonlinearity of the problem (see Fig. 4.20). The following database was computed:

$$\boldsymbol{u}_m(\boldsymbol{x}, t, A_d(\mu_2)) = \sum_{i=1}^{m} \boldsymbol{\Phi}_i(\boldsymbol{x})\, a_i^1(t)\, a_i^2(\mu_2) \tag{4.4}$$

Fig. 4.21 shows the damage map for three values of the parameter μ_2. The first thing to notice is that two zone are mostly damaged during the process. The node of the assembly is particularly affected during the loading. Another area, close to the in-hexapod cask (right

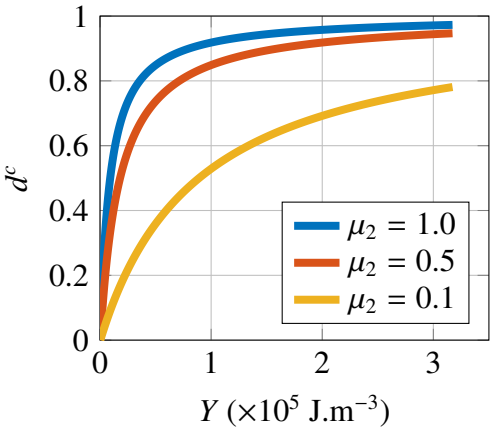

Figure 4.20: Evolution of damage d^c with the energy rate Y for different values of μ_2

part of the column), is also damaged. this is due to the rigid motion imposed to the casked elements that tends to create a high strain zone. This area may not exist during a real test as the boundary conditions are not perfect, and may allow rotations within the casks.

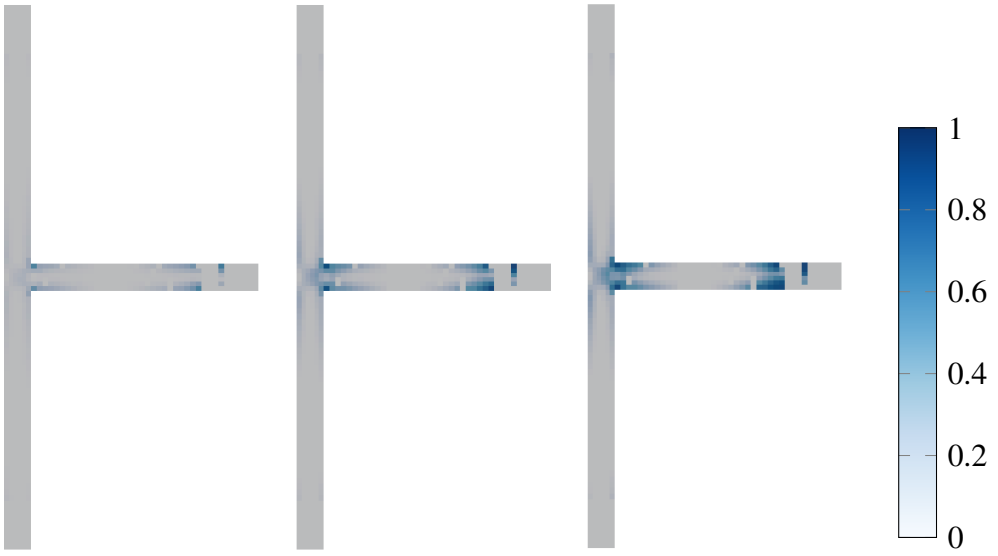

Figure 4.21: Post-treatment of the damage field for three values of $\mu_2 = 0.2$ (left), $\mu_2 = 0.4$ (center) and $\mu_2 = 0.8$ (right) at a given time step

One can also see that the damage zones are broader with the increase of the value of the parameter, as the behavior shifts to a very brittle configuration (see Fig. 4.20). This can be seen on Fig. 4.22 which gives a closer view on the node of the beam–column assembly. One can once again see the evolution of the damage pattern, similar to the one presented in [Iskef, 2016] for the Damage TC model [Costa et al., 2005] (which unlike our model considers two damage variables, one in tension and one in compression), as shown on Fig. 4.23 (which was however obtained for a more intense cyclic prescribed displacement –20 mm peak).

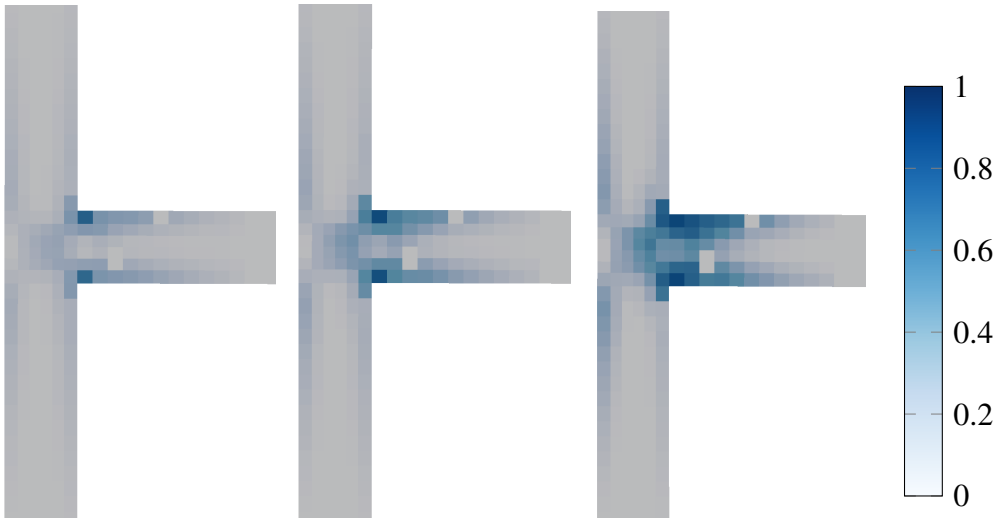

(a) $\mu_2 = 0.2$ (b) $\mu_2 = 0.4$ (c) $\mu_2 = 0.8$

Figure 4.22: Post-treatment of the damage field for $\mu_2 = 0.2$ (left), $\mu_2 = 0.4$ (center) and $\mu_2 = 0.8$ (right) – close-up view on the beam–column node

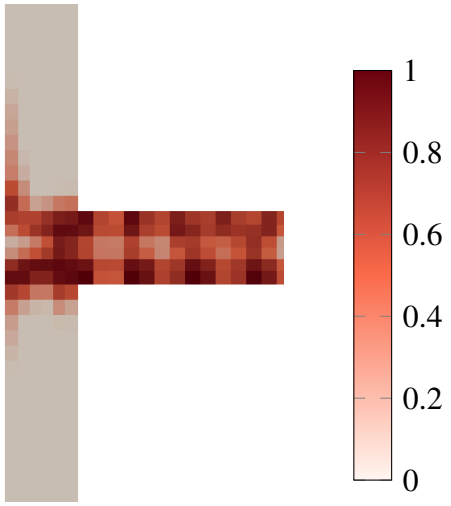

Figure 4.23: Damage field computed with the *Damage TC* model – close-up view on the beam-column node (courtesy of A. E. Iskef)

Figs. 4.25 and 4.24 respectively show spatial functions and the parametric functions of the decomposition (4.4). One can notice once again the three behaviors encountered for the first examples along the enrichment of the reduced order basis: (i) the spatial modes localizes the information to the more damaged zones. This comes from the fact that, starting from an elastic behavior (initialization), the strains (and as a consequence damage) concentrates in certain areas, the node for example, whereas the rest of the beam goes under an elastic unloading. This concentration increases along the iterations (progressive localization to several

areas); (ii) this correction is mostly achieved once again at the peaks of loading, as shown in Fig. 4.24a; (iii) the other parametric function modulates relatively smoothly the approximation.

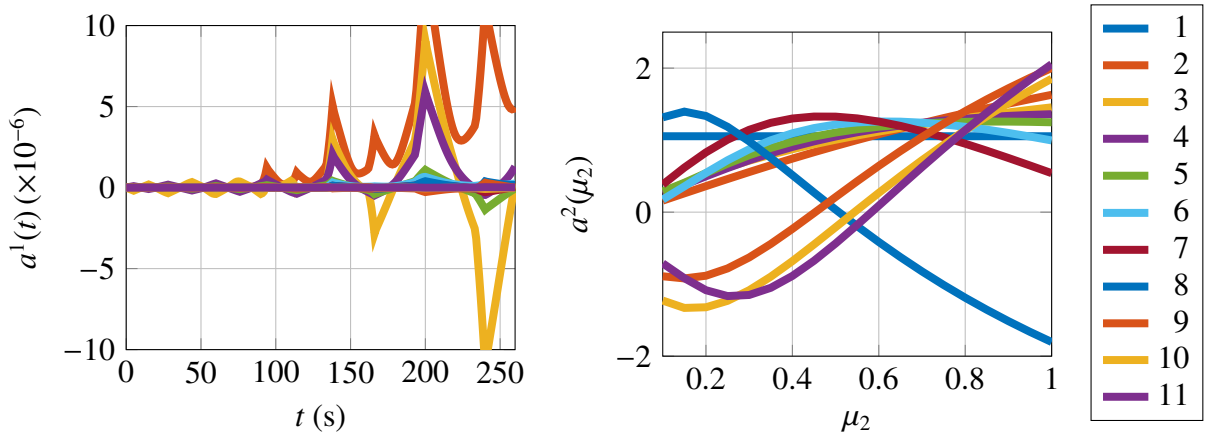

(a) Time functions $\{a_i^1(t)\}_{i=2\cdots11}$

(b) Functions associated with parameter μ_2 $\{a_i^2(\mu_2)\}_{i=1\cdots11}$

Figure 4.24: *SMART testing* test – parametric functions $\{a_i^1(t)\}_{i=2\cdots11}$ (left) and $\{a_i^2(\mu_2)\}_{i=1\cdots11}$ (right)

We showed in this example the ability to recover the damage patterns at the node of the beam–column assembly with a few iterations, with a variability on a parameter directly affecting the nonlinear part of the behavior law. This variability induces a local mechanical response that switches from a softening to a quasi-brittle behavior. This can be especially useful to determine the parameter A_d, which has to be identified during experiments.

4 Performances of the algorithm

Evaluating the performances of this algorithm is not an easy task, first because high performance computing has never been the goal of our study, which was to show the feasibility of the extension of the LATIN algorithm more than its efficiency compared to other solutions. However, some work has been done to improve some steps of the computation, especially using the parallel-processing options of Matlab. As a consequence, this section does not intend to compare the CPU cost of our method compared to other techniques (which is quite user-dependent) but rather to profile our algorithm and propose some improvements to be made for further HPC developments that could be done if implemented into an industrial code. For each test, 5 runs were made and the elapsed time of the different stages was averaged over those runs. Note that neither the pre-process (assembly of the FEM operators, boundary conditions, ...) nor the post-process (*.vtu* or *.pxdmf* exports) was taken into account. Three tests have been carried out as described in Tab. 4.6.

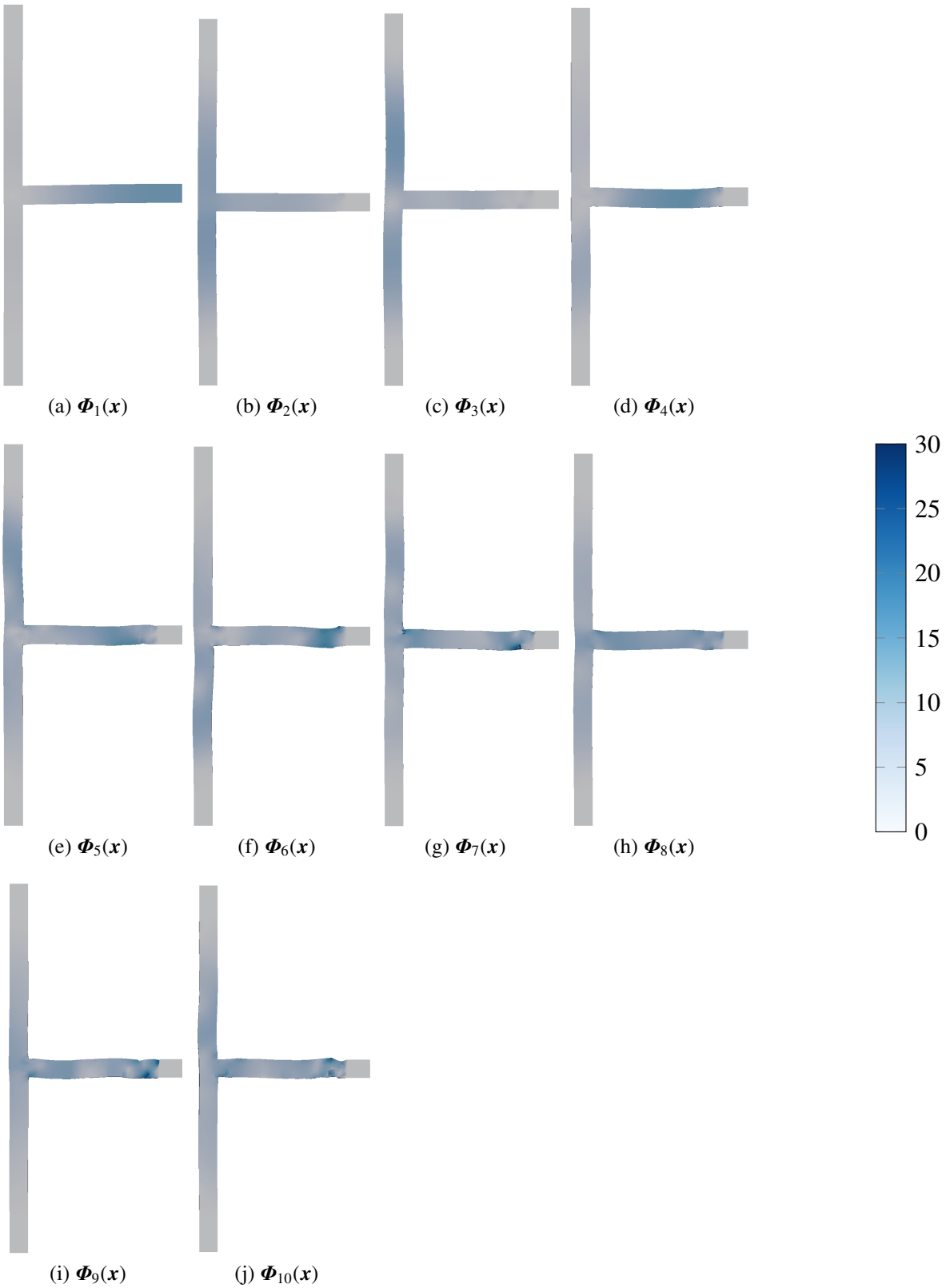

(a) $\boldsymbol{\Phi}_1(\boldsymbol{x})$ (b) $\boldsymbol{\Phi}_2(\boldsymbol{x})$ (c) $\boldsymbol{\Phi}_3(\boldsymbol{x})$ (d) $\boldsymbol{\Phi}_4(\boldsymbol{x})$

(e) $\boldsymbol{\Phi}_5(\boldsymbol{x})$ (f) $\boldsymbol{\Phi}_6(\boldsymbol{x})$ (g) $\boldsymbol{\Phi}_7(\boldsymbol{x})$ (h) $\boldsymbol{\Phi}_8(\boldsymbol{x})$

(i) $\boldsymbol{\Phi}_9(\boldsymbol{x})$ (j) $\boldsymbol{\Phi}_{10}(\boldsymbol{x})$

Figure 4.25: Magnitude of the space modes $\{\boldsymbol{\Phi}_i\}_{i=1\cdots10}$

Table 4.6: Profile test cases – dimension of the domains

	#elements (#Gauss points)	$\mu_1 \equiv t$	μ_2	μ_3	#CPUs
(1)	c: 360 (2, 280) r: 112 (112)	[0, 99] (100 val.)	[1, 12] (12 val.)	[0.8, 1.2] (9 val.)	1
(2)	c: 360 (2, 280) r: 112 (112)	[0, 99] (100 val.)	[1, 12] (12 val.)	[0.8, 1.2] (9 val.)	12
(3)	c: 2400 (19, 200) r: 232 (232)	[0, 99] (100 val.)	[1, 12] (12 val.)	[0.8, 1.2] (9 val.)	12

The first one associated with a first mesh was run for 3 parameters without enforcing the parallelization of the code. The overall profile of the LATIN–PGD algorithm is given in Fig. 4.26. The linear stage is decomposed into the update phase and the enrichment step (Fig. 4.26b). This computation is time-consuming as the local problem, even though the model is explicit, has to be computed at each Gauss point and for each value of parameters.

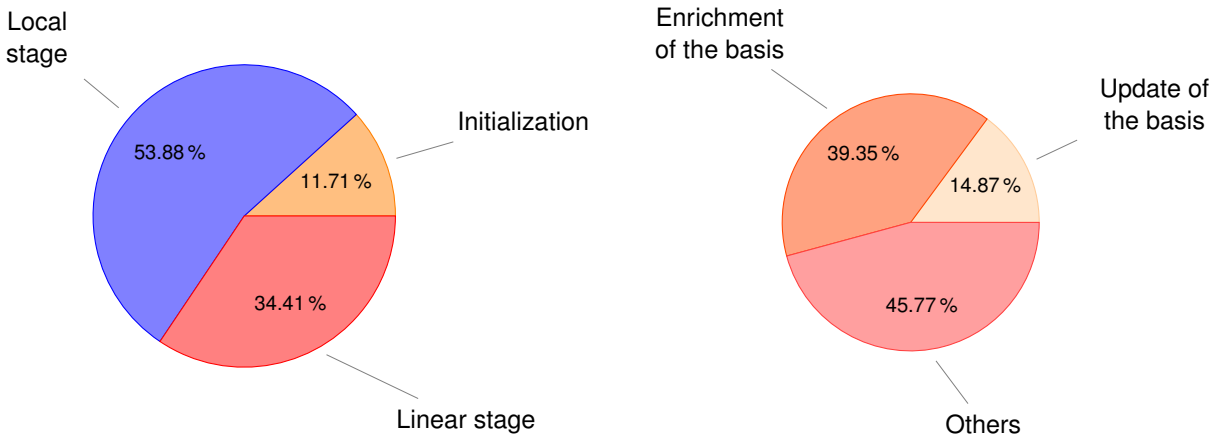

(a) Profile of the stages of the LATIN-PGD algorithm

(b) Detailed profile of the linear stage

Figure 4.26: Profile of test (1) (serial) (Fig. 4.26b details the linear stage)

The second example was carried out on the same mesh, but the parallelization of the process is enforced. This parallelization is particularly easy to implement as the parameters are independent one another and the model is local. It is to be mentioned that even if only the initialization and local stages are explicitly parallelized (using the *parfor* option), some other processes are "naturally" parallelized by Matlab. The profile associated with those runs is given on Fig. 4.27. One can notice that the division is quite similar for those two runs, especially when looking at the detailed profile of the linear stage (Figs. 4.26b and 4.27b).

However, the average time of the first (sequential) run was 4, 320 seconds, whereas the total time for the second run (parallelized over 12 cores) was 371 seconds, which means a speedup of 11.6.

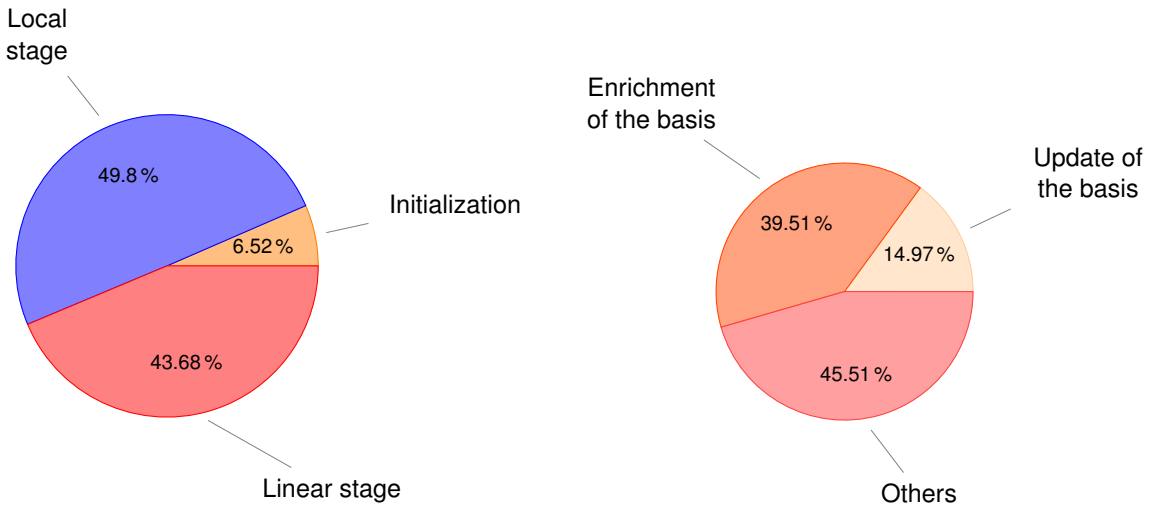

(a) Profile of the stages of the LATIN-PGD algorithm

(b) Detailed profile of the linear stage

Figure 4.27: Profile of test (2) (parallel) (FIG. 4.27b details the linear stage)

Finally, the last test was carried on a larger mesh. One can notice that the bigger (in terms of number of DOFs or GPs) the mesh gets the more expensive the linear stage becomes, especially the enrichment phase (generation of a new mode) which becomes more expensive as the spatial problem (resolution of a linear system, of size number of DOFs) is more heavy to solve in the fixed-point algorithm.

Those results highlight two issues: (i) the parallelization of the algorithm drastically reduces the computation cost associated with the resolution of the nonlinear problem and the construction of the approximation of the solution fields; (ii) the generation of the PGD modes becomes heavier with the size of the mesh, due to the resolution of a linear system in the fixed-point algorithm.

This parallelization could be enforced at deeper levels depending on the application, at every Gauss point of the local stage for example. This however requires a better parallel infrastructure than the one offered by Matlab and the integration into an industrial software should be considered to do so (for example in the Cast3M of CODE_ASTER codes)

Another interesting study would be to compare our method with the multi-parametric strategy, especially for the second test case (bending test), as it faces the strongest variability.

5 To put it in a nutshell ...

We presented in this chapter some numerical results computed thanks to the ROMlab demonstrator developed during this thesis (Matlab code relying on the *Tensor toolbox* [Bader and

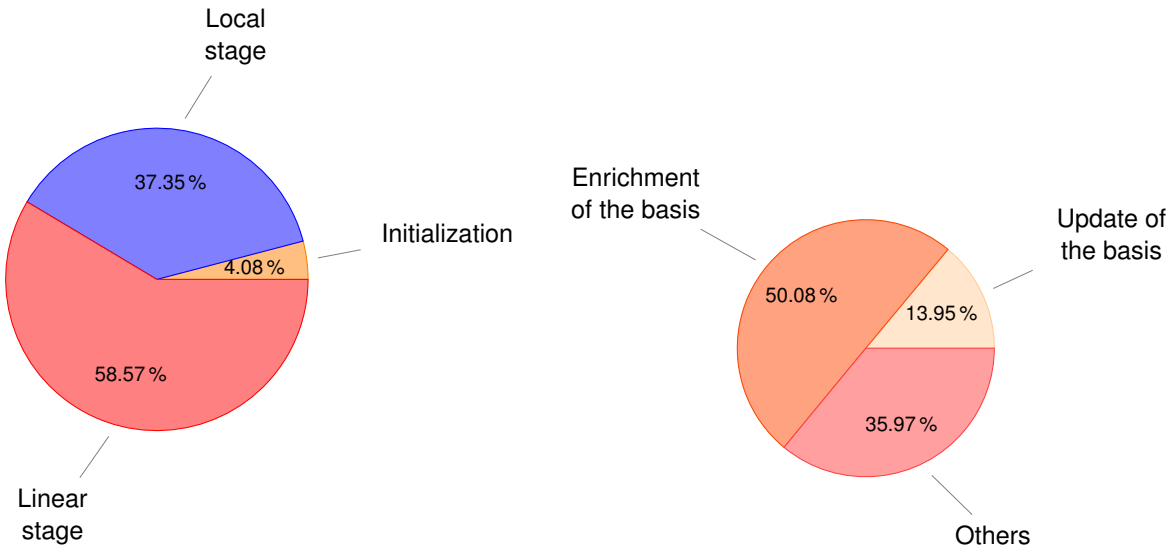

(a) Profile of the stages of the LATIN-PGD algorithm

(b) Detailed profile of the linear stage

Figure 4.28: Profile of test (3) (parallel) (FIG. 4.28b details the linear stage)

Kolda, 2007]). Those examples show the possibility to simulate reinforced concrete media with a highly nonlinear behavior, in a framework that enables an easy post-treatment of the database (thanks to the PXDMF plug-in). Different kinds of material and loading variabilities have been considered on structures of the size of a toy example to the size of industrial applications. In every case, about a dozen iterations were necessary to reach the stopping criterion.

We also showed in this chapter that the numerical cost associated with the computation of the database can be reduced by parallelizing the process, with in this particular case a really high scalability. However, some limits may occur when the number of degrees of freedom increase, mostly linked to the memory required to store some of the quantities computed at the local stage. Different ways to tackled this problem can be considered: (i) using CP-decompositions of those quantities; (ii) the RPM method could be used to approximate those operators; (iii) a PGD formulation of the local problem would both reduce the computation cost of this stage, but would also accelerate the resolution of the linear stage as most of the operations to be performed (integrations, Galerkin projections, ...) would be done in a separated representation framework.

Conclusion

The increasing complexity of numerical simulations led researchers to find more efficient tools able to solve quickly and accurately those problems. Among those issues, the case of parametric studies is an interesting one as it requires the resolution of the same physical model for numerous different sets of parameters of this model. A class of methods that has grown over the last decades and that has risen our interest in the work presented herein is the model-order reduction methods, based on the separation of the variables of the problem. Among those approaches, the proper generalized decomposition has shown interesting results as, unlike the other strategies, it does not require any pre-computed reduced-order basis to build the approximation, as the latter is constructed by successive enrichments over an iterative process. The application of such approaches to civil engineering problems is fairly new, mostly because, alone, those methods can not tackle the nonlinearity of the equations of the physical models at stake. To do so, PGD has to be coupled with a nonlinear solver, in our case the LATIN method. LATIN–PGD algorithms have been used for a couple of decades for numerous fields of applications, with for example interesting results for modeling the behavior of elasto-visco-plastic materials.

We proposed in this work the extension of the classical LATIN–PGD algorithm, relying on a time-space decomposition of the unknown fields, to a wider parametric dependency, where the parameters are all considered as coordinates of the quantities of interest. Algorithmic developments have been proposed and applied to a damage mechanics model, involving damage in tension and crack closure (unilateral effect) in compression. The main differences with the classical algorithm are the following: (i) the local stage of the LATIN method has to be solved for all the discrete values of parameters, at every Gauss point. It was shown that in our case, mostly due to the fact that the equations are local and because the formulation of the damage model is explicit, that the process can numerically be extensively parallelized with a high speedup; (ii) different methods for the generation of the new modes have been proposed, using high-order tensor decompositions. The field of application is also fairly new in this context, as several numerical results have been presented on a damage mechanics problem, involving strong local nonlinearities due to the quasi-brittle behavior of the concrete medium and the crack closure phenomenon. The first study was a simple tension test on a reinforced concrete beam, with a variability on the amplitude of the prescribed displace-

ment, in order to show the ability to quickly (11 modes) recover the local behavior as well as the global equilibrium of the structure. The second test was a 4-points bending test, for which both the amplitude of the loading and the Young modulus of the concrete medium, to show the ability to build larger databases but also its easy particularization for given sets of parameters thanks to the PXDMF plug-in. The post-process (computation of other quantities of interest, such as the Mises stress) is also much simpler to perform and the study of local quantities of interest has shown the impact of this variability on the mechanical response of the concrete medium. Finally, this method was used to model an industrial-like structure (40k Gauss points), a T-shaped reinforced concrete structure, as the one used in the *SMART testing* project at LMT, for which the brittleness coefficient, driving the post-peak behavior in the damage evolution law, was parametrized.

Those different studies showed the capabilities of the algorithm and provided great indications on the directions to take to improve the method: only a few iterations (however costly for our Matlab demonstrator) were necessary to reach the stopping criterion. Once computed, this database can be easily particularized or post-processed (computation of Mises stress, optimization studies, ...) and can be enriched once again if necessary by re-initializing the LATIN-PGD algorithm with the previously converged solution, which can be seen as an extension of the multi-parametric strategy.

However, some limits arose and must be mentioned: (i) the cost associated with the resolution of the local problem, which – if no special technique is used – increases exponentially with the number of parameters of the formulation. We showed however that this cost can be reduced by using HPC techniques, and such result is extremely encouraging for a future implementation in industrial parallel codes, but assembly of large operators is still required; (ii) the lack of guaranteed error indicators, taking into account both the error linked to the reduced-order modeling but also to the local phenomena that may occur (strain and damage concentrations, ...), is probably the biggest drawback of this approach. The extension of classical LATIN indicators to numerous parameters is not possible as it is computationally very expensive. In the particular case of damage mechanics, estimators based on the local quantities as well as the global response of the structure should be investigated.

From these observations, the prospects of this work are numerous, and can be separated according to their (estimated) complexity.

- The short term prospects deal with the enrichment of the model and the addition of mastered numerical tools to improve the demonstrator. Different approaches can be used to tackle the complexity of the local problem: the reference point method (RPM, [Capaldo, 2015]) can be used to reduce the cost associated with the resolution of the local behavior, as it provides a great framework for dealing with fields depending on many parameters. The enrichment of the model, by taking into account the plasticity in compression of the concrete medium and the elasto-visco-plastic behavior of the reinforcement is also necessary to increase the fidelity of the results. Different sampling techniques on the parametric spaces may also be investigated as a post-treatment of

the computed database of solutions, as the approximation is known for every set of parameters.

- The middle term prospects are more focused on alternate PGD decompositions or ways to deal with the parametric dependency. For example, a formulation based on the decomposition of the damage variable d (instead of $\boldsymbol{u}$) could be investigated, as the value of this quantity of interest (and its post-treatment to obtain the crack opening) drives the dimensioning of the structures. Another extension of the method could lie in a hybrid multi-parametric strategy / "extended" (in the sense of the number of parameters) LATIN-PGD approach, for which the repartition of the overall parameters between both techniques could be done for example in our case depending on the way they may affect the damage pattern: loading parameters –which affect the spatial localization– could be integrated into the PGD decomposition whereas the Young modulus or the brittleness coefficient A_d, which affect the intensity of the damage, could be covered in a MPS framework. PGD-based identification ([Marchand et al., 2015, Nadal et al., 2015, Signorini et al., 2016]) could be interesting as it can be easily implemented once the database is computed. Those procedures usually rely on recurring FE simulations which are not necessary anymore. Also, the computation of sensibility fields (gradients of the quantity of interest with respect to the parameters) is now really easy to achieve thanks to the format of the approximation. For example:

$$\frac{\partial \boldsymbol{u}(\boldsymbol{x},\boldsymbol{\mu})}{\partial \mu_i} = \sum_{k=1}^{m} \boldsymbol{\Phi}_k(\boldsymbol{x}) \frac{\mathrm{d}\, a_k^i}{\mathrm{d}\, \mu_i} \prod_{j=1,\, j\neq i}^{N^p} a_k^j(\mu_j) \tag{4.5}$$

  Some collaborations with the material department at LMT are expected on these aspects, with applications for real-time identification during digital image correlation testings. See also [Passieux and Périé, 2012] for a PGD–DIC algorithm.

- In the long term, more advanced numerical tools have to be developed and coupled with our algorithm to tackle problems linked to simulations involving variabilities on numerous parameters (dozens, hundreds), more complex loading conditions (seismic loading) or application to other fields. Among those possibilities, we consider the following: a full separated-variable decomposition algorithm could be investigated, with a lot of work to be done on the formulation of the local problem. This would however considerably reduce the cost associated with the storage of the local quantities. However, this approach may not be suitable for damage mechanics problems. The extension to the simulation of of the seismic response of structures could be done by considering a synthetic parametric seismic loadings. This aspect will be studied in collaboration with CEA Saclay. The extension of the PGD to a very large number of parameters will be investigated in the PhD of C. Paillet (2016–), in the continuity of his Master's thesis work that I co-supervised. The use of PGD virtual charts, coupled with multi-fidelity optimization algorithms (cokriging, ...) is also an interesting aspect, and will be developed in the PhD of S. Nachar (2016–). The application to the simulation of composite structures would be a great extension. However, while we are "lucky" that

the damage is localized in a low number of areas for our examples, the apparition of micro-damage in composites may be tougher to model as it localizes in numerous areas at the same time. As a consequence, the first PGD modes may not give a relevant idea of the space localization, and a strategy to "kill" the irrelevant modes may need to be implemented. Another important point focuses on error estimators: better error estimators for high-dimensional reduced order models are necessary, in the event the quantities of interest are very local, to validate the quality of the overall approximation. Finally, the implementation into an industrial software is necessary to investigate the possibilities of this algorithm. CODE_ASTER provides a good framework to do so thanks to its *Python* interface. Some ongoing work [Oumaziz et al., 2017] shows interesting results for a non-invasive implementation of the LATIN algorithm for frictional contact with domain decomposition.

Acknowledgment. This work carried out under the SINAPS@ project benefited French funding managed by the National Research Agency under the program "Future Investments" (SINAPS@ Reference No. ANR-11-RSNR-0022).

Appendix A

Regularization methods for fragile media

The non-objectivity of the numerical solutions is a classical problem when simulating the response of fragile media. The loss of ellipticity of the mechanical problem for softening materials, due to the loss of positive-definitiveness of the tangent operator, usually leads to a mesh dependence of the solutions. This fact can be easily illustrated on a simple 1-D homogeneous concrete beam problem in tension, solve using finite elements: let us consider two different discretization of the medium, one coarser than the other. For each problem, numerical approximations will simulate a defect on one element which will initiate the damage after a certain load is reached. Whereas the damage value will increase on this element, the rest of the beam will undergo an elastic unloading. In both cases, only one element will damage but the dissipated energy, linked to the size of the finite element mesh, will be different, as illustrated on FIG. A.1.

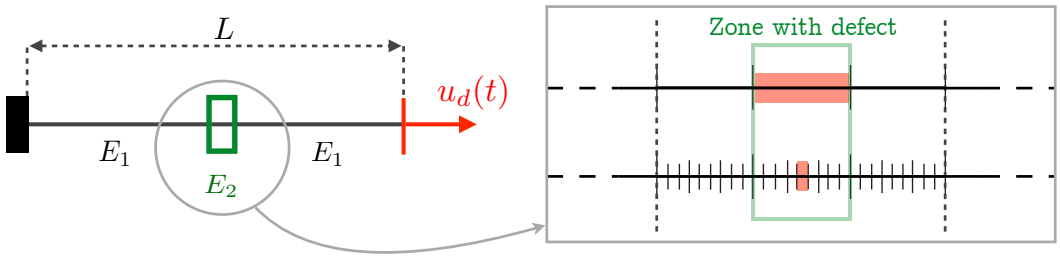

Figure A.1: Mesh dependency of the damage pattern. The green area has a weakest Young modulus $E_2 < E_1$. The red zone shows the element that damages in two mesh configurations.

This implies that changing the mesh leads to a change in the numerical solution, the most extreme configuration consisting in refining the mesh in order to have a size of elements tending to zero, which automatically leads to a dissipated energy also tending to zero, as if no energy was necessary to fracture the beam, which does not have a physical sense [Hill, 1958]. It is also noticeable that the dissipated energy not only depends on the size of the mesh, but also on its orientation and on the type of elements used for the numerical resolution.

To avoid this problem, localization limiters need to be implemented to guarantee that the dissipated energy value has a physical sense. Different regularization strategies are presented in the next sections. Some of those methods, such as nonlocal regularizations [Jirásek, 2007] or energy-based regularization [Hillerborg et al., 1976] rely on the definition of a characteristic length, related to the discretization of the finite element mesh.

Energy regularization

The dissipated energy depends on the size of the localization zone. For finite element simulations, the size of this zone corresponds for local models to the size of one finite element (or a band of elements). The method presented in [Hillerborg et al., 1976] consists in adjusting the softening part of the material model (herein the value of A_d) depending on the size of this element in order to obtain a dissipated energy independent from the mesh, by adapting the stress–jump of displacement relation of the process zone so that the surface energy dissipated by the creation of the surface of the crack is equal the critical energy restitution rate G_c of the material:

$$G_c = \int_0^{[\![\boldsymbol{u}_f]\!]} \boldsymbol{\sigma}\, \mathrm{d}[\![\boldsymbol{u}]\!] \tag{A.1}$$

where $[\![\square]\!]$ represents the jump of quantity $\square$ at the process zone. This approach however does not avoid the localization of the damage to one element, as it only corrects the damage evolution law to obtain a more physical meaning (in the sense of the dissipated energy). Also, the damage pattern remains dependent on the orientation of the mesh, as shown on Fig. A.2. To avoid this problem, non-local approaches have been developed and are presented in the next section.

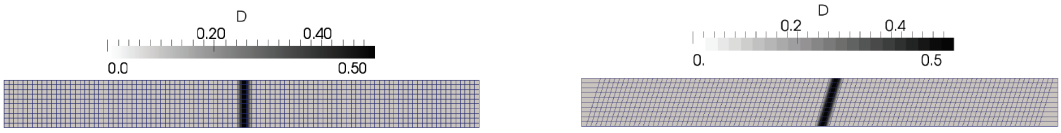

(a) (b)

Figure A.2: Mesh dependency of the damage pattern. (a) mesh with vertical bands; (b) mesh with tilted bands (courtesy of C. Giry)

Non-local regularization of internal variables

The idea behind non-local regularization approaches is to consider that, for each point, a local quantity is replaced by another quantity taking into account the influence of the neighboring points. These approaches consider the fact that the macroscopic response depends on lower-scale interactions in a zone proportional to the internal length l_c (also called characteristic

length) introduced at the macroscopic level. The numerical outcome of this assumption is that the damage does not evolve on only one band of elements but on a band that contains several elements, which size is proportional to l_c. The shape and size of the elements does not influence the dissipated energy nor the propagation of this zone of localization. [Jirásek, 2007] details those different approaches and provides a numerical comparison.

Integral approaches

Nonlocal integral regularization is really classical when working with softening materials (either modeled with plasticity or damage –or both). The idea behind these approaches is to replace a local variable $b(\boldsymbol{x})$ from the model by its average $\overline{b}(\boldsymbol{x})$ over a neighborhood of the considered point [Grassl and Jirásek, 2006]. The nonlocal average is given as the convolution product of the local function by a (classically Gaussian) weight function:

$$\overline{b}(\boldsymbol{x}) = \int_\Omega \frac{\phi_0(\boldsymbol{x}, \boldsymbol{s})}{\int_\Omega \phi_0(\boldsymbol{x}, \boldsymbol{s}) \mathrm{d}\, \boldsymbol{s}} b(\boldsymbol{s}) \, \mathrm{d}\, \boldsymbol{s} \tag{A.2}$$

where the weight function is used to determine the interactions between the different points. For example:

$$\phi_0(\boldsymbol{x}, \boldsymbol{s}) = \exp\left(-\left(\frac{4 \left\|\boldsymbol{x} - \boldsymbol{s}\right\|^2}{l_c^2}\right)\right) \tag{A.3}$$

This framework remains general and can be used either for plasticity [Jirásek and Rolshoven, 2003] or damage ([Saouridis and Mazars, 1992] for isotropic, [Desmorat et al., 2007] for anisotropic) models and can be applied to different variables [Jirásek, 2007]. However this technique is highly intrusive and requires heavy modifications of the numerical codes. Other numerical problems can arise for elements close to the boundaries of the domain, or when a point and its region or interest are too close from a crack (classical technique leads to numerical interaction between the Gauss points on each side of the crack. This issues has more recently been addressed in [Giry et al., 2011].

Differential approaches

The continuous model is enriched by adding higher-order derivative terms either to the local quantities (for example the strain or the internal variables) [De Borst and Mühlhaus, 1992]. This regularization can be either implicit or explicit, as detailed below.

Explicit gradient

Under its explicit form, this approach consists in adding to the local quantity b its Laplace quantity:

$$\overline{b}(\boldsymbol{x}) = b(\boldsymbol{x}) + l_c \, \nabla^2 \, b(\boldsymbol{x}) \tag{A.4}$$

where l_c is homogeneous to a length. This method is often said to be "weakly nonlocal" as it involves only the local value of the variables and its derivatives at the same point. However, this method requires to use richer (higher-order) finite elements (a C^1 continuity of the displacement field is then required).

Implicit gradient

An implicit method can also be used, for which the nonlocal form of the local variable b is defined implicitly:

$$\overline{b} + l_c \nabla^2 \overline{b} = b \tag{A.5}$$

This method is said to be "strongly" nonlocal. Its is that it is more robust than its explicit counterpart, and can be related to the integral version by considering a Green weight function [Peerlings et al., 2001]. However, it requires the additional resolution of a differential equation in the process which requires more degrees of freedom. Finally, it implies the loss of symmetry of the operator to be inversed, which requires to impose additional boundary conditions (for example a null flux).

Bounded rate concept – damage-delay

The damage-delay [Ladevèze, 1991, Dubé et al., 1996, Allix and Deü, 1997, Allix et al., 2003, Suffis et al., 2003] (or bounded rate concept [Allix, 2012]) method introduces a viscosity aspect in the evolution law of the damage variable, through a characteristic time parameter τ_c, in order to delay the peak of damage (see [Needleman, 1988] for elastic-plasticity). The advantage of such methods is that it set a maximum value of the damage rate, which regularizes the problem, whichever the strain rate (this aspect is not taken into account in [Dubé et al., 1996]). For example:

$$\dot{d} = \frac{1}{\tau_c} \left[1 - \exp(a \langle d_s - d \rangle_+) \right] \tag{A.6}$$

where d is the regularized damage variable and d_s is the damage variable calculated without regularization. This method provides a non-dependence on the mesh size and avoids the localization phenomenon, but the stability is really dependent on the characteristic time τ_c. Parameter a is usually equal to 1.

Appendix B

Tensor decompositions

This appendix presents basic notions for understanding matrix and tensor decompositions in a discrete framework. See [Bader and Kolda, 2007] for more information on the formalism and the implementation of those decompositions.

Classical SVD

Singular value decomposition (SVD) is a factorization of a real or complex matrix and is a generalization of the eigendecomposition of a positive semidefinite normal matrix to any $m \times n$ matrix. Let consider the matrix $\mathbf{A} \in \boldsymbol{\mathcal{M}}_{m,n}(\mathbb{R})$, with $m > n$.

(i) $\exists \mathbf{U} \in \boldsymbol{\mathcal{M}}_{m}(\mathbb{R})$ unitary (meaning $\mathbf{U}^{\mathrm{T}}\,\mathbf{U} = \mathbf{I}_m$);

(ii) $\exists \mathbf{V} \in \boldsymbol{\mathcal{M}}_{n}(\mathbb{R})$ unitary (meaning $\mathbf{V}^{\mathrm{T}}\,\mathbf{V} = \mathbf{I}_n$);

(iii) $\exists \boldsymbol{\Lambda} \in \boldsymbol{\mathcal{M}}_{m,n}(\mathbb{R})$;

such that:

$$\mathbf{A} = \mathbf{U}\,\boldsymbol{\Lambda}\,\mathbf{V}^{\mathrm{T}} \tag{B.1}$$

$$\mathrm{a}_{i_1,i_2} = \sum_{j_1}\sum_{j_2} \lambda_{j_1,j_2}\,\mathrm{u}_{i_1,j_1}\,\mathrm{v}_{i_2,j_2} \tag{B.2}$$

where the matrix $\boldsymbol{\Lambda}$ is defined as:

$$\boldsymbol{\Lambda} = \left(\begin{array}{ccc|c} \lambda_1 & & & \\ & \ddots & & \mathbf{0} \\ & & \lambda_m & \\ \hline & \mathbf{0} & & 0 \end{array}\right) \tag{B.3}$$

The $\{\lambda_i\}_{i=1\cdots m}$ are the singular values of $\mathbf{A}$. On a reduced-order modeling point of view, this can be rewritten:

$$\mathbf{A} = \sum_{i=1}^{m} \lambda_i \, \mathbf{U}_i \otimes \mathbf{V}_i^{\star} \tag{B.4}$$

where $\otimes$ represents the outer product of the vectors $\mathbf{U}_i$ and $\mathbf{V}_i^{\star}$ (first m vectors of $\mathbf{V}$).

High-order SVD

Whereas the classical SVD provides at the same time (a) a rank-R decomposition of a hermitian matrix $\mathbf{A}$ and (b) orthonormal raw/column matrices $\mathbf{U}$ and $\mathbf{V}$, those two properties are embodied by two different decompositions for higher order arrays. (a) can be computed using CP decomposition (see next paragraph). (b) is extended to higher order tensors by a method known as the Tucker decomposition, which enables to compute the orthonormal spaces associated with the different modes (axes) of a tensor.

• SVD

$$\begin{aligned} \mathbf{A} &= \mathbf{U}\,\mathbf{\Lambda}\,\mathbf{V}^{\mathrm{T}} \\ a_{i_1,i_2} &= \sum_{j_1}\sum_{j_2} \lambda_{j_1,j_2}\, \mathrm{u}_{i_1,j_1}\, \mathrm{v}_{i_2,j_2} \end{aligned}$$

• HO-SVD (Tucker decomposition)

$$\mathbf{A} = \mathbf{\Lambda} \times_{i=1}^{n} \mathbf{U}^{(i)} \tag{B.5}$$

$$\mathrm{a}_{i_1\cdots i_N} = \sum_{j_1} \cdots \sum_{j_N} \Lambda_{j_1\cdots j_N}\, \mathrm{u}^{(1)}_{i_1,j_1} \cdots \mathrm{u}^{(N)}_{i_N,j_N} \tag{B.6}$$

with $\times_k$ the mode-k tensor-matrix product and where $\mathbf{\Lambda}$ is here called the core tensor. Such decomposition must fulfill the following requirements:

(i) each $\mathbf{U} = [\mathrm{u}^{(n)}_{i,j}]_{\mathbf{I}_n \times \mathbf{I}_n}$ is an orthogonal matrix;

(ii) two sub-tensors of the core tensor $\mathbf{\Lambda}$ are orthogonal:

$$\left\langle \mathbf{\Lambda}_{j_n=p}, \mathbf{\Lambda}_{j_n=q} \right\rangle = 0 \text{ if } p \neq q \tag{B.7}$$

(iii) the sub-tensors in the core tensor $\mathbf{\Lambda}$ are ordered according to their Frobenius norm:

$$\left\|\mathbf{\Lambda}_{j_n=1}\right\| \geq \left\|\mathbf{\Lambda}_{j_n=2}\right\| \geq \cdots \geq \left\|\mathbf{\Lambda}_{j_n=\mathbf{I}_n}\right\| \text{ for } n = 1 \cdots N \tag{B.8}$$

Construction of the approximation The high-order SVD decomposition can be computed from several SVDs according to the following process:

1. given a tensor $\mathbf{A} \in \mathbb{F}^{n_1 \times \cdots \times n_N}$, construct the mode-$k$ flattening $\mathbf{A}_{(k)}$;
2. compute the singular value decomposition of $\mathbf{A}_{(k)}$:

$$\mathbf{A}_{(k)} = \mathbf{U}_{(k)} \, \mathbf{\Lambda}_{(k)} \, \mathbf{V}_{(k)}^{\mathrm{T}} \tag{B.9}$$

   and store the left singular vectors $\mathbf{U}_{(k)}$;
3. The core tensor $\mathbf{\Lambda}$ is the corresponding projection of $\mathbf{A}$ onto the tensor basis formed by the factor matrices $\{\mathbf{U}_{(n)}\}_{n=1 \cdots N}$, i.e.

$$\mathbf{\Lambda} = \mathbf{A} \times_{n=1}^{N} \mathbf{U}_{(n)}^{\mathrm{T}} \tag{B.10}$$

Tensor rank approximation

Considering a tensor space $\mathbb{F}^{n_1 \times \cdots \times n_N} = \mathbb{F}^{n_1} \otimes \cdots \otimes \mathbb{F}^{n_N}$ where $\mathbb{F} \in \mathbb{R}$ or $\mathbb{C}$, every order-N tensor $\mathbf{A}$ in this space may be represented as a linear combination of rank-1 tensors (as a Kruskal tensor):

$$\mathbf{A} = \sum_{i}^{r} \lambda_i \, \mathbf{U}_i^{(1)} \otimes \cdots \otimes \mathbf{U}_i^{(N)} \tag{B.11}$$

$$\tag{B.12}$$

where $\lambda_i \in \mathbb{F}$ and $\mathbf{U}_i^k \in \mathbb{F}^{n_k}$. r is called the rank of the tensor:

(i) if r is minimal, this approximation is referred to as "tensor rank decomposition", "minimal CP decomposition" or "canonical polyadic decomposition";

(ii) otherwise, it is called "r-term decomposition", "CANDECOMP/PARAFAC" or "polyadic decomposition".

Construction of the approximation Different methods exist to construct such approximation. Among them:

- alternating algorithms:
  - alternating least squares (the one used in this work);
  - alternating slice-wise diagonalization;
- algebraic algorithms:
  - simultaneous diagonalization;

  - simultaneous generalized Schur decomposition;

- optimization algorithms:
  - Levenberg-Marquardt;
  - nonlinear conjugate gradient;

- direct methods (direct multi-linear decomposition).

Appendix C

Orthonormalization of a reduced basis – extension to parametric problems

The orthonormalization of the reduced-order basis is done in the PGD framework using a Gram-Schmidt algorithm. Whereas this approach is trivial when dealing with time-space separation (or more generally two-variables representations), the extension to parametric decompositions requires high-order techniques. We give in this appendix the details in the discrete case.

Case 1: time-space representation

Input:

- the solution at iteration m:

$$\mathbf{u}_m(\mathbf{x}, \mathrm{t}) = \sum_{i=1}^{m} \mathrm{a}_i \, \mathbf{\Phi}_i \tag{C.1}$$

- the new mode just computed:

$$\Delta\mathbf{u}_m(\mathbf{x}, \mathrm{t}) = \mathrm{a}_{m+1} \, \mathbf{\Phi}_{m+1} \tag{C.2}$$

One seeks to orthonormalize the function $\mathbf{\Phi}_{m+1}$ with respect to the already computed orthonormal basis $\{\mathbf{\Phi}_i\}_{i=1}^{m}$ according to a given norm:

$$\langle \mathbf{\Phi}_i, \mathbf{\Phi}_j \rangle_{\mathbf{I}_\Omega} = \mathbf{\Phi}_i^{\mathrm{T}} \, \mathbf{I}_\Omega \, \mathbf{\Phi}_j = \begin{cases} 0 \text{ if } i \neq j \\ 1 \text{ if } i = j \end{cases} \tag{C.3}$$

where $\mathbf{I}_\Omega$ is defined such that:

$$\int_{\Omega} \boldsymbol{\Phi}^i(\boldsymbol{x}) \cdot \boldsymbol{\Phi}^j(\boldsymbol{x}) \, \mathrm{d}\boldsymbol{\Omega} \equiv (\mathbf{\Phi}^i)^{\mathrm{T}} \, \mathbf{I}_\Omega \, \mathbf{\Phi}^j \tag{C.4}$$

$\mathbf{u}_{m+1}$, the rank-$(m+1)$ time-space decomposition of $\mathbf{u}$, then writes:

$$\begin{aligned}
\mathbf{u}_{m+1} &= \sum_{i=1}^{m} \mathrm{a}_i\, \mathbf{\Phi}_i + \mathrm{a}_{m+1}\, \mathbf{\Phi}_{m+1} \\
&= \sum_{i=1}^{m} \mathrm{a}_i\, \mathbf{\Phi}_i + \sum_{i=1}^{m} \mathrm{a}_{m+1} \left[\langle \mathbf{\Phi}_i, \mathbf{\Phi}_{m+1} \rangle_{\mathbf{I}_\Omega}\, \mathbf{\Phi}_i + \tilde{\mathbf{\Phi}}_i \right] \\
&= \sum_{i=1}^{m} \underbrace{\left[\mathrm{a}_i + \mathrm{a}_{m+1} \langle \mathbf{\Phi}_i, \mathbf{\Phi}_{m+1} \rangle_{\mathbf{I}_\Omega} \right]}_{\tilde{\mathrm{a}}_i} \mathbf{\Phi}_i + \mathrm{a}_{m+1}\, \tilde{\mathbf{\Phi}}_{m+1} \\
&= \sum_{i=1}^{m} \tilde{\mathrm{a}}_i \mathbf{\Phi}_i + \mathrm{a}_{m+1}\, \tilde{\mathbf{\Phi}}_{m+1}
\end{aligned} \tag{C.5}$$

with:

$$\mathbf{\Phi}_{m+1} \leftarrow \tilde{\mathbf{\Phi}}_{m+1} = \mathbf{\Phi}_{m+1} - \sum_{i=1}^{m} \langle \mathbf{\Phi}_i, \mathbf{\Phi}_{m+1} \rangle_{\mathbf{I}_\Omega}\, \mathbf{\Phi}_i \tag{C.6}$$

The new function $\mathbf{\Phi}_{m+1}$ is then normalized:

$$\mathrm{a}_{m+1} \leftarrow \mathrm{a}_{m+1} \langle \mathbf{\Phi}_{m+1}, \mathbf{\Phi}_{m+1} \rangle_{\mathbf{I}_\Omega} \tag{C.7}$$

$$\mathbf{\Phi}_{m+1} \leftarrow \frac{\mathbf{\Phi}_{m+1}}{\langle \mathbf{\Phi}_{m+1}, \mathbf{\Phi}_{m+1} \rangle_{\mathbf{I}_\Omega}} \tag{C.8}$$

A criterion for rejecting the new mode is implemented if its norm (e.g. the norm of the function a_{m+1}) is lower than a certain threshold (meaning the $(m+1)^{\text{th}}$ mode does not enrich sufficiently the rank-m decomposition).

Case 2: extension to a parametric representation

Following the procedure explained in the previous section (method **B**), the orthonormalization procedure for parametric problems after the fixed point algorithm leads to:

$$\mathbf{u}_{m+1} = \sum_{i=1}^{m} \underbrace{\left[\mathbf{A}_i + \mathbf{A}_{m+1} \langle \mathbf{\Phi}_i, \mathbf{\Phi}_{m+1} \rangle_{\mathbf{I}_\Omega} \right]}_{\tilde{\mathbf{A}}_i} \mathbf{\Phi}_i + \mathbf{A}_{m+1}\, \tilde{\mathbf{\Phi}}_{m+1} \tag{C.9}$$

where $\mathbf{A}_{m+1} = \prod_k \mathrm{a}^k_{m+1}$, $\mathbf{A}_i \in \mathcal{M}_{\mathbf{D}}(\mathbb{R})$ and consequently $\tilde{\mathbf{A}}_i \in \mathcal{M}_{\mathbf{D}}(\mathbb{R})$. A rank-1 CP-decomposition of the terms $\tilde{\mathbf{A}}_i$ is performed in order to get the new functions $\{\{\tilde{\mathrm{a}}^k_i\}_{i=1}^m\}_{k=1}^{N^p}$ (using an alternating least squares algorithm as presented in Appendix B).

Once again the new mode is normalized (with the weight of the the function being put on

the "first" parametric function, in our case the time function):

$$\mathrm{a}^1_{m+1} \leftarrow \mathrm{a}^1_{m+1} \langle \boldsymbol{\Phi}_{m+1}, \boldsymbol{\Phi}_{m+1} \rangle_{\mathbf{I}_\Omega} \prod_{k=2}^{N^p} \langle \mathrm{a}^k_{m+1}, \mathrm{a}^k_{m+1} \rangle_{\mathbf{I}_{\mathbf{D}_i}} \tag{C.10}$$

$$\boldsymbol{\Phi}_{m+1} \leftarrow \frac{\boldsymbol{\Phi}_{m+1}}{\langle \boldsymbol{\Phi}_{m+1}, \boldsymbol{\Phi}_{m+1} \rangle_{\mathbf{I}_\Omega}} \tag{C.11}$$

$$\mathrm{a}^k_{m+1} \leftarrow \frac{\mathrm{a}^k_{m+1}}{\langle \mathrm{a}^k_{m+1}, \mathrm{a}^k_{m+1} \rangle_{\mathbf{I}_{\mathbf{D}_i}}} \qquad \forall k \in [2, N^p] \tag{C.12}$$

where $\mathbf{I}_{\mathbf{D}_i}$ is defined as:

$$\int_{\mathcal{D}_i} \boldsymbol{a}(\mu_i) \cdot \boldsymbol{b}(\mu_i) \, \mathrm{d}\mu_i \equiv \mathbf{a}^{\mathrm{T}} \, \mathbf{I}_{\mathbf{D}_i} \, \mathbf{b} \tag{C.13}$$

with $\mathbf{B}$ such that $\boldsymbol{\varepsilon}(\mathbf{u}) = \mathbf{B}\,\mathbf{u}$.

Appendix D

LATIN method

		References	Damage	PGD
Ref. works	Functional formulation	[Ladevèze, 1985]		**x**
	Internal variables formulation	[Ladevèze, 1989]		**x**
	English version	[Ladevèze, 1999]		**x**
Large deformations and plasticity		[Vauchez, 1991]		**x**
		[Liu, 1992]		**x**
Large deformations, co-rotational formulation		[Boucard, 1996]		**x**
		[Michel-Ponnelle, 2001]		**x**
Elasto-visco-plasticity, large number of cycles and thermo-elasticity		[Boisse, 1987]		**x**
		[Cognard, 1989]		**x**
		[Arzt, 1994]		**x**
		[Cognard et al., 1999]		**x**
Verification, viscoplasticity		[Pelle and Ryckelynck, 2000]		**x**
Nonlinear dynamics		[Royer, 1990]		**x**
Damage and composites	Integral behavior laws	[Allix and Ladevèze, 1992]	⋆	**x**
	Internal variables formulation	[Douchin and Ladevèze, 2001]	⋆	
	Multi-scale composite structures	[Trovalet, 2010]	⋆	
	Buckling-delamination coupling	[Saavedra Redlich, 2012]	⋆	
	Snap back in concrete	[Vandoren et al., 2013]	⋆	
Fast dynamic, pyrotechnic shocks		[Lemoussu et al., 2002]		
		[Derumaux, 2004]		
		[Gupta et al., 2005]	⋆	

		References	Damage	PGD
Assembly	2-D axisymmetric, static	[Danwé, 1993]		
	3-D (flange in static)	[Champaney, 1996]		
	Application, quasi-static	[Blanzé et al., 2000]		
	Dynamics, pyrotechnic shocks	[Ladevèze et al., 2000]		
	Optimization	[Boucard et al., 2009] [Soulier and Boucard, 2009]		
	Contact	[Giacoma et al., 2015]		**x**
	Non-invasive	[Oumaziz et al., 2017]		
DDM	Parallelism	[Lorong, 1994] [Dureisseix, 1997]		
	Multi-scale	[Ladevèze and Dureisseix, 2000] [Ladevèze et al., 2001]		
	Re-use strategy, stochastic	[Nouy, 2003] [Ladevèze et al., 2001]		
	Multi-physics	[Néron, 2004]		
	Coupling with XFem, cracking	[Guidault, 2005]		
	3-D multi-scale, C++	[Violeau, 2007]		
	Time multi-scale	[Passieux, 2008]		**x**
	Composites	[Kerfriden, 2008]	⋆	
	Dumping	[Caignot, 2009]		
	Reference points method, multi-scale	[Capaldo, 2015]		**x**
Multi-parametric	Assemblies	[Boucard and Champaney, 2003]		
	Multi-scale dynamics	[Odièvre, 2009]		
	Composite assemblies	[Roulet, 2012]	⋆	
	Buckling, elasto-visco-plasticity	[Boucard and Ladevèze, 1999]		**x**
	Elasto-visco-plasticity	[Relun, 2011]		**x**
	Optimal basis	[Heyberger et al., 2013]		**x**
	Optimization, assemblies	[Laurent, 2013] [Courrier, 2015]		
Identification		[Allix and Vidal, 2002]		**x**
Inverse problems		[Nguyen et al., 2008]		**x**

Appendix E

Extended summary in French

1 Introduction

L'étude de la variabilité intrinsèque aux matériaux est un sujet essentiel quant au dimensionnement des structures de génie civil. Cette variabilité peut provenir de la fabrication du matériau (choix de ses éléments constitutifs, procédés de fabrication), ou de la description de son modèle physique. Ainsi, il est évident que plus ces incertitudes seront importantes et plus la simulation du comportement de ce matériau sera complexe, quelle que soit l'échelle considérée pour l'étude (du point de vue microscopique à l'échelle macroscopique de la structure). C'est en particulier vrai pour le béton armé qui est utilisé de manière intensive depuis des décennies bien que son comportement à long terme ne soit toujours pas bien compris ni modélisé. La tenue mécanique de ces structures peut être modifié par des réactions chimiques ou des dégradations mécanique ce qui rend la prédiction de leur comportement à un aléas donné extrêmement complexe, et cela même avec des outils numériques de plus en plus performants. Parmi les nombreuses thématiques de recherche, l'étude de la réponse des structures en béton armé à un aléas sismique est extrêmement importante, en particulier depuis l'incident de Fukushima en 2011. Le projet *SINAPS@* a été lancé en réponse à cet incident, et a pour but de quantifier l'influence des incertitudes liées aux procédés physiques et aux méthodes utilisées pour qualifier le risque sismique sur la vulnérabilité des structures de l'industrie nucléaire. Son but est principalement de fournir des outils pour décrire le phénomène sismique ainsi que son impact sur des structures en béton armé, pour identifier les risques et proposer des recommandations quant à l'évolution des règles concernant le risque sismique.

L'étude présentée ici porte sur le fait que le calcul de la réponse d'une structure en béton armé à un aléas sismique, à un instant donné, nécessite la connaissance de l'histoire de ladite structure et des différentes dégradations qui ont pu lui être causées, celles-ci pouvant s'étaler sur plusieurs décennies. Ces phénomènes sont souvent complexes à modéliser, tout comme l'est le chargement sismique, ce qui rend ce type de calcul extrêmement coûteux à réaliser. L'objectif des travaux présentés ici n'est cependant pas de modéliser ces phénomènes aux longs termes mais d'en étudier les potentiels effets sur une structure soumise, à un instant

donné, à un chargement cyclique. Pour ce faire, nous considérons un milieu pour laquelle certains paramètres matériaux (mais aussi affectant le chargement) ne sont connus que par leur valeur moyenne et leur intervalle de variation, le but étant de déterminer la réponse d'une structure exacerbant un comportement fortement non-linéaire pour les différents jeux de paramètres associés à ces nouvelles variables du problème.

Il est évident que la prise en compte de ces paramètres dans la résolution d'un problème déjà délicat de part la nature du modèle utilisé (fortement non-linéaire, et qui est décrit dans la prochaine section) rend ce type d'étude très complexe en terme de coût de calcul avec les techniques de résolution usuelles. Cette double difficulté (non-linéarité, calcul paramétrique) est traitée ici en associant un algorithme itératif, la méthode LATIN [Ladevèze, 1999], et une méthode de réduction de modèle, la PGD [Ammar et al., 2012]. Les algorithmes de type LATIN–PGD on été utilisés à maintes reprises depuis les années 80 pour le traitement des problèmes non-linéaires d'évolution faisant intervenir des modèles de comportement visco-plastique, mais aussi plus récemment pour des problèmes multi-physiques ou avec décomposition de domaine. L'utilisation de ces algorithmes pour des études paramétriques a été faite dans le cadre de la stratégie multi-paramétrique [Boucard and Ladevèze, 1999]. Nous proposons ici une extension de l'algorithme classique, faisant intervenir une décomposition PGD temps-espace à une décomposition intégrant plus de variables, et l'application de cette méthode à un problème d'endommagement avec effet unilatéral. Le modèle de comportement matériaux est sommairement décrit dans la prochaine section, puis l'algorithme LATIN-PGD est donné en mettant l'accent sur les modifications apportées pour prendre en compte l'aspect paramétrique du problème. Cette méthode est enfin illustrée au travers de deux exemples (sollicitations de traction et flexion) avec variabilité sur des paramètres matériaux et affectant l'amplitude du chargement.

2 Le modèle étudié

La modélisation du milieu étudié découle de [Richard and Ragueneau, 2012] (pour la loi d'endommagement) et [Vassaux et al., 2015] (pour la loi de refermeture de fissure). Cette section rappelle les différents points du modèle, la variabilité considérée et l'influence sur le comportement mécanique du béton. Les quantités relatives au modèle de comportement du béton (respectivement de l'armature) seront notées $\square^c$ (respectivement $\square^r$).

2.1 Modèle d'endommagement avec effet unilatéral

La relation de comportement au niveau d'un point de Gauss est donnée Fig. E.1. On peut voir que deux phénomènes ici sont pris en compte. Un endommagement en traction, venant affecter la rigidité du matériau, et un regain de rigidité progressive lors de la phase de décharge et de compression, caractérisant le phénomène de refermeture progressive des fissures présentes dans le béton, et conférant au matériau une rigidité (en compression) proche de sa rigidité "saine" sont considérés. Il est à noter que contrairement à [Richard and Ragueneau, 2012], ni la plasticité en compression, ni les phénomènes hystérétiques liés au charge-

ment cyclique ne sont pris en compte. En terme de modélisation, cet état peut être obtenu en

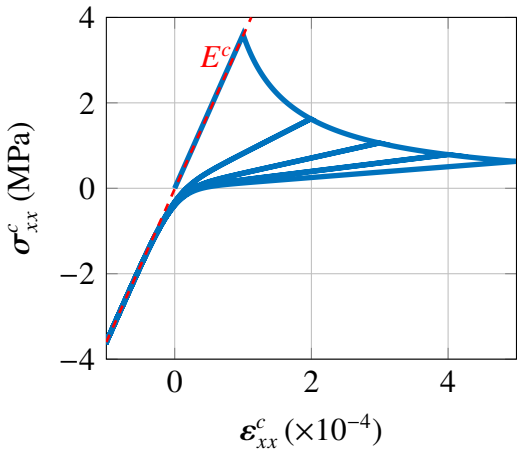

Figure E.1: Réponse mécanique $\sigma^c_{xx} = f(\varepsilon^c_{xx})$ au point de Gauss

scindant le tenseur des contraintes de Cauchy au sein du volume élémentaire représentatif en une somme de deux contributions indépendantes, la première liée à l'état de contrainte dans le milieu dans le milieu fissuré (en négligeant les interactions entre les fissures) et la seconde liée à l'état de contrainte dans les fissures une fois refermées :

$$\boldsymbol{\sigma}^c = \boldsymbol{\sigma}^{c,m} + \boldsymbol{\sigma}^{c,f} \tag{E.1}$$

Un résumé des différentes variables est donné Tab. E.1 et le lecteur peut se référer à Eqs. (E.2, E.3) pour un résumé des équations constitutives du problème.

Table E.1: Résumé des variables du modèle de comportement du béton

Mécanisme	Variable d'état	Variable interne	Force thermodynamique
Déformation totale	$\boldsymbol{\varepsilon}^c$		$\boldsymbol{\sigma}^c$
Élasticité		$\boldsymbol{\varepsilon}^{c,e}$	$\boldsymbol{\sigma}^{c,m}$
Endommagement isotrope		d^c	$-Y^c$
Écrouissage isotrope associé à l'endommagement		z^c	Z^c
Refermeture de fissure		$\boldsymbol{\varepsilon}^{c,f}$	$\boldsymbol{\sigma}^{c,f}$

Lois d'état

$$\begin{aligned}
\boldsymbol{\sigma}^{c,m} &= (1-d^c)\,\boldsymbol{C}^c : \boldsymbol{\varepsilon}^c \\
\dot{\boldsymbol{\sigma}}^{c,f} &= \nu\,\boldsymbol{C}^c : \dot{\boldsymbol{\varepsilon}}^{c,f} \\
Y^c &= \frac{1}{2}\,\langle\boldsymbol{\varepsilon}^c\rangle_+ : \boldsymbol{C}^c : \langle\boldsymbol{\varepsilon}^c\rangle_+ \\
Z^c &= \frac{\mathrm{d}\,H(z^c)}{\mathrm{d}\,z^c} \\
\boldsymbol{\sigma}^r &= \boldsymbol{C}^r : \boldsymbol{\varepsilon}^r
\end{aligned} \tag{E.2}$$

Lois d'évolution

$$\begin{aligned}
d^c &= 1 - \frac{1}{1 + A_d(Y^c - Y_0)} \\
z^c &= \frac{1}{1 + A_d(Y^c - Y_0)} - 1 \\
\boldsymbol{\varepsilon}^{c,f} &= d^c\,\boldsymbol{\varepsilon}^c \\
d^r &= 0
\end{aligned} \tag{E.3}$$

où C^c le tenseur de Hooke du béton, A_d un paramètre matériaux régissant le comportement adoucissant de la loi d'endommagement, Y_0 le seuil d'initiation d'endommagement.

2.2 Variabilité au sein du béton

Les procédés de fabrication, ainsi que le vieillissement des structures en béton armé, peuvent conduire à une évolution de certaines propriétés du matériau. Les incertitudes qui en découlent ont une influence directe sur la réponse mécanique globale des structures. Nous considérerons en particulier ici des variabilités sur des paramètres matériaux, ainsi que sur des paramètres liés au chargement (affectant notamment son amplitude). Une approche classique pour prendre en compte ces variabilités consiste à s'appuyer sur des outils probabilistes ou sur des données statistiques. Cependant, de telles approches nécessitent bien souvent un nombre de calculs numériques conséquent ou la mise en place de vastes (et coûteuses) campagnes expérimentales.

L'approche choisie ici consiste à considérer un ensemble de N^p paramètres $\boldsymbol{\mu} = \{\mu_i\}_{i=1\cdots N^p}$, affectant des variables matériaux ou l'amplitude du chargement, uniquement décrits par une distribution uniforme centrée sur la valeur moyenne de ces paramètres. Par exemple, on prendra $\boldsymbol{\mu} = \{\mu_1, \mu_2\}$ tel que μ_1 affecte le coefficient pilotant la phase adoucissante du béton $A_d = A_d(\mu_1)$ et μ_2 affecte le module d'Young de telle manière que $E^c = E^c(\mu_2)$.

Fig. E.2 montre la réponse mécanique, à l'échelle du point de Gauss, d'une structure en béton pour laquelle une variabilité sur le module d'Young du béton E^c (Fig. E.2a), sur le seuil initial d'endommagement Y_0 (Fig. E.2b) et sur le coefficient d'adoucissement A_d (Fig. E.2c) sont considérées (voir Tab. E.2). On peut voir la forte influence de cette variabilité sur la réponse mécanique du problème, en particulier pour la variabilité sur A_d pour laquelle

la variation d'énergie dissipée (aire sous la courbe de la partie adoucissante) est fortement impactée.

Table E.2: Paramètres étudiés, variabilité

Paramètre	Nom	Valeur moyenne	Variabilité	Intervalle de variation
E^c	Module d'Young	36×10^9 Pa	$+/-30\%$	$[25.2 - 46.8] \times 10^9$
A_d	Coefficient d'adoucissement	8×10^{-3} J^{-1}.m^3	$+/-20\%$	$[6.4 - 9.6] \times 10^{-3}$
Y_0	Seuil initial d'activation de l'endommagement	180 J.m^{-3}	$+/-20\%$	$[144 - 216]$

3 Réduction de modèle en non-linéaire et analyse paramétrique

La prise en compte de ces paramètres pour la simulation de problèmes structuraux complexes (tant bien émanant du modèle ou de la géométrie du milieu) est bien souvent rédhibitoire en terme de coût de calcul, aussi bien en temps de simulation qu'en capacité de stockage de la solution associée. L'approche choisie dans cette étude pour prendre en compte cette dépendance aux paramètres consiste à approximer les champs solution du problème sous une forme à variables séparées, comme une somme de produits de fonctions de chacune de ces variables, c'est à dire:

$$\boldsymbol{u}(\boldsymbol{x},\boldsymbol{\mu}) \approx \boldsymbol{u}_m(\boldsymbol{x},\boldsymbol{\mu}) = \sum_{k=1}^{m} \boldsymbol{\Phi}_k(\boldsymbol{x}) \prod_{i=1}^{N^p} a_k^i(\mu_i) \tag{E.4}$$

En particulier, cette approximation est construite de manière itérative en utilisant un algorithme Galerkin–PGD [Nouy, 2010]. Cependant, cette approche utilisée comme telle n'est pas efficace pour la résolution de problèmes fortement non-linéaires tels que ceux rencontrés dans le cas de notre étude. Ainsi, le couplage avec la méthode LATIN [Ladevèze, 1999] est étudié. Les algorithmes LATIN–PGD ont déjà été l'objet de nombreuses études, faisant intervenir une décomposition temps-espace du champ d'intérêt. Nous proposons ici l'extension de cette méthode à des problèmes paramétrés en s'appuyant sur une description telle que (E.4), et l'application de cette méthode à des problèmes structuraux tels que ceux rencontrés dans le domaine du génie civil.

3.1 Proper generalized decomposition

L'approche considérée ici consiste à prendre en compte l'intégralité des variables du problème dans la formulation PGD classique comme des coordonnées additionnelles de la décomposition [Ammar et al., 2012]. Un algorithme glouton est alors utilisé pour construire de manière itérative les différentes fonctions de la représentation. L'approche utilisée est la suivante : en considérant le problème discrétisé (noté avec des symboles droits) $\mathbf{L}\,\mathbf{u}_{m+1}(\boldsymbol{\mu}) = \mathbf{f}(\boldsymbol{\mu})$

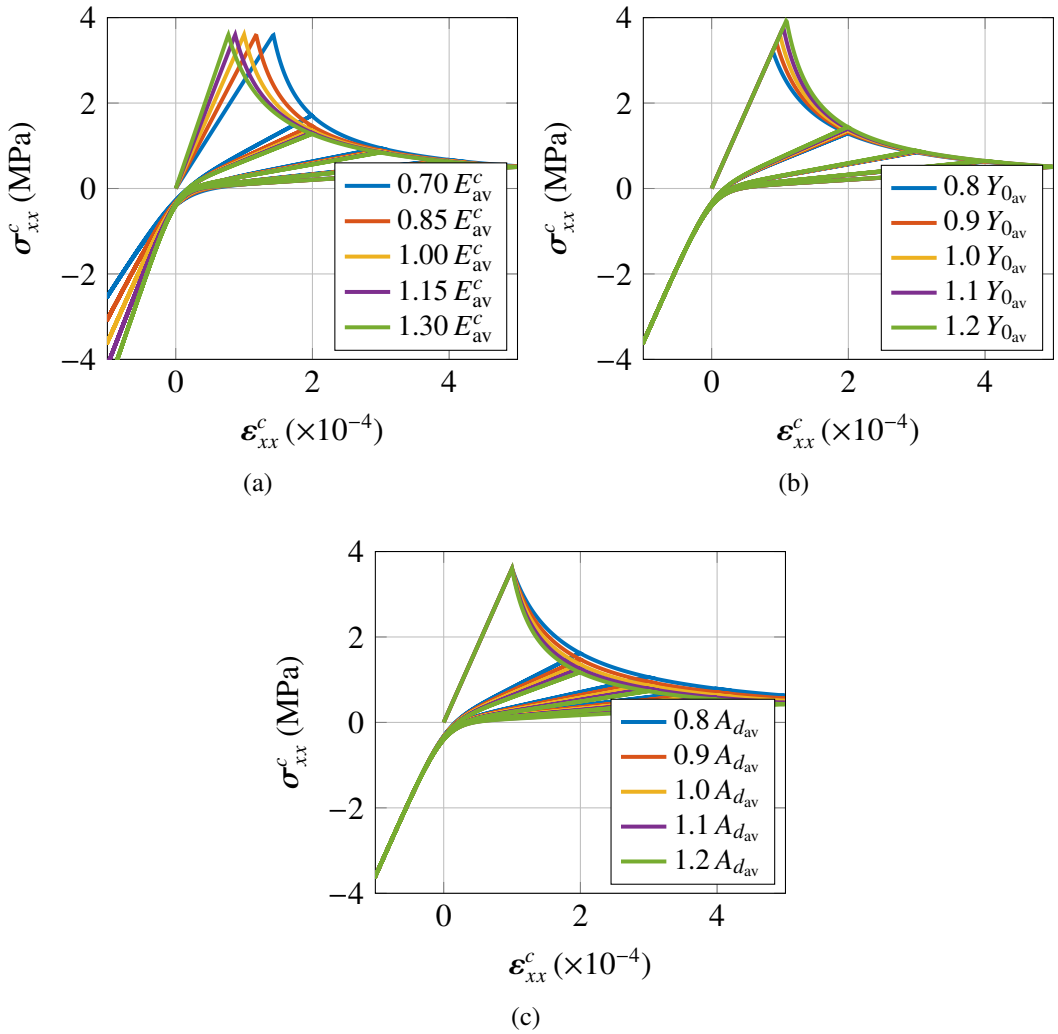

Figure E.2: Influence de la variabilité sur le module d'Young E^c (Fig. E.2a), le seuil d'activation de l'endommagement Y_0 (Fig. E.2b) et le coefficient d'adoucissement A_d (Fig. E.2c) sur la réponse mécanique au niveau d'un point de Gauss (les valeurs moyennes sont notées $\square_{\text{av}}$)

avec $\boldsymbol{\mu} \in \mathcal{D}$, où $\mathbf{L}$ est un opérateur linéaire, on cherche l'approximation de rang $\mathbf{u}_{m+1}$ comme une correction $\Delta\mathbf{u}_m$ apportée à l'approximation $\mathbf{u}_m$ obtenue à l'itération précédente, où $\Delta\mathbf{u}_m$ s'écrit :

$$\Delta\mathbf{u}_m = \mathbf{\Phi}_{m+1}\,\mathbf{A}_{m+1} \tag{E.5}$$

avec $\mathbf{A}_{m+1}(\mu) \in \mathcal{M}_{\mathbf{D}}(\mathbb{R})$ et $\mathbf{A}_m = \prod_{k=1}^{Np} \mathrm{a}_m^k$. La fonction test est choisie telle que :

$$\mathbf{u}^\star = \mathbf{\Phi}^\star\,\mathbf{A}_{m+1} + \mathbf{\Phi}_{m+1}\,\mathbf{A}^\star \tag{E.6}$$

Un point fixe est enfin utilisé pour déterminer les fonctions $\mathbf{\Phi}_{m+1}$ et $\mathbf{A}_{m+1}$:

(i) la fonction d'espace est calculée en résolvant l'équation suivante, en considérant $\mathbf{A}^\star = \mathbf{0}$:

$$\mathbf{\Phi}_{m+1} = \mathbf{L}^{-1}\left[\frac{\mathbf{f}_{m+1} \bar{\times}_{j+1} \left[\mathbf{I}_{\mathbf{D}_j}\, \mathrm{a}^j_{m+1}\right]}{\prod_{j=1}^{Np}\left[(\mathrm{a}^j_{m+1})^{\mathrm{T}}\, \mathbf{I}_{\mathbf{D}_j}\, \mathrm{a}^j_{m+1}\right]}\right] \tag{E.7}$$

(ii) en considérant $\mathbf{\Phi}^\star = \mathbf{0}$, $\mathbf{A}_{m+1}$ est calculée en résolvant le problème:

$$\mathbf{A}_{m+1} = \frac{\mathbf{\Phi}^{\mathrm{T}}_{m+1}\, \mathbf{f}_{m+1}}{\mathbf{\Phi}^{\mathrm{T}}_{m+1}\, \mathbf{L}\, \mathbf{\Phi}_{m+1}} \tag{E.8}$$

(iii) une décomposition CP [Hitchcock, 1927] de rang 1 de l'opérateur $\mathbf{A}_{m+1}$ est effectuée pour obtenir l'ensemble des fonctions de paramètres $\{\mathrm{a}^k_{m+1}(\mu_k)\}_{k=1\cdots Np}$.

où $\mathbf{f}_{m+1} = \mathbf{f} - \mathbf{u}_m$, $\bar{\times}_k$ est le produit tenseur-vecteur sur la k-ième dimension [Bader and Kolda, 2007] du tenseur $\mathbf{f}_{m+1}$ et les opérateurs d'intégration $\mathbf{I}_{\mathbf{D}_i}$ sont définis par :

$$\int_{\mathcal{D}_i} \boldsymbol{a}(\mu_i) \cdot \boldsymbol{b}(\mu_i)\, \mathrm{d}\mu_i \equiv \mathbf{a}^{\mathrm{T}}\, \mathbf{I}_{\mathbf{D}_i}\, \mathbf{b} \tag{E.9}$$

3.2 La méthode LATIN

Introduisons les espaces suivants :

(i) l'espace $\boldsymbol{A_d}$ des champs solutions admissibles $\boldsymbol{s}$ vérifiant les équations d'état;

(ii) l'espace $\boldsymbol{\Gamma}$ des champs admissibles $\boldsymbol{s}$ vérifiant les équations d'évolution.

La solution du problème vérifie à la fois les conditions d'admissibilité ainsi que les lois d'évolution, de sorte qu'elle se trouve à l'intersection des espace $\boldsymbol{A_d}$ et $\boldsymbol{\Gamma}$:

$$\boldsymbol{s} \in \boldsymbol{A_d} \cap \boldsymbol{\Gamma} \tag{E.10}$$

• **Initialisation de l'algorithme.** L'algorithme est initialisé en calculant la solution élastique, vérifiant les conditions d'admissibilité cinématique, de sorte que $\boldsymbol{s}_0 \in \boldsymbol{A_d}$. Le processus itératif commence ensuite par une étape locale.

• **L'étape locale.** Le but de l'étape locale est de trouver la solution $\hat{\boldsymbol{s}}_m \in \boldsymbol{\Gamma}$, vérifiant les équations de comportement locales (et dans notre cas non-linéaires) à partir de la solution $\boldsymbol{s}_m \in \boldsymbol{A_d}$ calculée à l'itération précédente, vérifiant l'équilibre global. La direction de rechercher $\boldsymbol{E}^+$ est définie de sorte que $(\hat{\boldsymbol{s}}_m - \boldsymbol{s}_m) \in \boldsymbol{E}^+$. Ce problème local est résolu de manière incrémentale (l'utilisation d'un algorithme de Newton-Raphson -par exemple- peut être nécessaire) en chaque point de Gauss de la structure et pour chaque valeur de paramètre.

• **L'étape linéaire.** L'étape linéaire consiste à trouver la solution $\boldsymbol{s}_{m+1} \in \boldsymbol{A_d}$ à partir de la solution calculée à l'étape locale précédente $\hat{\boldsymbol{s}}_m \in \boldsymbol{\Gamma}$ et la direction de recherche $\boldsymbol{E}^-$ définie telle que $(\boldsymbol{s}_{m+1} - \hat{\boldsymbol{s}}_m) \in \boldsymbol{E}^-$. Ce problème est global en espace et dépend des paramètres $\boldsymbol{\mu}$. Pour réduire le coût de calcul associé à cette résolution, la méthode PGD (telle que décrite précédemment) est implémentée pour approximer la solution $\boldsymbol{s}_{m+1}$ sous la forme d'une représentation à variables séparées, qui est successivement enrichie au fur et à mesure des itérations :

$$\boldsymbol{u}_{m+1} = \boldsymbol{u}_m + \Delta \boldsymbol{u}_m \tag{E.11}$$

et l'enrichissement $\Delta \boldsymbol{u}_m$ est déterminé à partir des équations (E.5–E.8). L'algorithme LATIN–PGD étendu aux problèmes paramétrés est résumé Alg. 10.

3.3 Critère d'arrêt de l'algorithme

L'algorithme s'arrête lorsque la norme $\boldsymbol{L}^2$ du nouveau mode $\varsigma = \left\|\mathrm{a}^1_{m+1}\right\|_{\boldsymbol{L}^2}$ devient plus petite qu'un certain critère ς_{crit}.

Algorithm 10: Algorithme LATIN–PGD

Data: $\mathbf{s}_0$, solution élastique vérifiant les conditions d'admissibilité cinématique;
Result: $\mathbf{u}_{m+1}$, approximation de rang-$m+1$ de $\mathbf{u}$;
while $\varsigma > \varsigma_{crit}$ **do**
  Étape locale :
  $\forall \mu_i \in \mathbf{D}_i$: résolution incrémentale du problème local : $\mathbf{s}_m \rightarrow \hat{\mathbf{s}}_m$;
  Étape linéaire :
  Enrichissement de la base réduite : algorithme de point fixe :
  $\rightarrow \Delta\mathbf{u}_m = \boldsymbol{\Phi}_{m+1} \prod_i \mathrm{a}^i_{m+1}$;
  $\rightarrow \mathbf{u}_{m+1} = \mathbf{u}_m + \Delta\mathbf{u}_m$
  Calcul de l'indicateur ς;
end

La faisabilité de ce couplage LATIN–PGD paramétrique a été illustrée pour un problème 1-D de diffusion thermique dans [Vitse et al., 2014]. La prochaine section présente des résultats concernant la simulation de structures en béton armé, avec le modèle endommageant avec refermeture de fissure présenté Sec. 2 et une variabilité sur l'amplitude du déplacement imposé lors d'un essai de traction-compression puis sur un essai de flexion 4 points sur une poutre en béton armé.

4 Exemples numériques

Cette section donne quelques résultats numériques concernant dans un premier temps l'étude d'une poutre en béton armé soumise à un chargement de traction–compression, puis dans

un second temps l'étude d'une poutre en béton armé soumise à un chargement de flexion 4 points, avec une variabilité à la fois sur l'amplitude du déplacement imposé ainsi que sur le module d'Young du béton (second exemple).

4.1 Essai de traction

On considère une poutre en béton armé soumise à un chargement de traction–compression. Sa géométrie est donnée Fig. E.3 et une variabilité sur l'amplitude du chargement est considérée, paramétrée par une variable μ_2 suivant la loi:

$$\boldsymbol{u}_d(t, \mu_2^i) = (0.75 + 0.25\,\frac{\mu_2^i}{\mu_2^{\max}})\,\mathbf{saw}(t) \tag{E.12}$$

Le modèle de comportement étudié est celui rappelé Sec. 2. Le but de cet étude est déterminer

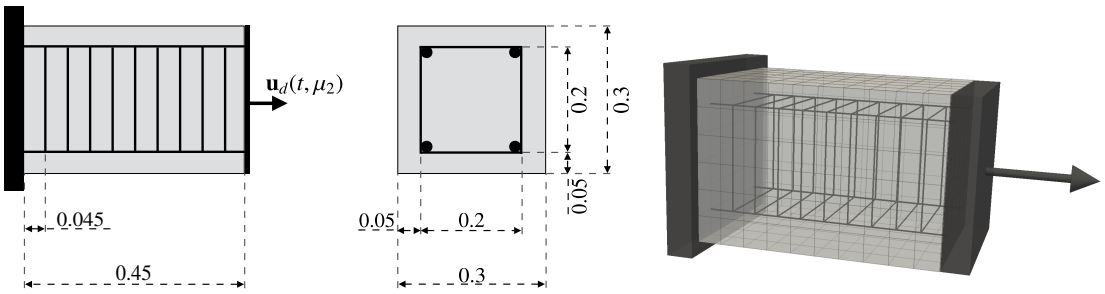

(a) Géométrie de l'éprouvette (b) Représentation 3-D

Figure E.3: Géométrie (gauche) et représentation 3-D (droite) du spécimen

l'approximation du champ de déplacement $\boldsymbol{u}$ sous la forme:

$$\boldsymbol{u}_m(\boldsymbol{x}, t, \boldsymbol{u}_d(\mu_2)) = \sum_{i=1}^{m} \boldsymbol{\Phi}_i(\boldsymbol{x})\, a_i^1(t)\, a_i^2(\mu_2) \tag{E.13}$$

Les informations relatives à la discrétisation du problème sont données dans le tableau E.3. La Fig. E.4 donne l'évolution temporelle du chargement pour quelques valeurs du paramètre

Table E.3: Discrétisation du premier exemple

Espace de définition		Intervalle of variation – discrétisation
$\boldsymbol{\Omega}$	Béton	3, 157 nœuds, 2, 400 éléments (9, 471 DDLs, 19, 200 PGs)
	Armature	80 nœuds, 112 éléments (240 DDLs, 112 PGs)
$\mathbf{D}_1 \equiv \mathcal{I}$	Temps	$t \in [0, 199]$ (200 pas de temps)
$\mathbf{D}_2$	Paramètre de chargement	$\mu_2 \in [1, 24]$ (24 valeurs)

μ_2 ainsi que la réponse globale associée, obtenue par particularisation du champ PGD déterminé en utilisant la méthode LATIN–PGD pour 11 itérations de l'algorithme présenté Sec. 3. L'indicateur d'erreur associé est donné Fig. E.5.

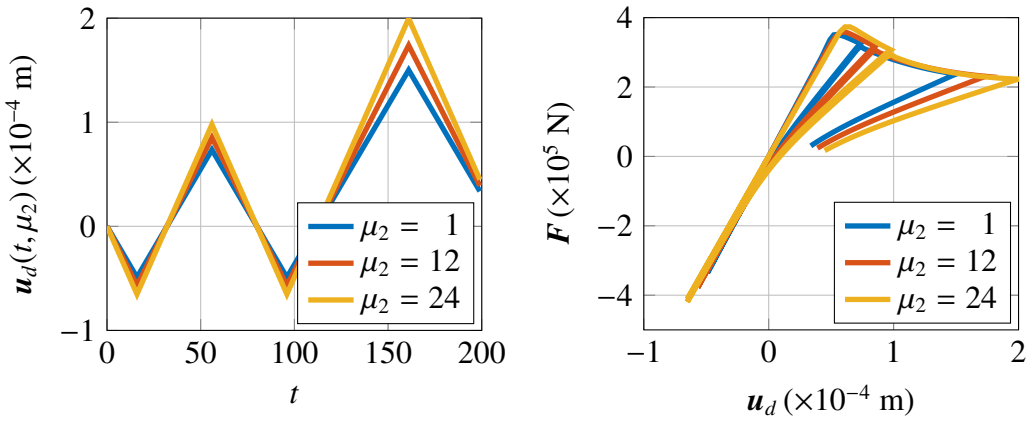

(a) Déplacement imposé pour trois valeurs de μ_2 (b) Réponse mécanique pour trois valeurs de μ_2

Figure E.4: $\boldsymbol{F}(\boldsymbol{u}_d)$ pour plusieurs valeurs de μ_2

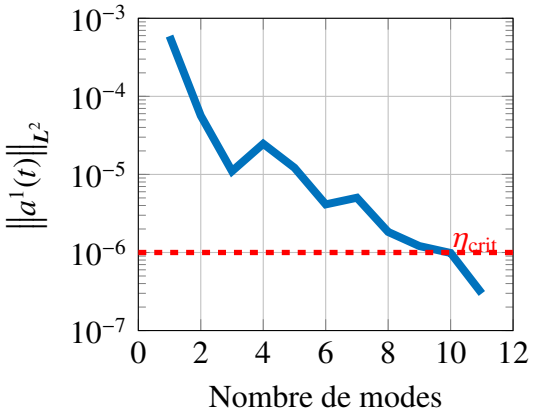

Figure E.5: Évolution de la norme $\mathcal{L}^2$ des modes dans la décomposition PGD

4.2 Essai de flexion 4 points

Le but de ce second exemple est de simuler le comportement d'une structure en béton armé, dont la géométrie est donnée Fig. E.6, lors d'un essai de flexion 4 points (la photographie d'une étude expérimentale d'A. Michou au LMT est donnée Fig. E.7).

La discrétisation spatiale de l'éprouvette ainsi que des espaces paramétriques est donnée Tab. E.4 et les conditions aux limites (encastrement et déplacement imposé) sont appliquées sur des bandes d'éléments sur la largeur de la poutre (en rouge sur la Fig. E.8).

Le déplacement imposé $\mathbf{u}_d(t,\mu_2)$ est paramétré par une variable μ_2, avec une variabilité de $+/-$ 30% qui affecte encore une fois son amplitude en suivant une loi similaire à celle présentée dans la section précédente (E.12) (ce chargement est particularisé pour trois valeurs de μ_2 Fig. E.9). Le module d'Young du béton est également paramétré par une variable μ_3 qui affecte sa valeur moyenne avec une variabilité de $+/-$ 15% ($E^c \in [21.61, 29.23]$ GPa).

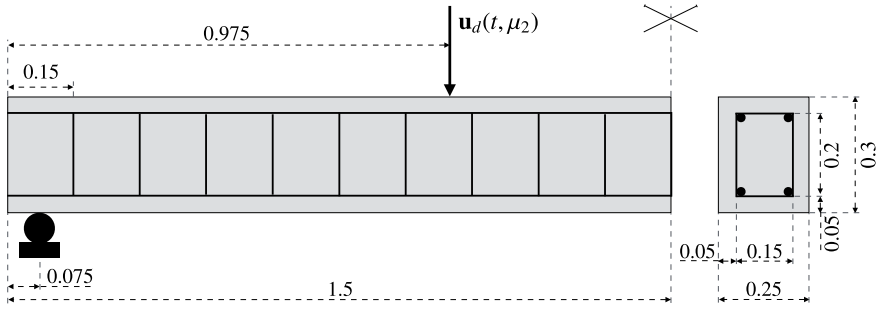

Figure E.6: Essai de flexion – coupes longitudinale (gauche) et transversale (droite) de la structure (en m)

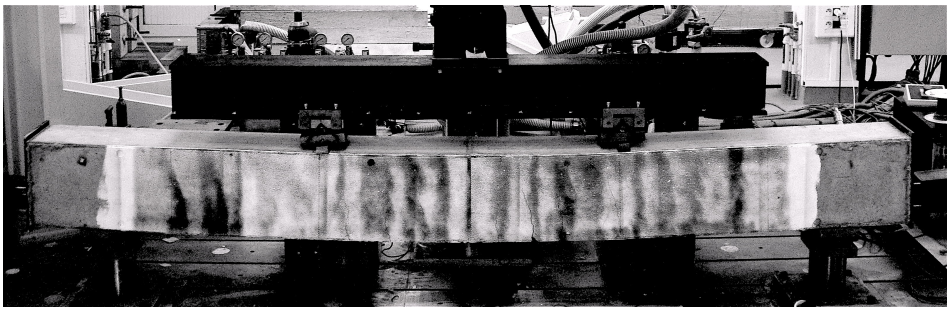

Figure E.7: Essai de flexion 4 points réalisé au LMT par A. Michou

Table E.4: Discrétisation du second exemple

Espace d'approximation		Intervalle de variation – discrétisation
$\boldsymbol{\Omega}$	Espace – béton	$3,157$ nœuds, $2,400$ éléments ($9,471$ DDLs, $19,200$ PGs)
	Espace – armature	160 nœuds, 232 éléments (480 DDLs, 232 PGs)
$\mathbf{D}_1 \equiv \mathcal{I}$	Temps	$\mu_1 \equiv t \in [0, 99]$ (100 pas de temps)
$\mathbf{D}_2$	Variabilité sur le chargement	$\mu_2 \in [1, 12]$ (12 values)
$\mathbf{D}_3$	Variabilité sur le module d'Young	$\mu_3 \in [0.85, 1.15]$ (9 valeurs)

La base de donnée suivante est ainsi calculée :

$$\boldsymbol{u}_m(\boldsymbol{x}, t, \boldsymbol{u}_d(\mu_2), E^c(\mu_3)) = \sum_{i=1}^{m} \boldsymbol{\Phi}_i(\boldsymbol{x})\, a_i^1(t)\, a_i^2(\mu_2)\, a_i^3(\mu_3) \tag{E.14}$$

Cet exemple est plus complexe dans le sens où cette forte variabilité, à la fois sur des paramètres affectant le chargement appliqué à la poutre et son matériau constitutif, conduit à des distributions d'endommagement et de contraintes complexes sur la structure.

Cela permet ainsi de montrer les possibilités de l'algorithme développé et en particulier

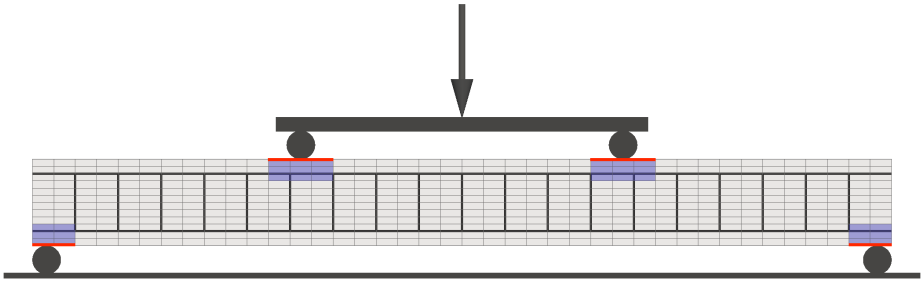

Figure E.8: Essai de flexion – zones d'applications des conditions aux limites (rouge)

l'avantage lié à l'utilisation de la représentation espace-paramètres de la PGD : cette décomposition permet tout d'abord de réduire le coût (mémoire et CPU) du problème linéaire et rend ainsi le post-traitement de la solution (visualisation de la réponse globale, calcul de quantités d'intérêt locales) bien plus facile à mettre en œuvre et rapide à effectuer, en particulier grâce au format PXDMF développé par F. Bordeu à l'École Centrale de Nantes[1].

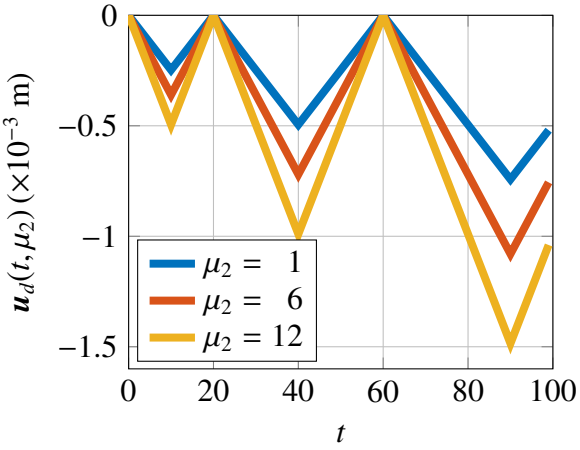

Figure E.9: Essai de flexion – variabilité sur le déplacement imposé $\boldsymbol{u}_d(t,\mu_2)$ pour quelques valeurs de μ_2

Les fonctions d'espace et paramétriques de la décomposition (E.14) sont respectivement données Figs. E.10 et E.11. On peut remarquer concernant les fonctions spatiales que les enrichissements sont de plus en plus localisés au fur et à mesure qu'augmente le nombre d'itérations. Concernant les fonctions du temps, présentées Fig. E.11a, on peut remarquer que les enrichissements sont localisés aux moments ou l'endommagement évolue : lorsque la charge dépasse le seuil initial lors du premier cycle (autour de $t = 10$s), ou lorsque la charge dépasse le pic atteint lors du cycle précédent (à $t = 40$s ou $t = 90$s). Les autres fonctions paramétriques sont cependant relativement régulières, ceci lié au fait que la variabilité sur le chargement semble prépondérante sur celle liée au module d'Young.

[1] `https://rom.ec-nantes.fr/`

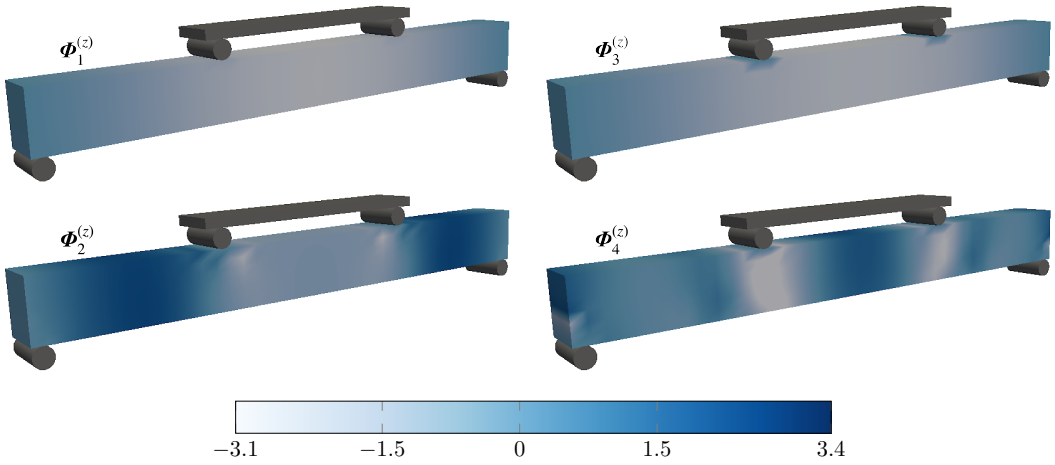

Figure E.10: Essai de flexion – composante suivant l'axe z des fonctions d'espace $\{\boldsymbol{\Phi}_i\}_{i=\{1,3,5,7\}}$ ($\boldsymbol{\Phi}_i^{(z)} = \boldsymbol{\Phi}_i \cdot z$)

La Fig. E.12 montre la particularisation du champ d'endommagement pour trois jeux de paramètres $\boldsymbol{\mu}_i = \{t^j, \mu_2^k, \mu_3^l\}_{i=1\cdots3}$ parmi $10,800$ possibles. On peut remarquer que les paramètres μ_2 et μ_3 influencent fortement l'intensité de l'endommagement dans certaines zones de la poutre, plus ou moins étendues selon les jeux choisis. Encore une fois, cette reconstruction est facilement et rapidement obtenue à partir de la base donnée grâce au plug-in PXDMF développé at École Centrale de Nantes[2] et utilisé au sein du logiciel ParaView [Ayachit, 2015], qui permet une combinaison en temps réel des différents modes, associée à un jeu de paramètres choisi par l'utilisateur, afin d'assembler la solution ainsi particularisée.

On retrouve ce résultat sur des aspects plus locaux : la Fig. E.13 montre l'évolution de la contrainte de von Mises $\boldsymbol{\sigma}_{\text{VM}}$ dans un élément endommagé pour l'ensemble des jeux de paramètres (μ_2, μ_3). Enfin, on peut remarquer sur la Fig. E.14 que la norme des modes décroît globalement avec le nombre d'itérations.

Seulement 11 itérations ont été nécessaires pour calculer la solution de ce problème exacerbant une forte variabilité à la fois sur des paramètres matériau et affectant le chargement imposé (pour un total de $10,800$ jeux de paramètres possibles). L'utilisation de la PGD dans ce cas est particulièrement intéressante car elle permet de grandement réduire le coût associé au traitement du problème linéaire du solveur LATIN, ainsi que de permettre très facilement l'étude de l'influence de ces paramètres sur les réponses mécaniques globales ou locales de la structure.

5 Conclusions et perspectives

La faisabilité du couplage LATIN-PGD avec une décomposition paramétrique a été montrée dans [Vitse et al., 2014] pour un problème 1-D et un premier résultat pour un problème 3-D

[2] `https://rom.ec-nantes.fr/`

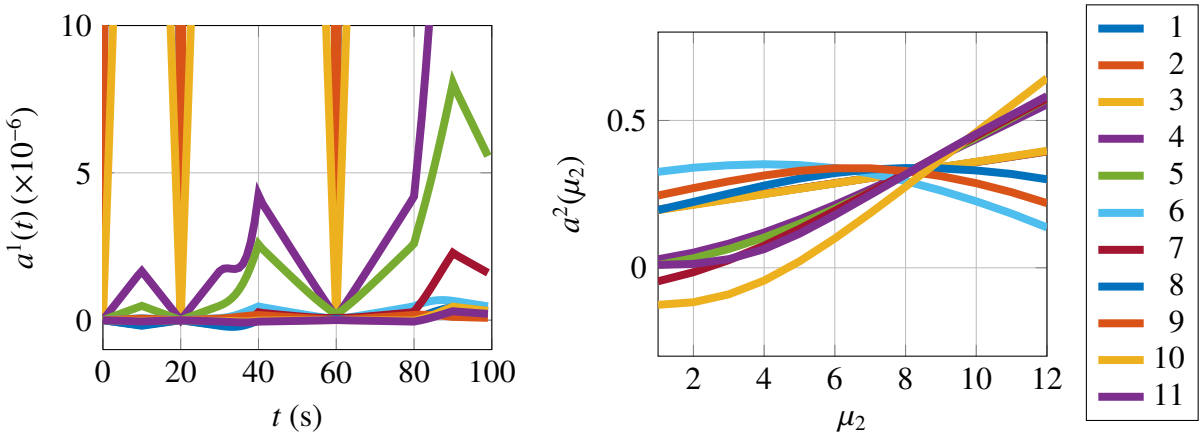

(a) Fonctions du temps $\{a_i^1(t)\}_{i=1\cdots11}$

(b) Fonctions associées au paramètre μ_2 $\{a_i^2(\mu_2)\}_{i=1\cdots11}$

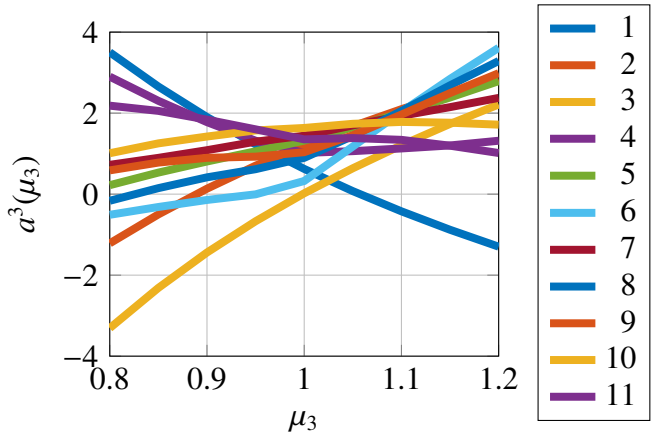

(c) Fonctions associées au paramètre μ_3 $\{a_i^3(\mu_3)\}_{i=1\cdots11}$

Figure E.11: Essai de flexion – fonctions paramétrique $\{a_i^1(t)\}_{i=1\cdots11}$ (Fig. E.11a), $\{a_i^2(\mu_2)\}_{i=1\cdots11}$ (Fig. E.11b) et $\{a_i^3(\mu_3)\}_{i=1\cdots11}$ (Fig. E.11c)

avec un modèle endommageant avec effet unilatéral a été présenté. Ces résultats sont encourageants car ils permettent, avec un faible nombre de termes dans la décomposition PGD, d'approximer le comportement global de la structure avec un modèle pourtant fortement nonlinéaire et une forte variabilité sur le déplacement imposé. L'analyse de structures massives avec des chargements plus complexes et une variabilité sur des paramètres matériaux et affectant le chargement sont nécessaires pour valider la méthode, et analyser ses performances numériques.

Les perspectives de ces travaux portent notamment sur le développement d'estimateurs d'erreurs permettant de caractériser la qualité du modèle réduit, reposant à la fois sur des critères globaux et locaux. L'utilisation d'approches de types points de référence [Capaldo, 2015] peut également s'avérer intéressante pour alléger le coût de calcul de l'étape locale de l'algorithme LATIN.

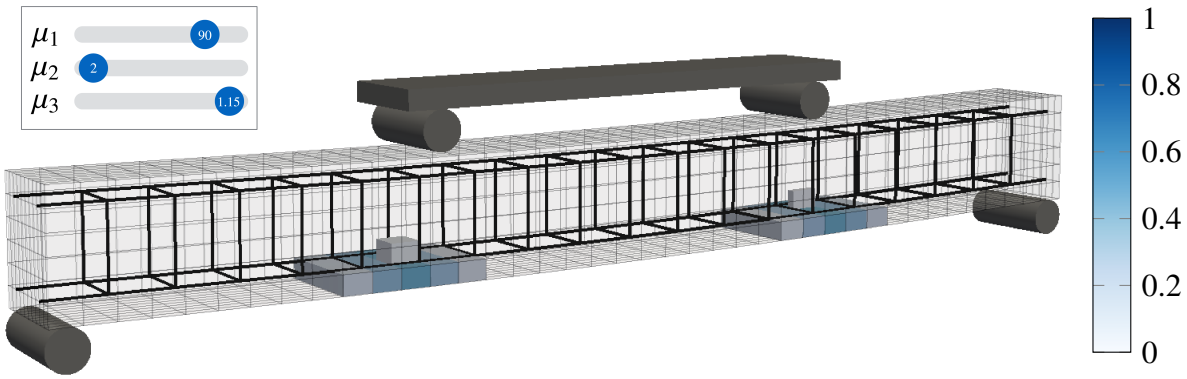

(a) Carte d'endommagement pour $\mu_1 = 90$, $\mu_2 = 2$ et $\mu_3 = 1.15$

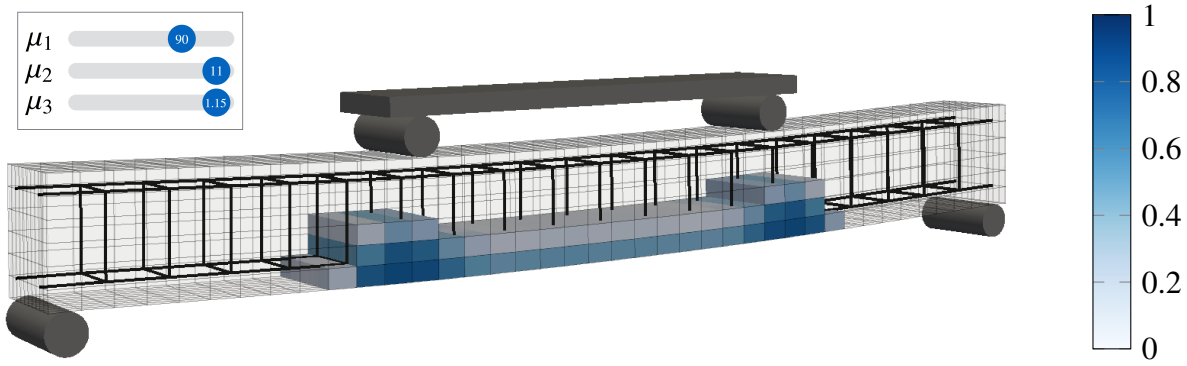

(b) Carte d'endommagement pour $\mu_1 = 90$, $\mu_2 = 11$ et $\mu_3 = 1.15$

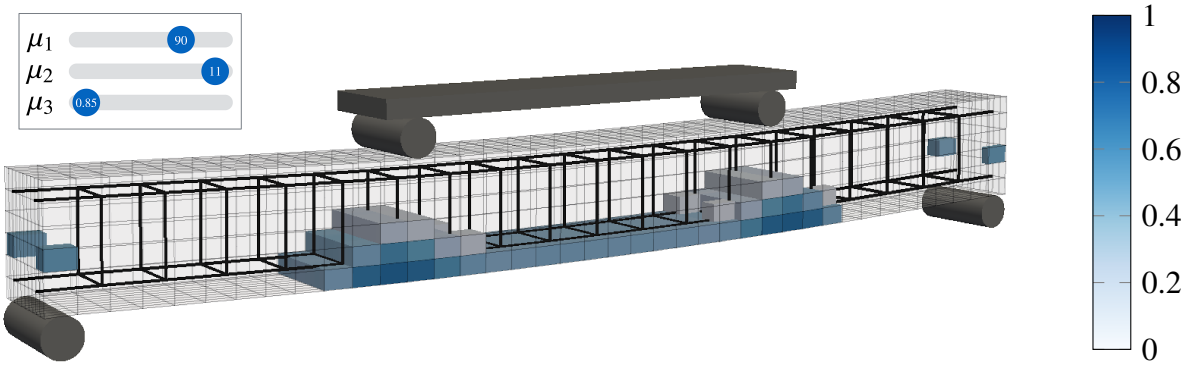

(c) Carte d'endommagement pour $\mu_1 = 90$, $\mu_2 = 11$ et $\mu_3 = 0.85$

Figure E.12: Essai de flexion – carte d'endommagement pour trois jeux de paramètres : (a) $(90, 2, 1.15)$; (b) $(90, 11, 1.15)$; (c) $(90, 11, 0.85)$

Remerciements

Ce travail réalisé au sein du projet SINAPS@ a bénéficié d'une aide de l'État gérée par l'Agence Nationale de la Recherche au titre du programme RSNR Investissements d'Avenir portant la référence No. ANR-11-RSNR-0022-04.

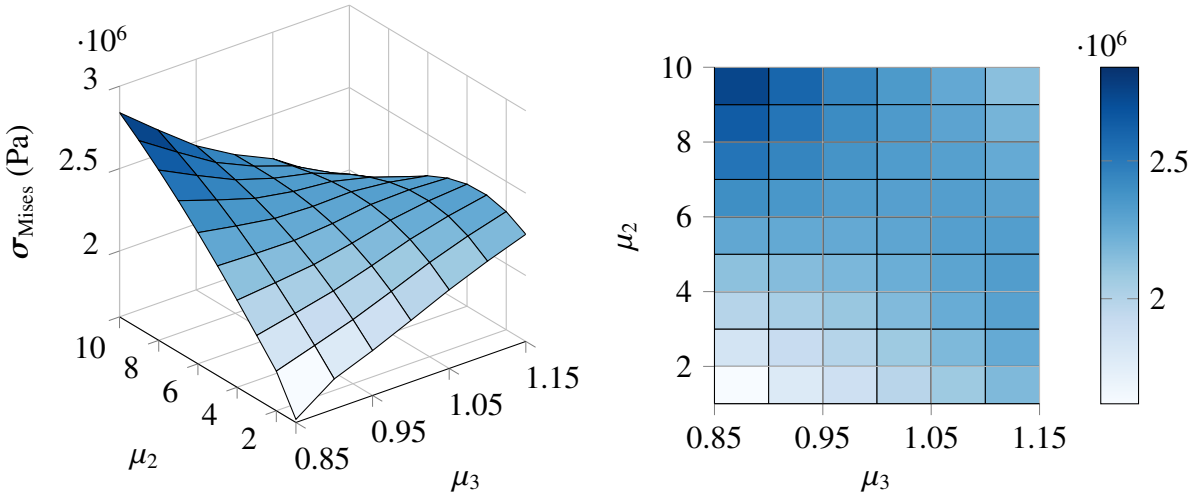

Figure E.13: Contrainte de von Mises stress dans un élément – surface de réponse (E.13a) et projection (E.13b)

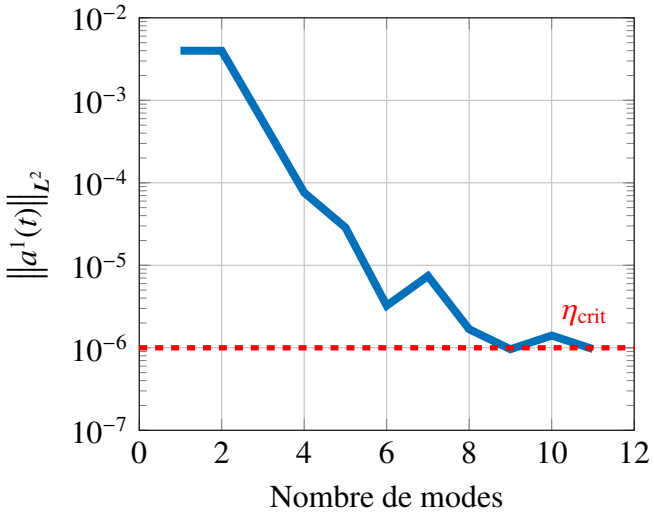

Figure E.14: Essai de flexion – évolution de la norme $\mathcal{L}^2$ des fonctions du temps avec le nombre de modes dans la décomposition

Bibliography

[Alfaro et al., 2015] Alfaro, I., González, D., Zlotnik, S., Díez, P., Cueto, E., and Chinesta, F. (2015). An error estimator for real-time simulators based on model order reduction. *Advanced Modeling and Simulation in Engineering Sciences*, 2(1):30.

[Allix, 2012] Allix, O. (2012). The bounded rate concept: A framework to deal with objective failure predictions in dynamic within a local constitutive model. *International Journal of Damage Mechanics*, 22:808–828.

[Allix and Deü, 1997] Allix, O. and Deü, J.-F. (1997). Delayed-damage modelling for fracture prediction of laminated composites under dynamic loading. *Engineering Transactions*, 45:29–46.

[Allix et al., 2003] Allix, O., Feissel, P., and Thévenet, P. (2003). A delay damage mesomodel of laminates under dynamic loading: basic aspects and identification issues. *Computers and Structures*, 81:1177–1191.

[Allix and Ladevèze, 1992] Allix, O. and Ladevèze, P. (1992). Interlaminar interface modelling for the prediction of delamination. *Composite Structures*, 22(4):235–242.

[Allix et al., 1989] Allix, O., Ladevèze, P., Gilletta, D., and Ohayon, R. (1989). A damage prediction method for composite structures. *International Journal for Numerical Methods in Engineering*, 27(2):271–283.

[Allix and Vidal, 2002] Allix, O. and Vidal, P. (2002). A new multi-solution approach suitable for structural identification problems. *Computer Methods in Applied Mechanics and Engineering*, 191(25-26):2727–2758.

[Ammar et al., 2012] Ammar, A., Chinesta, F., Cueto, E., and Doblaré, M. (2012). Proper generalized decomposition of time-multiscale models. *International Journal for Numerical Methods in Engineering*, 90:569–596.

[Ammar et al., 2010a] Ammar, A., Chinesta, F., Díez, P., and Huerta, A. (2010a). An error estimator for separated representations of highly multidimensional models. *Computer Methods in Applied Mechanics and Engineering*, 199(25-28):1872–1880.

[Ammar et al., 2014] Ammar, A., Huerta, A., Chinesta, F., Cueto, E., and Leygue, A. (2014). Parametric solutions involving geometry: A step towards efficient shape optimization. *Computer Methods in Applied Mechanics and Engineering*, 268:178–193.

[Ammar et al., 2010b] Ammar, A., Normandin, M., Daim, F., González, D., Cueto, E., and Chinesta, F. (2010b). Non incremental strategies based on separated representations: applications in computational rheology. *Commun. Math. Sci.*, 8:671–695.

[Arzt, 1994] Arzt, M. (1994). *Approche des phénomènes cycliques par la méthode à grand incrément de temps*. PhD thesis, Ecole Normale Supérieure de Cachan.

[Ayachit, 2015] Ayachit, U. (2015). *The ParaView Guide: a parallel visualization application*. Kitware.

[Azrar et al., 1993] Azrar, L., Cochelin, B., Damil, N., and Potier-Ferry, M. (1993). An asymptotic-numerical method to compute the postbuckling behaviour of elastic plates and shells. *International Journal for Numerical Methods in Engineering*, 36(8):1251–1277.

[Bader and Kolda, 2007] Bader, B. W. and Kolda, T. G. (2007). Efficient MATLAB computations with sparse and factored tensors. *SIAM Journal on Scientific Computing*, 30(1):205–231.

[Barrault et al., 2004] Barrault, M., Maday, Y., Nguyen, N. C., and Patera, A. T. (2004). An 'empirical interpolation' method: application to efficient reduced-basis discretization of partial differential equations. *Comptes Rendus Mathematique*, 339(9):667–672.

[Beringhier et al., 2016] Beringhier, M., Leygue, A., and Chinesta, F. (2016). Parametric nonlinear PDEs with multiple solutions: A PGD approach. *Discrete and Continuous Dynamical Systems - Series S*, 9(2):383–392.

[Blanzé et al., 2000] Blanzé, C., Champaney, L., and Vedrine, P. (2000). Contact problems in the design of a superconducting quadrupole prototype. *Engineering Computations*, 17(2):136–153.

[Bognet et al., 2014] Bognet, B., Leygue, A., and Chinesta, F. (2014). Separated representations of 3D elastic solutions in shell geometries. *Advanced Modeling and Simulation in Engineering Sciences*, 1(4):1–34.

[Boisse, 1987] Boisse, P. (1987). *Nouvel algorithme à grand incrément de temps pour le calcul des structures élastoplastiques*. PhD thesis, Université Pierre et Marie Curie.

[Boisse et al., 1990] Boisse, P., Bussy, P., and Ladevèze, P. (1990). A new approach in nonlinear mechanics: the large time increment method. *International Journal for Numerical Methods in Engineering*, 29(3):647–663.

[Boucard, 1996] Boucard, P.-A. (1996). *Approche à grand incrément de temps en grandes transformations*. PhD thesis, Ecole Normale Supérieure de Cachan.

[Boucard et al., 2009] Boucard, P.-A., Buytet, S., and Guidault, P.-A. (2009). A multiscale strategy for structural optimization. *International Journal for Numerical Methods in Engineering*, 78(1):101–126.

[Boucard and Champaney, 2003] Boucard, P.-A. and Champaney, L. (2003). A suitable computational strategy for the parametric analysis of problems with multiple contact. *International journal for numerical methods in engineering*, 57(9):1259–1281.

[Boucard and Ladevèze, 1999] Boucard, P.-A. and Ladevèze, P. (1999). A multiple solution method for non-linear structural mechanics. *Mechanical Engineering*, 50(5):317–328.

[Bouclier et al., 2013] Bouclier, R., Louf, F., and Chamoin, L. (2013). Real-time validation of mechanical models coupling PGD and constitutive relation error. *Computational Mechanics*, 52(4):861–883.

[Caignot, 2009] Caignot, A. (2009). *Prédiction par essais virtuels de l'amortissement dans les structures spatiales*. PhD thesis, Ecole Normale Supérieure de Cachan.

[Capaldo, 2015] Capaldo, M. (2015). *A new approximation framework for PGD-based nonlinear solvers*. PhD thesis, Université Paris-Saclay.

[Carlberg et al., 2013] Carlberg, K., Farhat, C., Cortial, J., and Amsallem, D. (2013). The GNAT method for nonlinear model reduction : Effective implementation and application to computational fluid dynamics and turbulent flows. *Journal of Computational Physics*, 242:623–647.

[Casanova et al., 2012] Casanova, A., Jason, L., and Davenne, L. (2012). Bond slip model for the simulation of reinforced concrete structures. *Engineering Structures*, 39:66–78.

[Champaney, 1996] Champaney, L. (1996). *Une nouvelle approche modulaire pour l'analyse d'assemblages de structures tridimensionnelles*. PhD thesis, Ecole Normale Supérieure de Cachan.

[Chatterjee, 2000] Chatterjee, A. (2000). An introduction to the proper orthogonal decomposition. *Current Science*, 78(7):808–817.

[Chaturantabut and Sorensen, 2010] Chaturantabut, S. and Sorensen, D. C. (2010). Nonlinear model reduction via discrete empirical interpolation. *SIAM Journal On Scientific Computing*, 32(5):2737–2764.

[Chinesta et al., 2010] Chinesta, F., Ammar, A., and Cueto, E. (2010). Recent advances and new challenges in the use of the proper generalized decomposition for solving multidimensional models. *Archives of Computational Methods in Engineering*, pages 1–24.

[Chinesta et al., 2013] Chinesta, F., Leygue, A., Bordeu, F., Aguado, J. V., Cueto, E., González, D., Alfaro, I., Ammar, A., and Huerta, A. (2013). PGD-Based computational vademecum for efficient design, optimization and control. *Archives of Computational Methods in Engineering*, 20(1):31–59.

[Choi and Kwon, 2000] Choi, B.-S. and Kwon, Y.-W. (2000). Probabilistic analysis of reinforced concrete beam and slab deflections using Monte Carlo simulation. *KCI Concrete Journal*, 12(2):11–21.

[Cochelin et al., 1994] Cochelin, B., Damil, N., and Potier-Ferry, M. (1994). Asymptotic-numerical methods and Padé approximants for non-linear elastic structures. *International journal for numerical methods in engineering*, 37(7):1187–1213.

[Cognard, 1989] Cognard, J.-Y. (1989). *Une nouvelle approche des problèmes de plasticité et de viscoplasticité : la méthode à grand incrément de temps*. PhD thesis, Université Pierre et Marie Curie.

[Cognard et al., 1999] Cognard, J.-Y., Ladevèze, P., and Talbot, P. (1999). A large time increment approach for thermo-mechanical problems. *Advances in Engineering Software*, 30(9–11):583–593.

[Costa et al., 2005] Costa, C., Pegon, P., Arêde, A., and Castro, J. (2005). Implementation of the Damage model in Tension and Compression with Plasticity in Cast3m. Technical report.

[Courard et al., 2016] Courard, A., Néron, D., Ladevèze, P., and Ballere, L. (2016). Integration of PGD-virtual charts into an engineering design process. *Computational Mechanics*, 57(4):637–651.

[Courrier, 2015] Courrier, N. (2015). *Couplage optimisation à convergence partielle et stratégie multiparamétrique en calcul de structures*. PhD thesis, Ecole Normale Supérieure de Cachan.

[Danwé, 1993] Danwé, R. (1993). *Une méthode simplifiée pour l'étude d'assemblage de structures*. PhD thesis, Ecole Normale Supérieure de Cachan.

[De Borst and Mühlhaus, 1992] De Borst, R. and Mühlhaus, H.-B. (1992). Gradient-dependent plasticity: formulation and algorithmic aspects. *International Journal for Numerical Methods in Engineering*, 35(October 1991):521–539.

[Derumaux, 2004] Derumaux, M. (2004). *Sur la modélisation / simulation de liaisons soumises à des chocs pyrotechniques*. PhD thesis, Ecole Normale Supérieure de Cachan.

[Desmorat et al., 2007] Desmorat, R., Gatuingt, F., and Ragueneau, F. (2007). Nonlocal anisotropic damage model and related computational aspects for quasi-brittle materials. *Engineering Fracture Mechanics*, 74(10):1539–1560.

[Douchin and Ladevèze, 2001] Douchin, B. and Ladevèze, P. (2001). Mise en œuvre numérique d'un mésomodèle d'endommagement des stratifiés. *Revue européenne des éléments finisuropéenne des éléments finis*, 10:473–487.

[Drohmann et al., 2012] Drohmann, M., Haasdonk, B., and Ohlberger, M. (2012). Reduced Basis Approximation for Nonlinear Parametrized Evolution Equations based on Empirical Operator Interpolation. *SIAM Journal on Scientific Computing*, 34(2):937–969.

[Dubé et al., 1996] Dubé, J.-F., Pijaudier-Cabot, G., and La Borderie, C. (1996). Rate Dependent Damage Model for Concrete in Dynamics. *ASCE Journal of Engineering Mechanics*, 122(10):939–947.

[Dureisseix, 1997] Dureisseix, D. (1997). *Une approche multi-échelles pour des calculs de structures sur ordinateurs à architecture parallèle*. PhD thesis, Ecole Normale Supérieure de Cachan.

[Dureisseix et al., 2003] Dureisseix, D., Ladevèze, P., and Schrefler, B. (2003). A LATIN computational strategy for multiphysics problems: Application to poroelasticity. *International Journal for Numerical Methods in Engineering*, 56(10):1489–1510.

[El Halabi et al., 2016] El Halabi, F., González, D., Sanz-Herrera, J. A., and Doblaré, M. (2016). A PGD-based multiscale formulation for non-linear solid mechanics under small deformations. *Computer Methods in Applied Mechanics and Engineering*, 305:806–826.

[Farhat et al., 2014] Farhat, C., Avery, P., Chapman, T., and Cortial, J. (2014). Dimensional reduction of nonlinear finite element dynamic models with finite rotations and energy-based mesh sampling and weighting for computational efficiency. *International Journal for Numerical Methods in Engineering*, 98(9):625–662.

[Ghanem and Spanos, 1991] Ghanem, R. G. and Spanos, P. D. (1991). *Stochastic Finite Elements: A Spectral Approach*. Springer New York, New York, NY.

[Giacoma et al., 2016] Giacoma, A., Dureisseix, D., and Gravouil, A. (2016). An efficient quasi-optimal space-time PGD application to frictional contact mechanics. *Advanced Modeling and Simulation in Engineering Sciences*, 3(1):12.

[Giacoma et al., 2015] Giacoma, A., Dureisseix, D., Gravouil, A., and Rochette, M. (2015). Toward an optimal a priori reduced basis strategy for frictional contact problems with LATIN solver. *Computer Methods in Applied Mechanics and Engineering*, 283:1357–1381.

[Giry et al., 2011] Giry, C., Dufour, F., and Mazars, J. (2011). Stress-based nonlocal damage model. *International Journal of Solids and Structures*, 48(25-26):3431–3443.

[Glüsmann and Kreuzer, 2009] Glüsmann, P. and Kreuzer, E. (2009). On the application of Karhunen-Loève transform to transient dynamic systems. *Journal of Sound and Vibration*, 328(4-5):507–519.

[Grassl and Jirásek, 2006] Grassl, P. and Jirásek, M. (2006). Plastic model with non-local damage applied to concrete. *International Journal for Numerical and Analytical Methods in Geomechanics*, 30(1):71–90.

[Grepl et al., 2007] Grepl, M. A., Maday, Y., Nguyen, N. C., and Patera, A. T. (2007). Efficient reduced-basis treatment of nonaffine and nonlinear partial differential equations. *ESAIM: mathematical modelling and numerical analysis*, 41:575–605.

[Guidault, 2005] Guidault, P.-A. (2005). *Une stratégie de calcul pour les structures fissurées : analyse locale-globale et approche multiéchelle pour la fissuration*. PhD thesis, Ecole Normale Supérieure de Cachan.

[Gupta et al., 2005] Gupta, J. S., Allix, O., Boucard, P.-A., Fanget, A., and Héreil, P.-L. (2005). Fracture prediction of a 3D C/C material under impact. *Composites Science and Technology*, 65(3–4):375–386.

[Heyberger et al., 2012] Heyberger, C., Boucard, P.-A., and Néron, D. (2012). Multiparametric analysis within the proper generalized decomposition framework. *Computational Mechanics*, 49(3):277–289.

[Heyberger et al., 2013] Heyberger, C., Boucard, P.-A., and Néron, D. (2013). A rational strategy for the resolution of parametrized problems in the PGD framework. *Comput. Methods Appl. Mech. Engrg.*, 259:40–49.

[Hilaire et al., 2014] Hilaire, A., Benboudjema, F., Darquennes, A., Berthaud, Y., and Nahas, G. (2014). Modeling basic creep in concrete at early-age under compressive and tensile loading. *Nuclear Engineering and Design*, 269:222–230.

[Hill, 1958] Hill, R. (1958). A general theory of uniqueness and stability in elastic-plastic solids. *Journal of the Mechanics and Physics of Solids*, 6:236–249.

[Hillerborg et al., 1976] Hillerborg, A., Modéer, M., and Petersson, P.-E. (1976). Analysis of crack formation and crack growth in concrete by means of fracture mechanics and finite elements. *Cement and Concrete Research*, 6:773–782.

[Hitchcock, 1927] Hitchcock, F. L. (1927). The expression of a tensor or a polyadic as a sum of products. *J. Math. Phys.*, 6:164–189.

[Iskef, 2016] Iskef, A. E. (2016). *Technologies informatiques pour l'étude du comportement expérimental et numérique d'un assemblage poutre-poteau en béton armé*. PhD thesis, Université Paris-Saclay.

[Jirásek, 2007] Jirásek, M. (2007). Nonlocal damage mechanics. *Revue Européenne de Génie Civil*, 11(7-8):993–1021.

[Jirásek and Rolshoven, 2003] Jirásek, M. and Rolshoven, S. (2003). Comparison of integral-type nonlocal plasticity models for strain-softening materials. *International Journal of Engineering Science*, 41(13-14):1553–1602.

[Jung et al., 2009] Jung, N., Haasdonk, B., and Kroner, D. (2009). Reduced Basis Method for quadratically nonlinear transport equations. *International Journal of Computing Science and Mathematics*, 2(4):334.

[Karhunen, 1946] Karhunen, K. (1946). *Zur spektraltheorie stochastischer prozesse*. Suomalainen tiedeakatemia.

[Kerfriden, 2008] Kerfriden, P. (2008). *Stratégie de décomposition de domaine à trois échelles pour la simulation du délaminage dans les stratifiés*. PhD thesis, Ecole Normale Supérieure de Cachan.

[Kerfriden et al., 2011] Kerfriden, P., Gosselet, P., Adhikari, S., and Bordas, S. P. A. (2011). Bridging proper orthogonal decomposition methods and augmented Newton-Krylov algorithms: An adaptive model order reduction for highly nonlinear mechanical problems. *Computer Methods in Applied Mechanics and Engineering*, 200(5-8):850–866.

[Kerfriden et al., 2012] Kerfriden, P., Passieux, J.-c., and Bordas, S. P. A. (2012). Local/global model order reduction strategy for the simulation of quasi-brittle fracture. *International Journal for Numerical Methods in Engineering*, 89(2):154–179.

[Kosambi, 1943] Kosambi, D. D. (1943). Statistics in function space. *J. Indian Math. Soc*, 7(1):76–88.

[Ladevèze, 1985] Ladevèze, P. (1985). Sur une famille d'algorithmes en mécanique des structures. *Comptes-rendus des séances de l'Académie des sciences. Série 2, Mécanique-physique, chimie, sciences de l'univers, sciences de la terre*, 300(2):41–44.

[Ladevèze, 1989] Ladevèze, P. (1989). The large time increment method for the analyze of structures with nonlinear constitutive relation described by internal variables. *CR Acad Sci Paris*, 309(1095-1099).

[Ladevèze, 1991] Ladevèze, P. (1991). About a damage mechanics approach. In *Mechanics and Mechanisms of Damage in Composites and Multi-materials*, pages 119–141. Baptiste, D. ed, London, mechanical edition.

[Ladevèze, 1997] Ladevèze, P. (1997). Une technique de calcul d'intégrales en temps et en espace relative à la LATIN méthode. Technical report, LMT Cachan.

[Ladevèze, 1999] Ladevèze, P. (1999). *Nonlinear computational structural mechanics: new approaches and non-incremental methods of calculation*. Springer.

[Ladevèze and Dureisseix, 2000] Ladevèze, P. and Dureisseix, D. (2000). A micro / macro approach for parallel computing of heterogeneous structures. *International Journal for Computational Civil and Structural Engineering*, 1:18–28.

[Ladevèze et al., 2000] Ladevèze, P., Lemoussu, H., and Boucard, P.-A. (2000). A modular approach to 3-D impact computation with frictional contact. *Computers & Structures*, 78(1–3):45–51.

[Ladevèze et al., 2001] Ladevèze, P., Loiseau, O., and Dureisseix, D. (2001). A micro–macro and parallel computational strategy for highly heterogeneous structures. *International Journal for Numerical Methods in Engineering*, 52(1-2):121–138.

[Ladevèze et al., 2010] Ladevèze, P., Néron, D., and Passieux, J.-c. (2010). On multiscale computational mechanics with time-space homogenization. *Multiscale methods - Bridging the scales in Science and Engineering*, 1(January 2008):247–282.

[Ladevèze and Nouy, 2003] Ladevèze, P. and Nouy, A. (2003). On a multiscale computational strategy with time and space homogenization for structural mechanics. *Computer Methods in Applied Mechanics and Engineering*, 192(28-30):3061–3087.

[Laurent, 2013] Laurent, L. (2013). *Stratégie multiparamétrique et métamodèles pour l'optimisation multiniveaux de structures*. PhD thesis, Ecole Normale Supérieure de Cachan.

[Lemoussu et al., 2002] Lemoussu, H., Boucard, P.-A., and Ladevèze, P. (2002). A 3D shock computational strategy for real assembly and shock attenuator. *Advances in Engineering Software*, 33(7–10):517–526.

[Leygue et al., 2013] Leygue, A., Chinesta, F., Beringhier, M., Nguyen, L. T., Grandidier, J.-C., Schrefler, B., and Pesavento, F. (2013). Towards a framework for non-linear thermal models in shell domains. *International Journal of Numerical Methods for Heat & Fluid Flow*, 23(1):55–73.

[Liang et al., 2002] Liang, Y., Lee, H., Lim, S., Lin, W., Lee, K., and Wu, C. (2002). Proper Orthogonal Decomposition and Its Applications—Part I: Theory. *Journal of Sound and Vibration*, 252(3):527–544.

[Liu, 1992] Liu, B. (1992). *Simulation numérique de l'emboutissage. Méthode à grand incrément de temps*. PhD thesis, Université Pierre et Marie Curie.

[Lorong, 1994] Lorong, P. (1994). *Sur une approche parallèle pour le calcul des structures : comportement sur calculateurs parallèles*. PhD thesis, Ecole Normale Supérieure de Cachan.

[Maday and Ronquist, 2004] Maday, Y. and Ronquist, E. M. (2004). The reduced basis element method: application to a thermal fin problem. *SIAM Journal on Scientific Computing*, 26(1):240–258.

[Mantoglou and Wilson, 1982] Mantoglou, A. and Wilson, J. L. (1982). The turning bands method for simulation of random fields using line generation by a spectral method. *Water Resources Research*, 18(5):1379–1394.

[Marchand et al., 2015] Marchand, B., Chamoin, L., and Rey, C. (2015). Real-time updating of structural mechanics models using Kalman filtering , modified Constitutive Relation Error , and Proper Generalized Decomposition. *International Journal for Numerical Methods in Engineering*, pages 1–31.

[Matallah et al., 2010] Matallah, M., La Borderie, C., and Maurel, O. (2010). A practical method to estimate crack openings in concrete structures. *International Journal for Numerical and Analytical Methods in Geomechanics*, 34(January):1615–1633.

[Mazars, 1984] Mazars, J. (1984). *Application de la mécanique de l'endommagement au comportement non linéaire et à la rupture du béton de structure*. PhD thesis, Université Pierre et Marie Curie.

[Mazars et al., 1990] Mazars, J., Berthaud, Y., and Ramtani, S. (1990). The unilateral behaviour of damaged concrete. *Engineering Fracture Mechanics*, 35(415):607.

[Metoui et al., 2014] Metoui, S., Prulière, E., Ammar, A., Dau, F., and Iordanoff, I. (2014). The proper generalized decomposition for the simulation of delamination using cohesive zone model. *International Journal for Numerical Methods in Engineering*, 99(13):1000–1022.

[Michel-Ponnelle, 2001] Michel-Ponnelle, S. (2001). *Modélisation et simulation de structures élastomères endommageables en grandes transformations*. PhD thesis, Ecole Normale Supérieure de Cachan.

[Mihai and Jefferson, 2011] Mihai, I. C. and Jefferson, A. D. (2011). A material model for cementitious composite materials with an exterior point Eshelby microcrack initiation criterion. *International Journal of Solids and Structures*, 48(24):3312–3325.

[Nadal et al., 2015] Nadal, E., Chinesta, F., Díez, P., Fuenmayor, F. J., and Denia, F. D. (2015). Real time parameter identification and solution reconstruction from experimental data using the Proper Generalized Decomposition. *Computer Methods in Applied Mechanics and Engineering*, 296:113–128.

[Needleman, 1988] Needleman, A. (1988). Material rate dependence and mesh sensitivity in localization problems. *Computer Methods in Applied Mechanics and Engineering*, 67(1):69–85.

[Néron, 2004] Néron, D. (2004). *Sur une stratégie de calcul pour les problèmes multiphysiques*. PhD thesis, Ecole Normale Supérieure de Cachan.

[Néron et al., 2015] Néron, D., Boucard, P.-A., and Relun, N. (2015). Time-space PGD for the rapid solution of 3D nonlinear parametrized problems in the many-query context. *International Journal for Numerical Methods in Engineering*, 103(4):275–292.

[Néron and Dureisseix, 2008] Néron, D. and Dureisseix, D. (2008). A computational strategy for poroelastic problems with a time interface between coupled physics. *International Journal for Numerical Methods in Engineering*, 73(June 2007):783–804.

[Nguyen et al., 2008] Nguyen, H.-M., Allix, O., and Feissel, P. (2008). A robust identification strategy for rate-dependent models in dynamics. *Inverse Problems*, 24(6):65006.

[Niroomandi et al., 2010] Niroomandi, S., Alfaro, I., Cueto, E., and Chinesta, F. (2010). Model order reduction for hyperelastic materials. *International Journal for Numerical Methods in Engineering*, 81(9):1180–1206.

[Niroomandi et al., 2012] Niroomandi, S., Alfaro, I., Cueto, E., and Chinesta, F. (2012). Accounting for large deformations in real-time simulations of soft tissues based on reduced-order models. *Computer Methods and Programs in Biomedicine*, 105(1):1–12.

[Nocedal and Wright, 1999] Nocedal, J. and Wright, S. J. (1999). *Numerical Optimization*. Springer.

[Nouy, 2003] Nouy, A. (2003). *Une stratégie de calcul multiéchelle avec homogénéisation en temps et en espace pour le calcul de structures fortement hétérogènes*. PhD thesis, Ecole Normale Supérieure de Cachan.

[Nouy, 2010] Nouy, A. (2010). A priori model reduction through proper generalized decomposition for solving time-dependent partial differential equations. *Computer Methods in Applied Mechanics and Engineering*, 199(23-24):1603–1626.

[Odièvre, 2009] Odièvre, D. (2009). *Sur une stratégie de calcul en dynamique transitoire en présence de variabilité paramétrique*. PhD thesis, Ecole Normale Supérieure de Cachan.

[Oseledets, 2011] Oseledets, I. V. (2011). Tensor-Train Decomposition. *SIAM Journal on Scientific Computing*, 33(5):2295–2317.

[Oumaziz et al., 2017] Oumaziz, P., Gosselet, P., Boucard, P.-A., and Guinard, S. (2017). A non-invasive implementation of a mixed domain decomposition method for frictional contact problems (submitted). *Computational Mechanics*.

[Passieux, 2008] Passieux, J.-C. (2008). *Approximation radiale et méthode LATIN multi-échelle en temps et espace*. PhD thesis, Ecole Normale Supérieure de Cachan.

[Passieux and Périé, 2012] Passieux, J.-c. and Périé, J.-N. (2012). High resolution digital image correlation using proper generalized decomposition: PGD-DIC. *International Journal for Numerical . . .* , 92(June):531–550.

[Patera and Rozza, 2007] Patera, A. T. and Rozza, G. (2007). *Reduced basis approximation and a posteriori error estimation for parametrized partial differential equations*. M.I.T.

[Peerlings et al., 2001] Peerlings, R. H. J., Geers, M. G. D., De Borst, R., and Brekelmans, W. A. M. (2001). A critical comparison of nonlocal and gradient-enhanced softening continua. *International Journal of Solids and Structures*, 38(44-45):7723–7746.

[Pelle and Ryckelynck, 2000] Pelle, J.-P. and Ryckelynck, D. (2000). An efficient adaptive strategy to master the global quality of viscoplastic analysis. *Computers & Structures*, 78(1–3):169–183.

[Potier-Ferry, 1979] Potier-Ferry, M. (1979). Perturbed bifurcation theory. *Journal of Differential Equations*, 33:112–146.

[Radermacher and Reese, 2014] Radermacher, A. and Reese, S. (2014). Model reduction in elastoplasticity: proper orthogonal decomposition combined with adaptive substructuring. *Computational Mechanics*, 54:677–687.

[Relun, 2011] Relun, N. (2011). *Approche multiparamétrique pour la conception robuste en fatigue*. PhD thesis, Ecole Normale Supérieure de Cachan.

[Relun et al., 2013] Relun, N., Néron, D., and Boucard, P.-A. (2013). A model reduction technique based on the PGD for elastic-viscoplastic computational analysis. *Computational Mechanics*, 51(1):83–92.

[Richard and Ragueneau, 2012] Richard, B. and Ragueneau, F. (2012). Continuum damage mechanics based model for quasi brittle materials subjected to cyclic loadings: Formulation, numerical implementation and applications. *Engineering Fracture Mechanics*, 98:383–406.

[Richard et al., 2010] Richard, B., Ragueneau, F., Cremona, C., and Adelaide, L. (2010). Isotropic continuum damage mechanics for concrete under cyclic loading: Stiffness recovery, inelastic strains and frictional sliding. *Engineering Fracture Mechanics*, 77(8):1203–1223.

[Roulet, 2012] Roulet, V. (2012). *Stratégie multiparamétrique pour la simulation d'assemblages de structures stratifiées*. PhD thesis, Ecole Normale Supérieure de Cachan.

[Royer, 1990] Royer, C. (1990). *Une Approche des problèmes de dynamique non-lineaires par la méthode à grand incrément de temps*. PhD thesis, Université Pierre et Marie Curie.

[Rozza et al., 2008] Rozza, G., Huynh, D. B. P., and Patera, A. T. (2008). Reduced basis approximation and a posteriori error estimation for affinely parametrized elliptic coercive partial differential equations. *Archives of Computational Methods in Engineering*, 15(3):229–275.

[Rozza and Veroy, 2007] Rozza, G. and Veroy, K. (2007). On the stability of the reduced basis method for Stokes equations in parametrized domains. *Computer Methods in Applied Mechanics and Engineering*, 196(7):1244–1260.

[Ryckelynck, 2005] Ryckelynck, D. (2005). A priori hyperreduction method: an adaptive approach. *Journal of Computational Physics*, 202(1):346–366.

[Ryckelynck et al., 2011] Ryckelynck, D., Missoum Benziane, D., Cartel, S., and Besson, J. (2011). A robust adaptive model reduction method for damage simulations. *Computational Materials Science*, 50(5):1597–1605.

[Ryckelynck et al., 2012] Ryckelynck, D., Vincent, F., and Cantournet, S. (2012). Multidimensional a priori hyper-reduction of mechanical models involving internal variables. *Computer Methods in Applied Mechanics and Engineering*, 225-228:28–43.

[Saavedra Redlich, 2012] Saavedra Redlich, K. (2012). *Stratégie multiéchelle pour l'analyse du couplage flambage-délaminage de composites stratifiés*. PhD thesis, Ecole Normale Supérieure de Cachan.

[Saouridis and Mazars, 1992] Saouridis, C. and Mazars, J. (1992). Prediction of the failure and size effect in concrete via a bi-scale damage approach. *Engineering computations*, 9(3):329–344.

[Sellier et al., 2013] Sellier, A., Casaux-Ginestet, G., Buffo-Lacarrière, L., and Bourbon, X. (2013). Orthotropic damage coupled with localized crack reclosure processing. Part I: constitutive laws. *Engineering Fracture Mechanics*, 97:148–167.

[Signorini et al., 2016] Signorini, M., Zlotnik, S., and Díez, P. (2016). Proper generalized decomposition solution of the parameterized Helmholtz problem: application to inverse geophysical problems. *International Journal for Numerical Methods in Engineering*, (62).

[Soulier and Boucard, 2009] Soulier, B. and Boucard, P.-A. (2009). A multiparametric strategy for the large-scale multilevel optimization of structural assemblies. In *8th World Congress on Structural and Multidisciplinary Optimization*, Lisbon, Portugal.

[Suffis et al., 2003] Suffis, A., Lubrecht, T. A. A., and Combescure, A. (2003). Damage model with delay effect: Analytical and numerical studies of the evolution of the characteristic damage length. *International Journal of Solids and Structures*, 40(13–14):3463–3476.

[Sutton, 2013] Sutton, M. A. (2013). Computer vision based , non-contacting deformation and shape measurements: a revolution in progress. *Journal of the South Carolina Academy of Science*, 11(1).

[Terrien, 1980] Terrien, M. (1980). Emission acoustique et comportement mécanique postcritique d'un béton sollicité en traction. *Bulletin de liaison des Laboratoires des Ponts et Chaussées*, (105):65–72.

[Trovalet, 2010] Trovalet, M. (2010). *Sur un modèle micro pour le calcul des structures en composites stratifiés*. PhD thesis, Ecole Normale Supérieure de Cachan.

[Vandoren et al., 2013] Vandoren, B., De Proft, K., Simone, A., and Sluys, L. J. (2013). A novel constrained LArge Time INcrement method for modelling quasi-brittle failure. *Computer Methods in Applied Mechanics and Engineering*, 265:148–162.

[Vassaux et al., 2015] Vassaux, M., Richard, B., Ragueneau, F., and Millard, A. (2015). Regularised crack behaviour effects on continuum modelling of quasi-brittle materials under cyclic loading. *Engineering Fracture Mechanics*, 149:18–36.

[Vauchez, 1991] Vauchez, P. (1991). *Simulation numérique des processus de mise en forme par la méthode à grand increment de temps*. PhD thesis, Université Pierre et Marie Curie.

[Violeau, 2007] Violeau, D. (2007). *Une stratégie de calcul pour l'analyse à l'échelle "micro" des endommagements jusqu'à rupture des composites stratifiés*. PhD thesis, Ecole Normale Supérieure de Cachan.

[Vitse et al., 2014] Vitse, M., Néron, D., and Boucard, P.-A. (2014). Virtual charts of solutions for parametrized nonlinear equations. *Computational Mechanics*, 54(6):1529–1539.

[Willcox, 2006] Willcox, K. (2006). Unsteady flow sensing and estimation via the gappy proper orthogonal decomposition. *Computers and Fluids*, 35(2):208–226.

[Zlotnik et al., 2015] Zlotnik, S., Díez, P., Modesto, D., and Huerta, A. (2015). Proper generalized decomposition of a geometrically parametrized heat problem with geophysical applications. *International Journal for Numerical Methods in Engineering*, 103(10):737–758.

université PARIS-SACLAY
ÉCOLE DOCTORALE
Sciences mécaniques et énergétiques, matériaux et géosciences (SMEMAG)

Titre : Réduction de modèle pour l'analyse paramétrique de l'endommagement dans les structures en béton armé

Mots clefs : PGD, méthode LATIN, mécanique de l'endommagement, problèmes paramétriques

Résumé : Ces travaux de thèse sont consacrés au développement d'un algorithme de résolution de problèmes non-linéaires pour lesquels il existe une variabilité sur certains paramètres du modèle ou du chargement définis par leur interval de définition. Le cadre d'étude est le projet SINAPS@, qui a pour but d'évaluer les incertitudes dans les structures de génie civil, et de quantifier leur influence sur la réponse mécanique globale d'une structure sujette à un aléas sismique. Contrairement aux approches statistiques ou probabilistes classiques, une résolution déterministe est privilégiée dans notre étude. Cependant, afin de réduire le coût de calcul de cette famille de problèmes, une approche de type réduction de modèle PGD est mise en place, pour laquelle les paramètres incertains sont considérés comme des variables supplémentaires du problème. Cette méthode est mise en place au sein de l'algorithme LATIN, qui utilise une approche itérative pour résoudre le caractère non-linéaire des équations rencontrées lors de la résolution du problème mécanique. Ces travaux présentent donc l'extension de l'algorithme classique temps-espace LATIN–PGD à des problèmes paramétriques, pour lesquels les paramètres sont considérées comme des variables additionnelles dans la définition des quantités d'intérêt, ainsi que l'application de cette méthode à un modèle endommageant avec refermeture de fissure, présentant une variabilité à la fois sur des paramètres matériaux et sur l'amplitude du chargement. La faisabilité de ce couplage est illustrée par des exemples numériques sur des structures en béton armé pour divers types de chargement cycliques (traction–compression, flexion).

Title : Model-order reduction for the parametric analysis of damage in reinforced concrete structures

Keywords : PGD, LATIN method, damage mechanics, parametric problems

Abstract : This thesis is dedicated to the development of an algorithm for the resolution of nonlinear problems for which there is a variability on some of the model parameters or on the loading conditions, which are only described by their intervals of variation. This study is part of the SINAPS@ project, which aims at evaluating the uncertainties in civil engineering structures and to quantify their influence on the global mechanical response of a structure to a seismic hazard. Unlike statistical or probabilistic approaches, we rely here on a deterministic approach. However, in order to reduce the computation cost of such problems, a PGD-based reduced-order modeling approach is implemented, for which the uncertain parameters are considered as additional variables of the problem. This method was implemented into the LATIN algorithm, which uses an iterative approach to solve the nonlinear aspect of the equations of the mechanical problem. This work present the extension of the classical time-space LATIN–PGD algorithm to parametric problems for which the parameters are considered as additional variables in the definition of the quantities of interest, as well as the application of such method to a damage model with unilateral effect, highlighting a variability on both material parameters and the loading amplitude. The feasibility of such coupling is illustrated on numerical examples for reinforced concrete structures subjected to different types of cyclic loading conditions (tension–compression, bending).

Université Paris-Saclay
Espace Technologique / Immeuble Discovery
Route de l'Orme aux Merisiers RD 128 / 91190 Saint-Aubin, France